UNIVERSITY OF TURKU

Flexible Electrode Array System for Sweat Analysis in Vitro

Information and Communication Technology
Department of Computing, Faculty of Technology
Master of Science in Technology Thesis

Author(s):
Yichen Shao

Supervisor(s):
Assoc. Prof. Tomi Westerlund
Assoc. Prof. Guoping Chen

June.2022

University of Turku
Department of Computing, Faculty of Technology
Master of Science in Technology Thesis

Subject: Information and Communication Technology
Author(s): Yichen Shao
Title: Flexible Electrode Array System for Sweat Analysis in Vitro
Supervisor(s): Assoc. Prof. Tomi Westerlund
Number of pages: 88 pages
Date: June.2022

Abstract.

Sweat is a kind of liquid secreted to the body surface by human sweat glands, and its composition is highly related to the physiological state of the human body. Flexible wearable devices can dynamically monitor the change of sweat composition and the state of motion in real-time, which makes it become an important means for clinical and physiological research. In this thesis, a sensing system based on the flexible electrode array, which mainly includes a flexible electrode array and portable signal acquisition and processing system module, is designed and used for dynamic sweat detection. The system is characterized by high sensitivity, high selectivity, and repeatability, enabling online sweat composition analysis in vitro or wearable situations.

Flexible electrode array mainly includes ion-selective electrodes (ISEs), enzyme electrodes, and reference electrodes. The ISEs include sodium and potassium selective electrodes. Enzyme electrodes include glucose and lactate oxidase electrodes. Reference electrodes are two pseudo-Ag/AgCl reference electrodes, both of which also act as counter electrodes. Signal acquisition and processing module mainly include voltage signal amplification, current signal amplification, filtering, signal selection, and A/D conversion circuit.

This thesis studies the response characteristics of the electrode array to four kinds of sweat components. The sensitivity of ISEs and enzyme electrodes can be obtained by using an electrochemical workstation: The voltage response sensitivity of potassium ISE is 60.8 mV/lg[c(K$^+$)]; The voltage response sensitivity of sodium ISE is 45.9 mV/lg[c(Na$^+$)]; The current response sensitivity of glucose oxidase electrode is 2.28 µA·L/mmol; The current response sensitivity of lactate oxidase electrode is 45 nA·L/mmol. At the same time, the selectivity of ISEs is studied, and the experiment shows that both potassium and sodium ISE have a good anti-interference ability with low sensitivity against temperature.

The sensitivity of potassium, sodium, glucose and lactate electrodes can still maintain a good linear relationship and meet the sensitivity requirements by using the portable signal acquisition and processing system. Combined with the "Clip Plate Method", sodium ion, glucose, and lactate of sweat sample collected from sportive volunteers are measured and analyzed, and the detecting of oxygen saturation and heart rate is also carried out in real-time, through which it can be found that the composition of sweat will change with the motion state and individual differences, providing a reference for the follow-up single targeted detection.

In the thesis, a new type of enzyme electrode based on viologen compounds is developed, which has simple technological process and good stability, and the current response sensitivity of glucose and lactate oxidase electrode based on sulfhydryl viologen is measured as -0.234 µA·L/mmol and -41.7 nA·L/mmol, which shows improved linearity and stability compared with conventional enzyme electrode.

Key words: flexible electrode array, sensing, ion-selective electrode, enzyme electrode, electrochemistry, sensitivity, circuit system, sweat composition, viologen.

Contents

List of Figures

List of Tables

List of Abbreviations

3D	Three Dimension
AC	Alternating Current
A/D	Analog/Digital
ADC	Analog-to-Digital Converter
CM	Common Mode
CMRR	Common Mode Rejection Ratio
CO., LTD.	Company Limited
CP	Chronopotentiometry
CV	Cyclic Voltammetry
D-glucose	Dextrorotation Glucose
DC	Direct Current
DEC	Decimal
DM	Differential Mode
DOS	Bis (2-Ethylhexyl) Sebacate
EDOT	3,4-Ethylene Dioxythiophene
F127	Polyethylene-polypropylene Glycol
FET	Field-effect Transistors
FPC	Flexible Printed Circuit
GBP	Gain-bandwidth Product
HEX	Hexadecimal
HR	Heart Rate
HRP	Horseradish Peroxidase
IA	Instrument Amplifier
ISE	Ion-selective Electrode
L-lactate	Levogyration Lactate
LSB	Least Significant Bit
MSPS	Million Samples per Second
MWCNT	Multi-walled Carbon Nanotubes
Na-TFPB	Sodium Tetrakis [3,5-Bis (Trifluoromethyl) Phenyl] Borate
NaPSS/PSS	Poly (Sodium 4-Styrenesulfonate)
NFC	Near Field Communication
PB	Prussian Blue
PBS	Phosphate Buffered Saline

PCB	Printed Circuit Board
PEDOT	Poly (3, 4-Ethylenedioxythiophene)
PEDOT:PSS	Poly (3, 4-Ethylenedioxythiophene)-Poly (Sodium p-Styrene Sulfonate) Copolymer
PET	Polyethylene Glycol Terephthalate
PVB	Polyvinyl Butyral
PVC	Polyvinyl Chloride
PVD	Physical Vapor Deposition
RC	Resistor-capacitance
REF	Reference
RMS	Root Mean Square
SpO$_2$	Percutaneous Arterial Oxygen Saturation
SWCNT	Single-walled Carbon Nanotube
TIA	Trans-impedance Amplifier

1 Introduction and Background

1.1 Background and Developing Status of Sweat Analysis

1.1.1 Introduction and Significance

Sweat is a kind of biological fluid that has not been applied and developed in biomedicine. It contains some important physiological information and metabolic information [1]. This information can be collected and analyzed to generate data and indicators that are valuable for relevant health status assessments. There are almost as many health indicators that can be detected in sweat as there are in the blood. However, a blood sample is necessary for blood tests, while sweat tests can be done in vitro, and that makes sweat tests more convenient than blood tests [2-3].

Sweat contains many biological elements, including ions such as sodium, potassium, chlorine, calcium, magnesium, zinc, copper ions, and trace elements; including organic compounds such as glucose, lactate, urea, and other metabolites; as well as protein, nucleic acid, and other macromolecules [4-5]. Through monitoring and analyzing these components in sweat, we can get the information of electrolyte imbalance, sweat glucose level, and dehydration degree of the human body which are important for assessing the vital signs of the human body [6].

Sweat monitoring is the process of analyzing the sweat compositions on the surface of the skin to obtain desired health information, and the accuracy of capturing sweat in its current state is key to the process. There are many ways to obtain sweat, such as natural sweating. Some means can also be used for sweating such as exercise, heating, local chemical induction, iontophoresis, etc. [7-10]. Among them, exercise-based sweating is currently the main means of obtaining sweat due to its advantages of non-invasive, safety, and the quantity and quality of sweat samples [7]. In 2016, G. Liu et al. from the University of California prepared a sweat sensor with a sweat collector structure by using 3D printed plastic molds and sweat gland hydraulic pumping [11]. In the same year, Ahyeon Koh et al. from the University of Illinois used microfluidic to guide sweat into the measurement and analysis area [12]. As shown in Figure 1.1 [11-12].
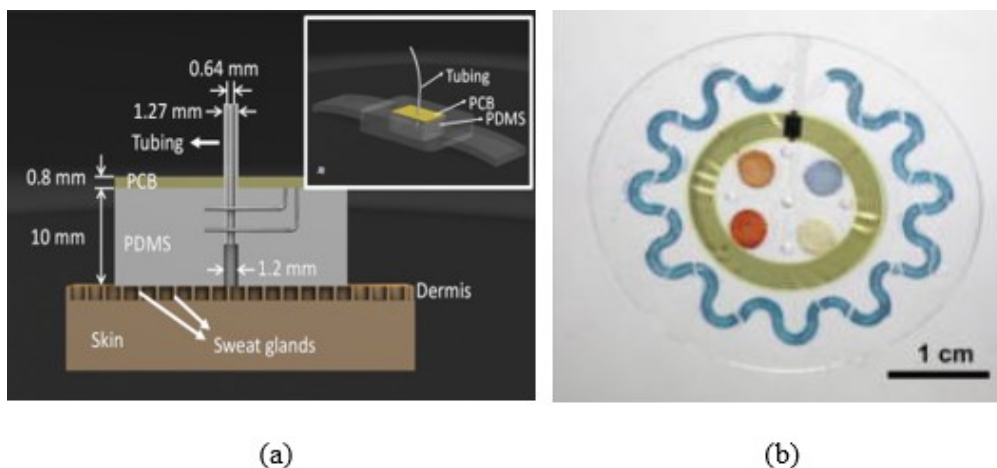
Figure 1.1 Sensor with sweat collecting function. (a) Sweat sensor with sweat gland hydraulic pumping [11] (b) Sweat sensor with microfluidic technologies [12]

The human skin typically has hundreds of sweat glands per square centimeter, and their density varies from area to area [13]. This means that in vitro, sweat is currently the most readily available biological fluid in the field of chemical sensing [14-15]. Therefore, it is of great significance to analyze and monitor sweat.

1.1.2 Methods for Sweat Analysis

Due to the low concentration of substances in sweat and the high demand for real-time performance, sweat analysis requires a short response time, high sensitivity, and high selectivity [16]. Generally, the analysis of sweat components can be divided into two categories according to the response mechanism of substances and different operation methods: electrochemical method and optical method respectively, as shown in Figure 1.2 [1]. In addition to the two methods mentioned above, Field-effect Transistors (FETs) are also gradually being used in the sensing field based on the similarity between the structure of a transistor and an electrochemical system.

The FET has been developed and widely used as transducers thanks to the development of transistors fabrication technology in recent years [17]. FET is commonly accepted for molecular detection and mobile diagnostics due to its miniaturization [18-19].
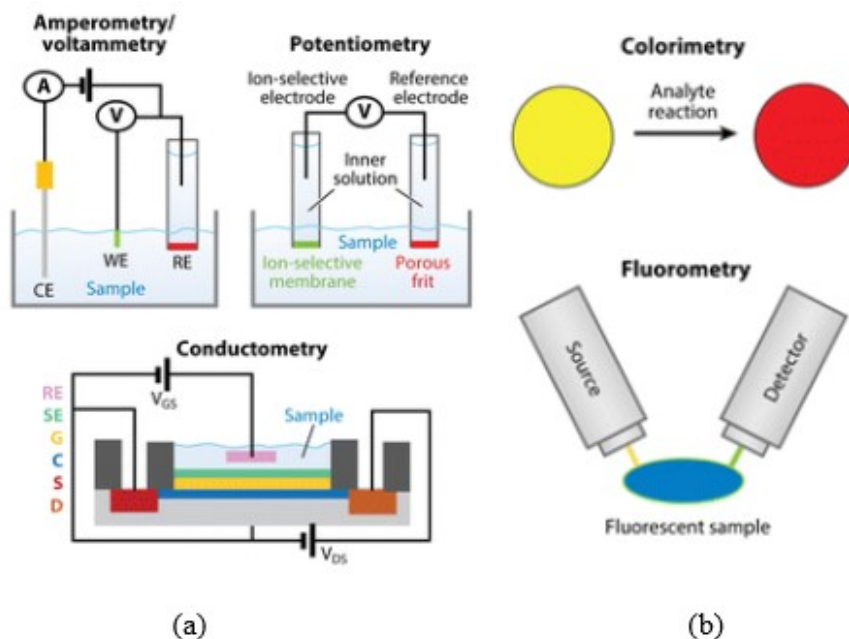
Figure 1.2 Method of sensing. (a) Electrochemical method of sensing [1] (b) Optical method of sensing [1]

1.1.3 Current Status and Challenges

Previously, sweat was detected in vitro by absorbent pads or microtubules attached to the skin to collect sweat samples, and the samples were then evaluated physically and chemically by laboratory instruments [20]. With the development of flexible electronic devices and technologies, sweat detection is becoming portable and wearable. At present, many wearable systems have been developed [11-12, 21-23]. These wearable systems can monitor sweat in real-time while minimizing the impact on people's movements. The system may have the characteristics of good adhesion and flexible location selection based on the material selection and the structural design, which make wearable systems have a very broad application prospect [24]. Among many wearable sensors, electrochemical detection is the most commonly used, and the typical structure is a hybrid system consisting of electrodes and circuits integrated on a flexible substrate [7, 11, 25-27]. Figure 1.3 illustrates several representative wearable sweat sensor systems [25-29].

Figure 1.3(a) presents an integrated wearable device in the form of a wristband for sweat measurement and sweat glucose content detection in patients with cystic fibrosis [25]. The paper shows the specific structure of the sensor: it adopts the method of iontophoresis and can be programmed to induce sweating with different stimulus signals. Meanwhile, the platform can measure the target substances in sweat in real-time. The electrode pattern is located on a

PET substrate and is in direct contact with the skin via hydrogel and stainless-steel contacts. Flexible PCB boards and electrodes are integrated for iontophoresis, signal acquisition, and processing, as well as control and wireless communication. The system allows continuous and non-invasive detection and controls the rate of sweat production.

Figure 1.3(b) shows a skin patch device for sweat capture, collection, and electrolyte analysis [28]. The device does not have a circuit structure. Instead, it adopts physical and chemical structures, such as a pinch valve, an effervescent pump, etc. to achieve microfluidic functions. The device also automatically releases substances like capsaicin and menthol when the amount of sweat exceeds a preset value, alerting the user to the situation of dehydration.

Figure 1.3(c) shows a wearable wristband microelectrode array, of which the main function is to simultaneously monitor the concentration of heavy metal ions in human sweat. The sensor is measured by square wave anodic stripping voltammetry using gold or bismuth electrodes on a PET substrate [26]. The electrode array is connected with external equipment through FPC, and thus realizes the detection of heavy metals in sweat under the state of exercise, which is an important reference value for personal health and physiological status.

The sensor array in Figure 1.3(d) mainly focuses on the measurement of lactate, glucose, sodium, and potassium ions in sweat [27]. The signal processing and analysis circuit, as well as control and communication module, are added based on the previous research, so as to achieve a high degree of integration.

Figure 1.3(e) sense and detect the lactate and potassium ions in sweat through the structure of glasses [29]. Electrodes are on the nose pads of the glasses, subtly making contact with the skin. The support circuit part is fixed on the leg of the glasses to realize the signal processing function while ensuring comfort. Compared with other electrode arrays and sensors, there is no need to attach additional electrodes or sensors to the body, which provides great convenience.

The sensor array introduced above is based on the premise of wearability, because this method can perform sweat detection better and realize real-time performance to the maximum extent. However, there are still many problems and challenges in wearable sensing devices [6].
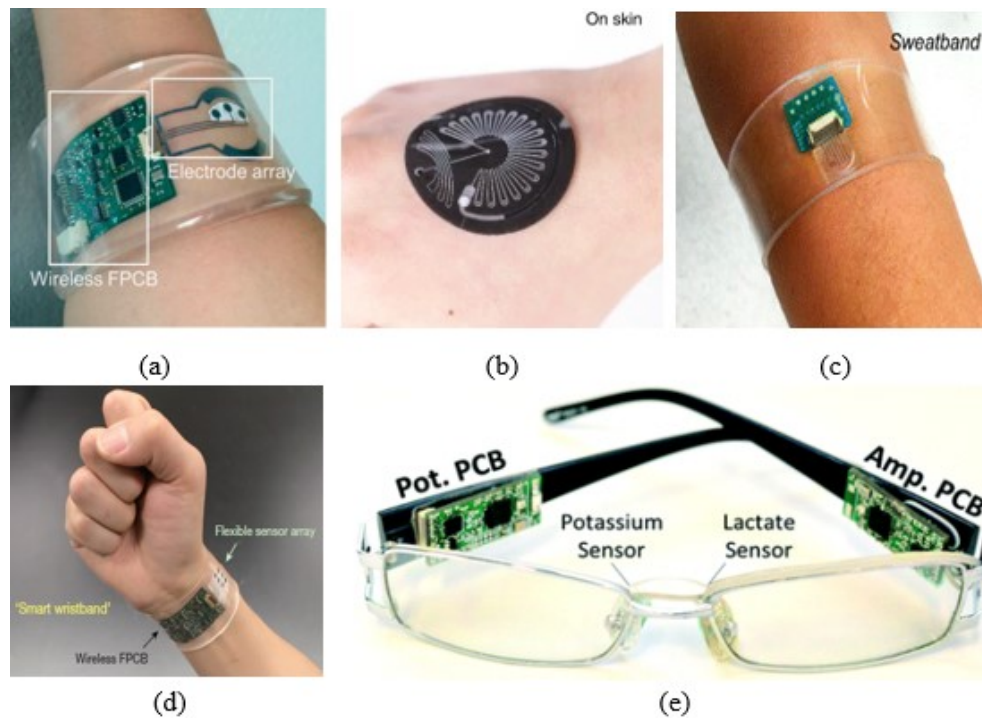
Figure 1.3 Some of the typical sweat sensing systems that have been developed recently. (a) An integrated wearable device in the form of a wristband for glucose detection of patients with cystic fibrosis [25] (b) A skin patch device for sweat capture, collection, and electrolyte analysis [28] (c) A wearable wristband microelectrode array for heavy metals measuring [26] (d) A wearable wristband microelectrode array for sodium, potassium, glucose and lactate measuring [27] (e) Eyeglasses based lactate and potassium sensing platform [29]

First is the sweat contamination. Since sweat is less productive and the skin surface is not completely clean, the effect of contaminants from the skin surface on sweat is significant [30]. In addition, newly generated sweat samples can also be contaminated with previous sweat due to the mixing of sweat samples on the skin surface over time, resulting in changes in components concentration.

Secondly, the concentration of substances in sweat doesn't indicate changes of concentration in the body fluids [31]. Sweat is just the liquid produced by sweat glands, and its composition is different from body fluids such as blood.

Thirdly, for the electrodes themselves, there are also many problems to be solved. For example, sports will cause a lot of wear on the sensor parts of wearable devices; sweat will corrode the equipment to a certain extent; power consumption and size of wearable devices also need to be considered.

Therefore, there still has much room for improvement of the current sweat analysis system.

1.2   Method of Immobilization of Enzyme

At present, glucose and lactate sensors generally use the corresponding oxidase to carry out specific recognition, so as to measure accordingly [1, 3, 4, 8, 25, 27, 29]. Therefore, the immobilization of enzymes on the surface of the electrode array is a very important step.

The method of enzyme immobilization is to fix the free enzyme on the carrier, which makes the enzyme cannot move freely. The characteristics of an immobilized enzyme are determined by the immobilized carrier and immobilized method. The immobilized enzyme can effectively improve the stability of the enzyme catalytic process and maintain stable enzyme activity. The fixation methods mainly include physical adsorption, embedding, covalent bonding, crosslinking, and heat treatment [32].

Adsorption method is through the electrostatic action, Van der Waals Force, and other ways to combine enzyme with the carrier, so as to achieve enzyme immobilization. This method is very simple to operate and the immobilization process is easy and efficient which makes it a very common method. But its disadvantage is that the combination is not stable enough and the enzyme is easy to detach.

The embedding method refers to the method of immobilizing enzymes in the carrier network structure. This method has little effect on enzyme structure and a high recovery rate of immobilized enzyme activity [33]. However, this method has a diffusion limitation, which has a certain influence on the catalytic reaction.

Covalent binding refers to the method of forming covalent bonds between enzyme molecules and carriers [34]. This method is very robust, stable, and reusable. The disadvantage is that the conditions for forming covalent bonds are more stringent.

Crosslinking method is to use reagents to connect the active groups of enzyme molecules to the carrier to form covalent bonds [35]. This method has a good fixation effect, but it has complicated operations and tedious steps.

Heat treatment is the process by which enzymes are fixed to a specific carrier or cell by heating. This method is not commonly used because it requires enzymes to be temperature insensitive.

As for the selection of carriers, inorganic oxides and carbon-based materials with good absorbability can be selected, as well as biopolymers and synthetic polymers to achieve a better fixation effect [36]. In this thesis, chitosan, single-walled carbon nanotubes, and Nafion are

combined used to fix the enzyme. The enzyme is fixed on the single-walled carbon nanotubes and further crosslinked with chitosan, which not only improves the fixation effect but also further improves the electron transfer rate [37]. By dropping Nafion onto the layer for overall embedding, enzyme shedding can be further prevented.

1.3 Research Content and Innovation Points

In this thesis, a sweat composition analysis system based on a flexible electrode array is explored. Thereinto, the electrochemical sensing mode of the electrode array is mainly studied, the feasibility of the method is verified, and the corresponding circuit has been designed. At the same time, the electrochemical sensing of enzyme electrodes based on viologen is preliminarily studied.

I. Combining the sensing principles of different substances, an electrode array on flexible substrates is prepared and insulated by means of photolithography and parylene evaporation.

II. The electrochemical performance of the electrode is tested to verify the relationship between the concentration of the substance and the electrical signal response, which is used as the basis for the design of the subsequent circuit.

III. The signal acquisition circuit is designed and the whole system-level verification is carried out. After successful verification, the system is applied to measure human sweat in a real motion state.

IV. The electrochemical response of enzyme electrodes based on viologen is preliminarily studied and compared with previous electrodes.

The innovation points of this thesis are as follows:

● The electrode array system can dynamically reflect the relationship between sweat composition and key human indicators under exercise combined with blood oxygen physiology, heart rate and body temperature, which provides a new method for precise medical treatment and personalized exercise detection.

● The output signals of the electrode array are collected simultaneously through self-designed collection circuits, and the signal is switched and selected as output through a

selector controlled by the wireless terminal, thereby reducing the amount of wireless transmission data, simplifying the circuit, and reducing data crosstalk.

● A sweat measurement method based on in vitro conditions called the "Clip Plate Method" is adopted. This method can realize real-time performance, repeatability and reduce the interference of external conditions such as temperature and friction, which lays a good foundation for the subsequent realization of wearable and in vitro measurement.

● A self-assembled enzyme electrode fabrication method based on viologen compounds is used, and its electrochemical response is studied. Compared with simple physical adsorption, the viologen electrode has similar stability and linearity, but greatly simplifies the preparation process, which is more conducive to the later application and development of electrode arrays.

1.4   Structure of Thesis

Chapter 1 is the introduction, which summarizes the background and methods of sweat analysis and the current status of sweat analysis research, and lists the shortcomings of sweat analysis.

Chapter 2 introduces the basic sensing principle and the fabrication process of flexible electrode substrate. The preparation of sodium and potassium ISEs, glucose, and lactate oxidase electrodes is also described.

Chapter 3 introduces the electrochemical responses of sodium and potassium ion electrodes, glucose and lactate oxidase electrodes, and the standard curves are drawn and analyzed.

Chapter 4 introduces the electronic circuit design of the signal acquisition module and carries out system-level verification and human sweat measurement under the condition of real motion.

Chapter 5 introduces the preliminary exploration of enzyme electrodes based on viologen, including electrochemical response measurement and standard curve drawing and analysis.

Chapter 6 summarizes the research content of this thesis and expounds on the prospect of future work.

2 Fabrication of Flexible Electrode Array for Sweat Composition Analysis System

The previous chapter introduces the current development status of wearable sweat sensors, as well as the existing problems and challenges. In this chapter, four typical components of sweat are used as measurements to introduce the design and fabrication of an electrode array.

The main content of this chapter is mainly divided into the following aspects: the basic sensing principle of sweat composition of the flexible electrode array, the introduction of experimental reagents and equipment, evaporation and insulation of flexible electrode array substrate pattern, preparation of sodium, potassium ISE electrode and glucose, lactate oxidase electrode.

2.1 Basic Principles of Sweat Sensing

The water in sweat accounts for the vast majority of more than 99%, and the rest mainly includes sodium chloride, potassium chloride, lactate, a small amount of glucose, magnesium, calcium, urea nitrogen, and other ions and organic compounds. By selecting four representative substances in sweat such as Na^+, K^+, lactate, and glucose which are to be analyzed, it can not only reflect the movement and health status of the testee to a certain extent at the molecular level but also avoid the invasion of the human body and reduce the risk of injury. Whether it's sodium and potassium ion or lactate and glucose, the response is based on electrochemical sensing technology.

2.1.1 Electrochemical Sensing Technology

Electrochemical sensing technology refers to the technology of sensing detection and analysis utilizing electrochemical reaction mechanism and analysis method, which converts the concentration, activity, and other property of a targeted object into potential, current, electric quantity, and other electrical quantities.

Electrochemical sensors can be divided into different types according to different output signals and different detection substances. According to the output signal, the electrochemical sensor can be divided into the potential sensor, current sensor, conductivity sensor, etc. According to the detection substances, electrochemical sensors can be divided into ion sensors, gas sensors, biosensors, and so on. Regardless of the classification method, the structure of electrochemical sensors is similar. To receive, recognize and transform the parameters of the substance to be

measured, the electrode is a necessary structure. A basic electrochemical two-electrode structure shown in Figure 2.1(a) consists of a working electrode (or sensing electrode), a counter electrode, and an electrolyte. Another typical electrochemical structure consists of a three-electrode system shown in Figure 2.1(b) added with a reference electrode that only has a single reversible reaction and forms a stable reference potential with the electrolyte.

(a)   (b)
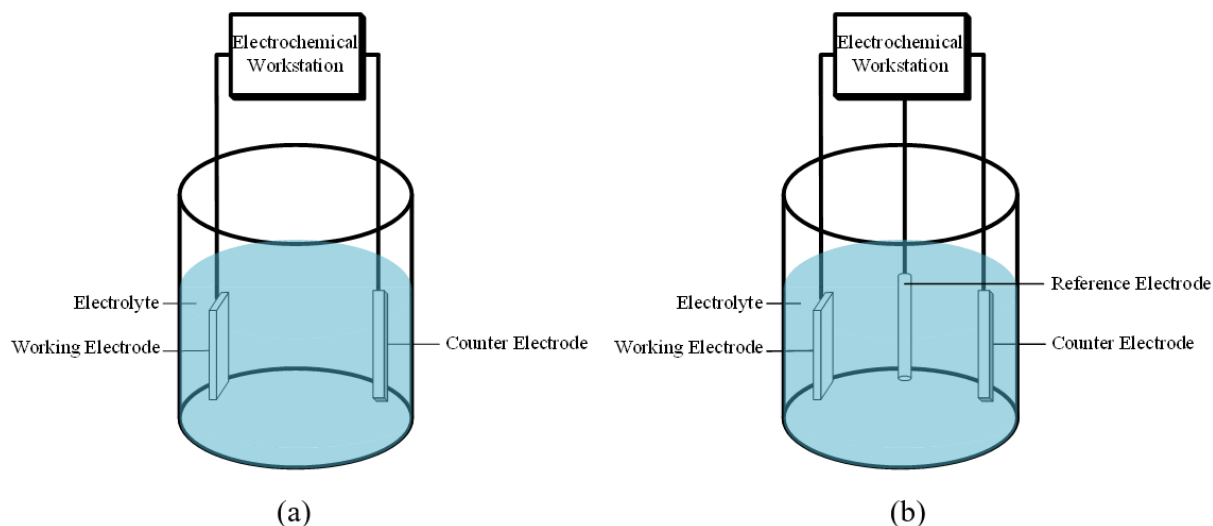
Figure 2.1 Electrochemical sensing structure. (a) Two-electrode system; (b)Three-electrode system

The electrode materials usually choose chemically stable precious metals, such as platinum and gold, which have good electrical conductivity and do not affect the response of the electrolyte under test. Because the electrochemical reaction occurs on the contact surface of the electrode and electrolyte, the surface performance of the electrode has a great influence on the sensing effect [38]. By modifying the surface of the working electrode or adding surfactants, the electrode may achieve optical sensitivity, specific selectivity, etc., resulting in high sensitivity and response values [39].

According to different responses, electrochemical sensors should adopt different analysis methods, the followings are several commonly used chemical analysis methods [40]:

I. Potentiometric Analysis. This method can be considered when the concentration or activity of the analyte can be converted into a potential signal. Under normal circumstances, the electrode potential should be measured in an open state to reduce the impact of current on the potential. The determination of substance content by this method is usually calculated by using the Nernst equation, so it is usually suitable for ion concentration measurement.

II. Chronoamperometry. This method can be used when the concentration and activity of a substance can be converted into regular changes in electric current (electrons). Whether a reference electrode is needed depends on whether an initial potential is applied externally. In general, the relationship between the current response and concentration can be determined from the order of the chemical reaction.

III. Voltammetry. This method is very commonly used for quantitative and qualitative analysis by measuring the variation of voltage-current parameters in the process of electrolysis. According to the voltage scanning mode and different operations, voltammetry can be subdivided into a variety of different methods: such as pulse voltammetry, cyclic voltammetry, etc.

In addition, electrochemical analysis methods include conductance analysis, AC impedance analysis, and so forth. The main components of sweat and their possible analysis methods are shown in Table 2.1.

Table 2.1 Main components of sweat and their analysis methods

Substance	Analysis method
Na^+	Open circuit potentiometry [41]
K^+	Open circuit potentiometry [41]
Cl^-	Open circuit potentiometry [42]
Ca^{2+}	Open circuit potentiometry [43]
Mg^{2+}	Open circuit potentiometry [42]
H^+ (pH)	Open circuit potentiometry [43]
Glucose	Chronoamperometry [40]
Lactate	Chronoamperometry [40]
Uric acid	Cyclic voltammetry [40]
Cortisol	Chronoamperometry [44]
Ethanol	Chronoamperometry [45]

2.1.2 Ion Sensing Mechanism

Ion sensing usually uses an ion-selective electrode (ISE). It is based on a solid or liquid-sensitive membrane, which can selectively respond to specific ions in the solution. There is no electron transfer on ISE and the potential difference is caused by ion exchange and diffusion on both sides of the sensitive membrane. The electrode potential has a linear relationship with the logarithm of ion activity. The linear relationship can be briefly deduced below:

By definition, for an ideal substance A, with Gibbs Free Energy G_A and content c_A, the chemical potential of A at position x is:

$$u_A(x) = G_A + kTlnc_A(x) \tag{2.1}$$

Where T is temperature and k is Boltzmann constant equal to 1.380649×10^{-23} *J/K.*

If A is an ion substance with n numbers of electric charges, then its electrochemical potential can be described as:

$$u_A'(x) = u_A(x) + ne\psi(x) \tag{2.2}$$

Where e is the elementary charge and ψ is the position function.

If A is assumed to be in a one-dimensional system, then the potential is only a function of position. If the system is in equilibrium, the electrochemical potential of A should be equal at all positions. For any position x_1 and x_2, according to Equation (2.1) and (2.2), we can obtain:

$$G_A + kTlnc_A(x_1) + ne\psi(x_1) = G_A + kTlnc_A(x_2) + ne\psi(x_2) \tag{2.3}$$

After simplification, we can get:

$$\psi(x_1) - \psi(x_2) = -\frac{kT}{ne} ln\frac{c_A(x_2)}{c_A(x_1)} \tag{2.4}$$

Given the gas constants $R=N_A k$ and Faraday constant $F=eN_A$, since the electric potential is only a function of position, Equation (2.4) can be further transformed as:

$$\varphi(x_2) = \varphi(x_1) + \frac{RT}{nF} ln\frac{c_A(x_2)}{c_A(x_1)} \tag{2.5}$$

Where $\varphi(x)$ is the electric potential of substance A at position x.

By Equation (2.5), we can get the linear relationship between potential and logarithm of ion activity. In addition, Equation (2.5) is also one of the forms of the Nernst equation.

ISE can be further classified according to different electrical signal response mechanisms and structures. The detailed classification of ISE [46] is shown in Figure 2.2.
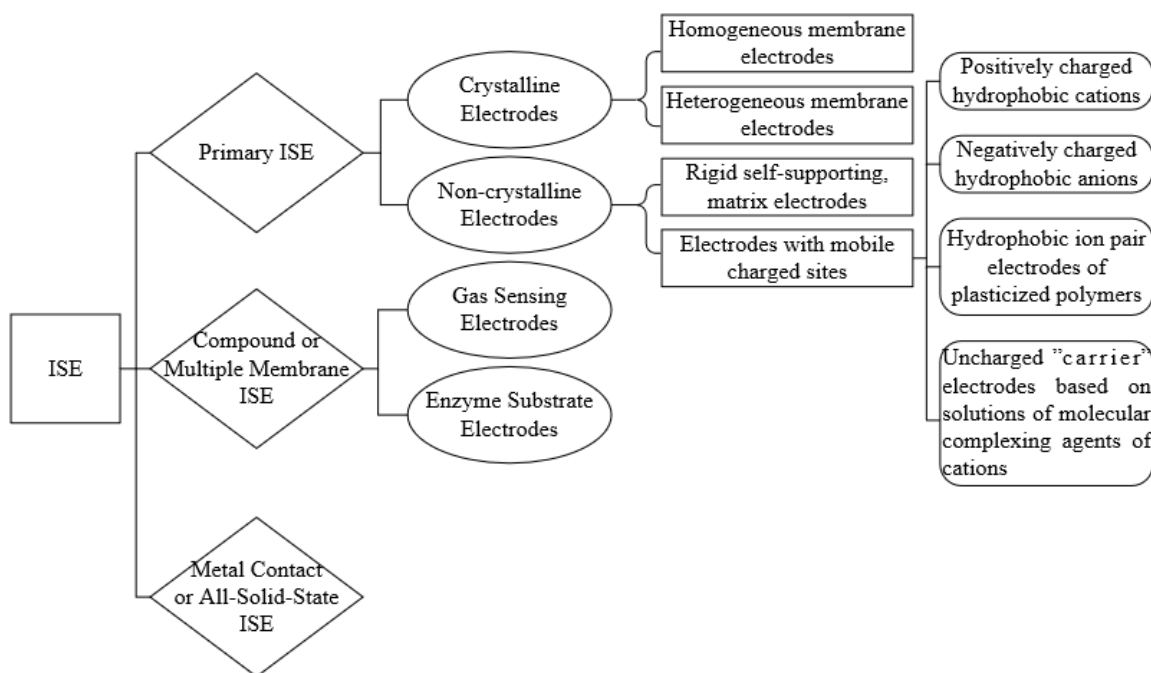
Figure 2.2 Classification of ISE

2.1.3 Enzyme Sensing Mechanism

An enzyme sensor is a device that uses an immobilized enzyme as a molecular recognition element to specifically identify measured substances. It is an instrument that is sensitive to biological substances and converts its concentration or activity into electric signals. Enzyme electrodes can be divided into amperometric enzyme electrodes and potentiometric enzyme electrodes according to the difference of electrical signals. Figure 2.3 is a schematic diagram of the enzyme electrode response mechanism. Among them, the function of intermediary includes promoting the process of electron transfer, broadening the linear range of response, reducing the working potential of the electrode, and so forth.
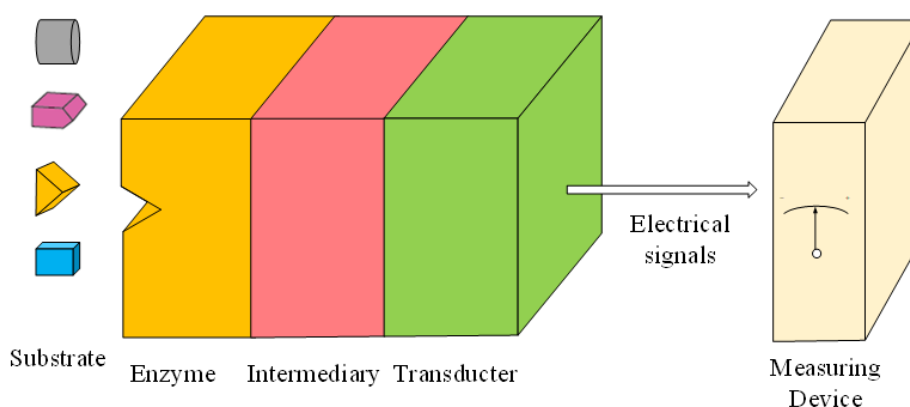
Figure 2.3 Mechanism of enzyme electrode response

Due to the presence of enzymes and intermediates, specific molecules will undergo oxidation or reduction reactions on the electrode surface. The potentiometric enzyme electrode indirectly measures the concentration of the original substance through the change of ions generated by the reaction, so its principle is roughly the same as ISE. Similarly, the amperometric enzyme electrode measures changes in current. The activity or concentration of a biological component can be determined by obtaining the relationship between the electrical signals and the activity or concentration of the measured object.

Oxidase is the most commonly used enzyme to make biosensors. Catalyzed by oxidases, the substrate reacts to form hydrogen peroxide. The sweat sensor in this thesis includes the detection of D-glucose and L-lactate, based on glucose oxidase and lactate oxidase electrodes.

In the presence of glucose oxidase, 1 molecule of glucose is catalyzed to 1 molecule of gluconic acid, producing 1 molecule of hydrogen peroxide. Similarly, in the presence of lactate oxidase, 1 molecule of lactate is catalyzed to 1 molecule of pyruvate, producing 1 molecule of hydrogen peroxide. Equation (2.6) and (2.7) shows their reaction formula:

$$H_2OH(CHOH)_4CHO + H_2O + O_2 \xrightarrow{GOD} CH_2OH(CHOH)_4COOH + H_2O_2 \qquad (2.6)$$

$$CH_3CH(OH)COOH + O_2 \xrightarrow{LOD} CH_3COCOOH + H_2O_2 \qquad (2.7)$$
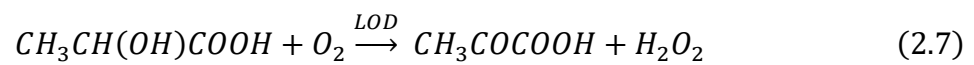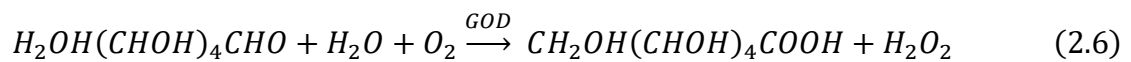
$$V = \frac{V_M[S]}{K_S + [S]} \qquad (2.8)$$

Where S is the concentration of free substrate, V_M is the maximum reaction rate, and K_s is the saturation constant.

In the case of low substrate concentration, S is far less than K_s, so the reaction rate increases linearly with the increase of substrate concentration, resulting in first-order reaction kinetics. On the contrary, when S is much higher than Ks, the reaction rate does not change with the substrate concentration, resulting in zero-order reaction kinetics [47].

Therefore, when substrate concentration and enzyme amount are appropriate, the current response of lactate and glucose oxidase electrode is linear with substrate concentration. Based on this relationship, we can design and develop a sweat enzyme sensor with application value.

2.2 Experimental Base Materials, Reagents, and Equipment

2.2.1 Base Materials and Reagents

Fabrication of electrode substrate: Polyethylene terephthalate (PET) is obtained from Suqian Dongsheng Suye CO., LTD. Gold, silver, and chromium target materials are procured from Beijing Dream Material Technology CO., LTD. Di-p-xylylene (Parylene N) is procured from Maggie Nano Technology (Suzhou) CO., LTD. Photoresist S1818 is obtained from Jiangyin R&J Electronics CO., LTD. Anhydrous ferric chloride, methanol, ethanol, acetone, isopropanol, hydrochloric acid, sodium hydroxide are procured from China National Pharmaceutical Group CO., LTD. (Sinopharm).

Fabrication of ISE: Poly sodium 4-styrenesulfonate (NaPSS), sodium tetrakis [3,5-bis (trifluoromethyl) phenyl] borate (Na-TFPB), sodium ionophore X, polyethylene-polypropylene glycol (F127) are purchased from Shanghai Macklin Biochemical CO., LTD. Valinomycin, polyvinyl butyral (PVB), polyvinyl chloride (PVC), bis (2-ethylhexyl) sebacate (DOS), Multi-walled carbon nanotubes (MWCNT), 3,4-ethylene dioxythiophene (EDOT) are purchased from Shanghai Aladdin Biochemical Technology CO., LTD. Tetrahydrofuran, sodium chloride, potassium chloride, magnesium chloride, calcium chloride are procured from China National Pharmaceutical Group CO., LTD. (Sinopharm).

Fabrication of enzyme electrode: lactate oxidase is purchased in batches from Sigma-Aldrich and Shanghai Guchen Biological CO., LTD. Nafion perfluorinated resin solution (5 wt.% in a mixture of aliphatic alcohols and 45% water) is obtained from Sigma-Aldrich. Single-walled carbon nanotube (SWCNT), glucose oxidase, L-lactate, D-glucose are purchased from Shanghai Aladdin Biochemical Technology CO., LTD. Sodium dihydrogen phosphate, disodium phosphate, chitosan, acetic acid, potassium chloride, anhydrous ferric chloride, hydrochloric acid, potassium ferricyanide are procured from China National Pharmaceutical Group CO., LTD. (Sinopharm).

Pure water is provided by the school laboratory. Without special instructions, all reagents used in the experiment are analytical reagents.

2.2.2 Equipment

The instruments used in the experiment are shown in Table 2.2.

Table 2.2 Experimental instruments

Instrument	Type	Company
Magnetic Stirrers	LC-DMS-H	Shanghai Lichen-BX Instrument Technology CO., LTD.
Digital Thermostat Water Bath	HH-1	Shanghai Lichen-BX Instrument Technology CO., LTD.
Custom Vacuum Spin Coater	AC300-S-CTM	Jiangyin Jiatu Technology CO., LTD.
Ultra Violet Lithography Machine	URE-2000/25	Institute of Optics and Electronics, Chinese Academy of Sciences
Parylene Vacuum Coating Machine	MQP-3001	Maggie Nano Technology (Suzhou) CO., LTD.
Vacuum Resistance Evaporation Coating Machine	ZHD-300M2	Beijing Technol Sincine CO., LTD.
Electrochemical Workstation	CHI660E	Shanghai Chinstruments CO., LTD.
High-Speed Tabletop Centrifuge	TGL-16C	Shanghai Anting Scientific Instrument Factory
Environmental Protection Constant Temperature Platform	P-20	Shenzhen Jinglianghe Technology CO., LTD.
Analytical Balance	FA1004	Changzhou XINGYUN Electronic Equipment CO., LTD.
Ultrasonic Cleaner	/	Shenzhen Huashen Science Industry CO., LTD.
Pipette	/	DLAB Scientific CO., LTD.
Optical Microscope	VH-Z500R	Keyence (China) CO., LTD.
Digital Multimeters	17B+	Fluke Test Instrumentation (Shanghai) CO., LTD.

2.3 Fabrication of Electrode Arrays Substrate and Pattern

2.3.1 Electrode Arrays Design

According to the function, the whole electrode array can be divided into three parts: reference electrode, ion-selective electrode (ISE), and enzyme electrode. The reference electrode is Ag/AgCl electrode. The ISE includes sodium ion working electrode and potassium ion working electrode. The response of the ion-selective electrode is measured by open-circuit potential analysis, and the current is zero, so the counter electrode is not needed. The enzyme electrodes include a lactate electrode and a glucose oxidase electrode. The reference electrode is used as the counter electrode because the enzyme electrode response is measured by chronoamperometry without applied voltage.

To obtain a specific electrode pattern, a metal mask is required for evaporation. The parameters and physical picture of the mask used in the experiment are shown in Figure 2.4.

The desired pattern can be obtained by attaching the flexible material to the mask surface and performing metal evaporation.
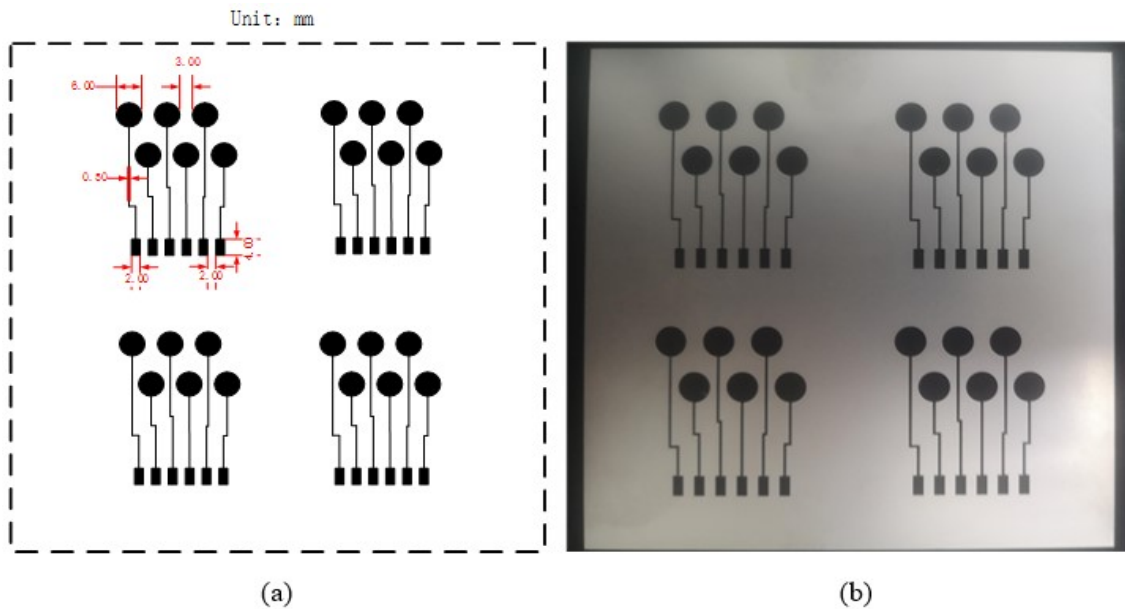
Figure 2.4 Parameter and physical picture of the mask. (a) Schematic diagram of mask plate size (b)Picture of real masks

2.3.2 Preparation of PET Substrate

First of all, cut the PET slice according to the size of the mask plate. During the operation, try not to scratch the surface, so as not to affect the evaporation. The PET substrate is completely immersed in pure water, isopropyl alcohol, and pure water in sequence for ultrasonic cleaning, the cleaning time is 10min, 20min, and 10min respectively. Then the PET substrate is dried on a hot plate at 80 degrees Celsius in a dust-free environment.

After the PET substrate is completely dried, it is fixed on the evaporation mask. When fixing, ensure that PET and mask fit perfectly, and pay attention to the adiabatic tape that does not block the evaporation hole on the plate.

2.3.3 Metal Evaporation

Metal evaporation is also known as physical vapor deposition (PVD). It works by using joule heat generated by a high current and resistance in a high vacuum to evaporate the raw material into metallic vapor, which is then deposited on the substrate. In the process of evaporation, the

evaporation rate of the source material and the thickness of the metal electrode can be controlled by adjusting the current. In addition to metals, it can also deposit small molecular organic materials [48]. Figure 2.5 is the picture of the vacuum resistance evaporation coating machine.

Specific electrode evaporation steps are as follows:

(1). Turn on the power supply and compressor of the cooling machine, and then turn on the power supply, the nitrogen inlet valve, and the vent valve of the vacuum coating machine in sequence, so that the air pressure in the evaporation room is balanced with the outside air pressure.

(2). Open the evaporation room, fix the mask on the coating platform, put chromium target material on evaporation source 1, put crucible and gold target material on evaporation source 2, and then close the evaporation room.

(3). Turn off the vent valve, turn on the mechanical pump and the front valve of the coating machine, wait until the pressure shown by the resistance vacuum gauge is less than 5 Pa, and then switch on the molecular pump. Wait until the pressure indicated by the ionization vacuum gauge is less than $5*10^{-4}$ Pa.

Figure 2.5 Vacuum resistance evaporation coating machine

(4). Set the type of coating metal and the required coating thickness, open evaporation source 1, and adjust the current at about 23 A. The specific current is adjusted according to the evaporation speed (0.1-1 Å/s) shown by the film thickness monitor, 30 nm of chromium metal layer is plated.

(5). Reduce the current of evaporation source 1 to 0, close evaporation source 1, and operate evaporation source 2, in the same way, to evaporate gold metal layer, with the current of generally about 102 A.

(6). Similarly close evaporation source 2 and wait for cooling for 30 minutes before switching off the molecular pump. Turn off the mechanical pump and the front valve, open the nitrogen inlet valve and the vent valve of the coating machine to balance the air pressure in the evaporation room. Open the evaporation room and take out the mask and PET substrate.

(7). Cover the part except for the reference electrode with adiabatic tape, and repeat steps (2), (3), and (4) to evaporate the silver metal layer with the current of generally about 80 A.

2.3.4 Electrode Characterization

Chromium evaporation is done before gold to increase the metal adhesion with the PET substrate. The electrode array pattern and microscopic characterization after evaporation are shown in Figure 2.6, while the resistance characterization of the electrode array measured by digital multimeter is shown in Table 2.3.

Table 2.3 Resistance characterization

Electrode	Length of wire	Resistance	Electrode	Length of wire	Resistance
No.1 Au	29.6 mm	35.6 Ω	No.4 Ag	19.0 mm	20.5 Ω
No.2 Au	28.6 mm	38.4 Ω	No.5 Au	18 mm	30.2 Ω
No.3 Ag	28.4 mm	25.3 Ω	No.6 Au	18.9 mm	29.2 Ω
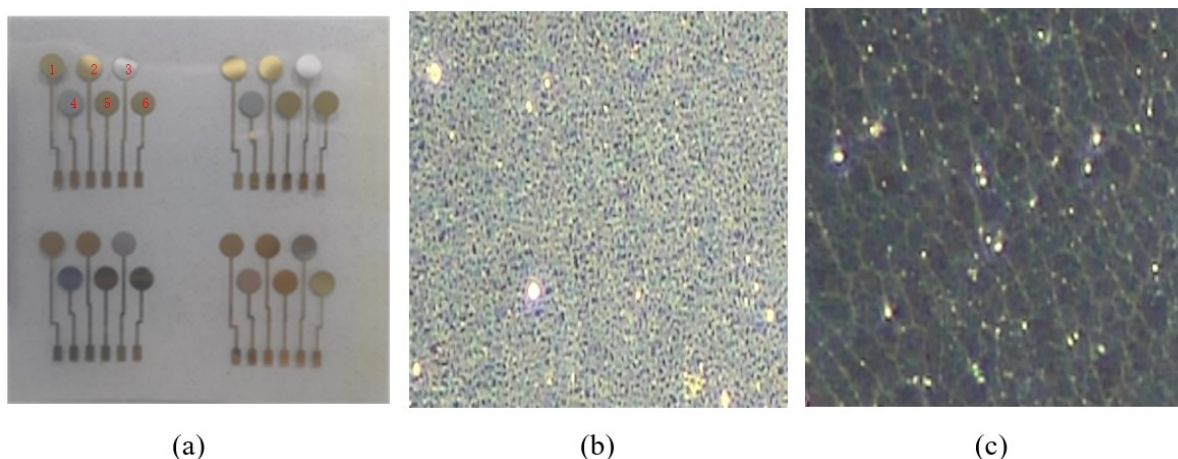
Figure 2.6 Photograph of Electrode array. (a) Electrode arrays pattern (b) Microscopic characterization of gold electrode (c) Microscopic characterization of silver electrode

2.3.5　Insulating and Protective Layer Treatment

The insulating layer is treated by two different methods: photoresist insulation and thermal evaporation of parylene. Both methods have their advantages while ensuring insulation and protection.

The advantages of using a photoresist to prepare an insulating layer are that the overall operation time is short and accurate insulation can be achieved, that is, only the electrode and the interface are photolithographic and exposed. The specific operation steps of photolithographic insulation are as follows:

(1). The PET piece is heated for 60 seconds on a hot plate at 100 ℃, and then fixed on the spinning coater.

(2). Appropriate amount of photoresist S1818 is dropped until the substrate pattern is covered. Set the spinning coater parameters to 500 r/min, 5 s, and 4000 r/min successively, 60 s, and start spinning.

(3) After (2) is finished, heat it for 120 s on the hot plate at 180 ℃.

(4) Prepare 0.5% (wt.%) NaOH developer for use. The PET substrate is fixed in the corresponding position, exposed for ten seconds, placed in the NaOH developer for 45 s, and then immediately transferred to acetone and pure water for 20 seconds successively. After removal, the substrate is placed on a hot table of 100 ℃ and dried.

The photoetching pattern and effect after photoetching is shown in Figure 2.7.

However, the disadvantages of this method are also significant. First of all, because PET substrate size has reached the centimeter level, the photoresist is more difficult to spin evenly; Secondly, a specific photomask is required for photoetching; Thirdly, the photoresist is not friendly to the human body and may contaminate sweat sample. By contrast, parylene is a kind of highly secure medical material. In addition, its uniformity is better by using machine evaporating, only insulation tape covering is needed for the position doesn't need to be insulated. Figure 2.8 shows the parylene vacuum coating machine used in the experiment. The procedure for parylene evaporation insulation is as follows:

(1). Add parylene N powder to a metal pan in furnace 1 and put PET substrate in the evaporation room. Check their sealability and lock it. Do not open the lid during coating.

(2). Turn on the main switch at the back of the machine and press the button to turn on the machine. After observing the yellow light flashing, set the evaporation time and temperature at the control panel: The temperature of furnace 1 controls the evaporation rate, which is generally 80-120 degrees Celsius; the temperature of furnace 2 controls the cracking process, the 680 degrees Celsius is set for parylene N powder.

(3). Turn on the film thickness monitor, and set the parameters; After all settings are complete, click automatic coating on the control panel and wait for the machine to complete.

(4). When the coating is finished, the machine will give out a warning sound. Take out the PET substrate and wait for the machine to cool off.

(a)   (b)
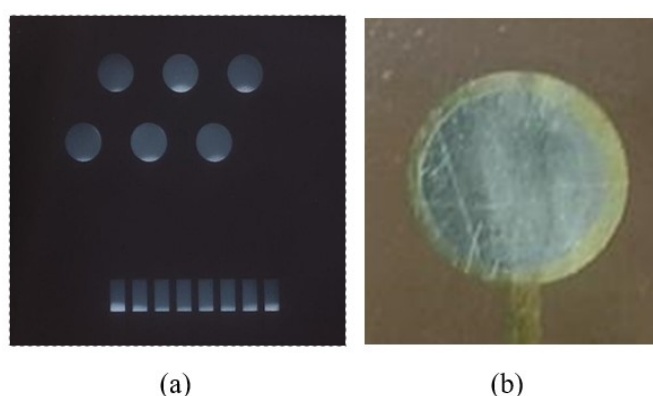
Figure 2.7 Photograph of photoetching mask and electrode (a) Photoetching pattern (b) Ag electrode after photolithography
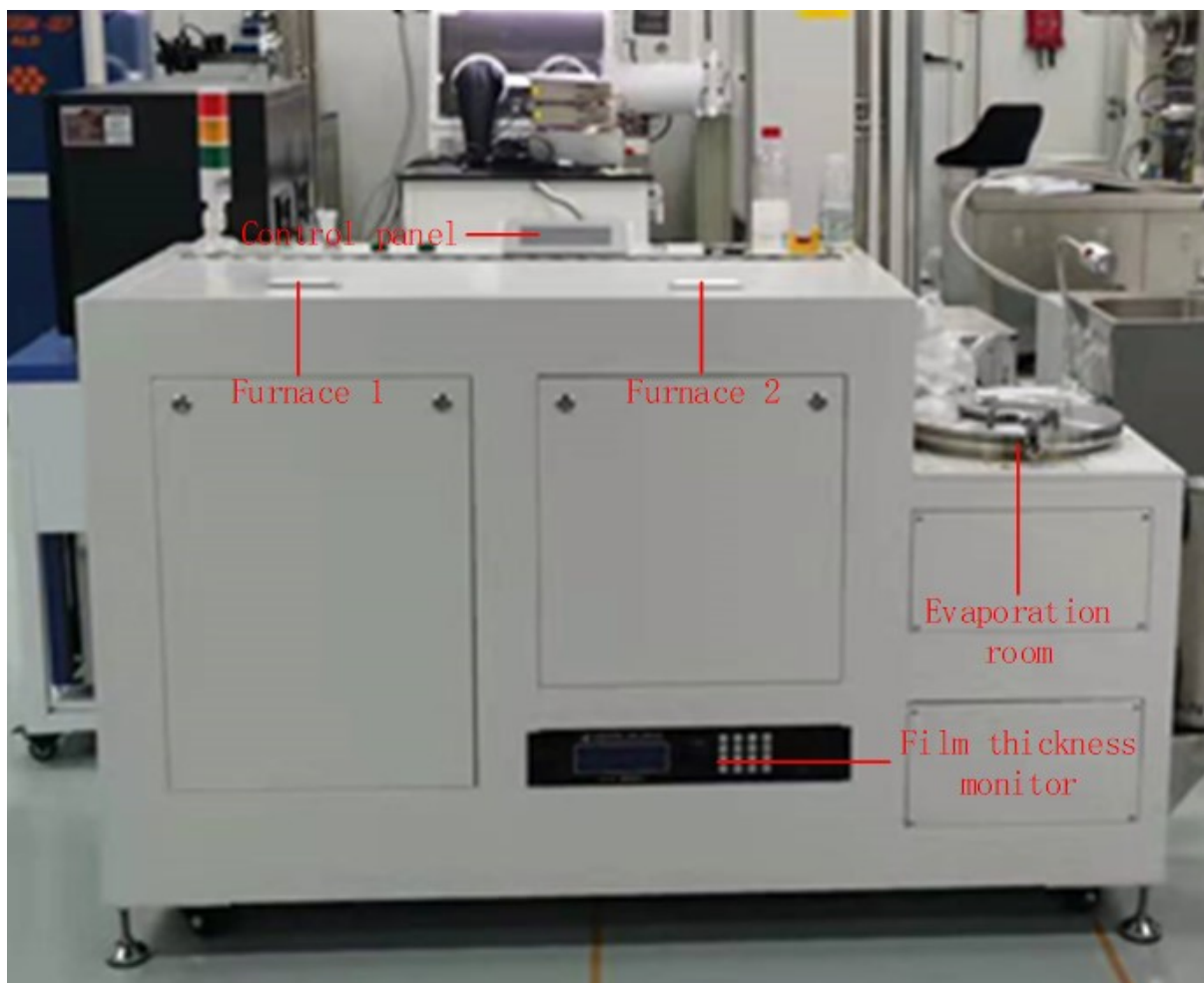
Figure 2.8 Parylene vacuum coating machine

2.3.6 Activation of Gold Electrodes

During the use of the gold electrode, it is easy to passivate, which leads to the decrease of sensitivity and fluctuation of reading, and will affect the overall stability of the electrode. Therefore, cyclic voltammetry curve activation is required before electrodeposition of PEDOT: PSS and Prussian Blue. The oxidation film on the electrode surface can be removed by activation, and the organic and inorganic impurities on the electrode surface can also be removed. The electrodes are usually polarized by dipping them in dilute acid, producing hydrogen atoms that reduce the surface oxides. For good results, the polarization should go through multiple cycles.

In this thesis, dilute sulfuric acid with a concentration of 0.5 mol/L is used to activate the gold electrode. The dissolved oxygen in dilute sulfuric acid is removed by bubbling nitrogen, and the gold electrode, commercial counter electrode, and commercial Ag/AgCl reference electrode are connected to the corresponding clamps of the electrochemical platform. The voltage range

of scanning is -0.2-1.5 V, and the scanning rate is 100 mV/s. After 20 cycles of scanning, the gold electrode can be removed and cleaned for further experiments. Figure 2.9 shows the scanning curve.
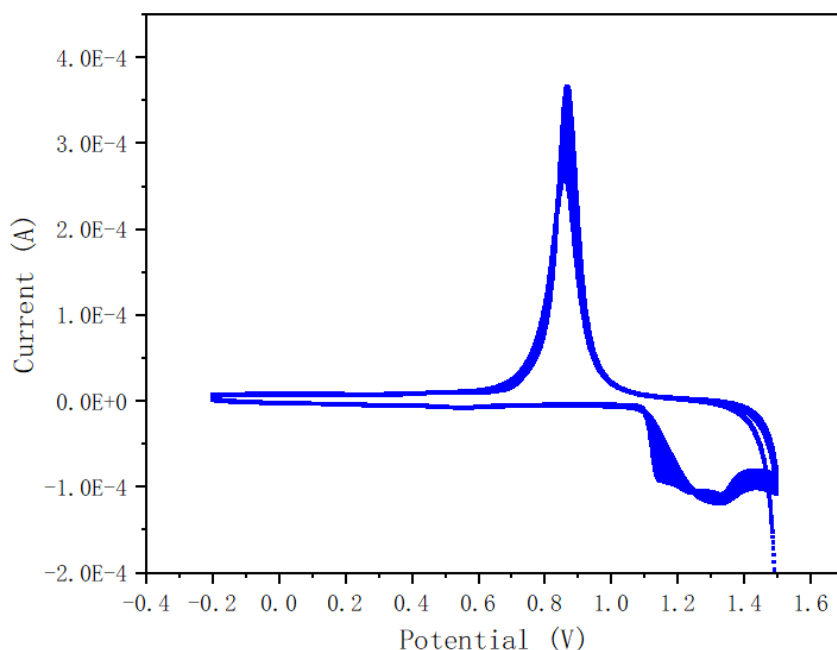
Figure 2.9 Activation CV curve of the gold electrode
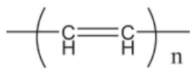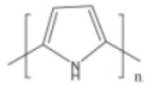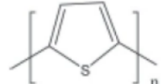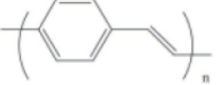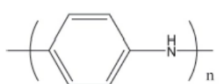
2.4 Fabrication of Ion-selective Electrodes

2.4.1 Introduction to Conductive Polymers

The charge transfer between the electrode and the ion-selective membrane can be promoted by inserting materials with electronic and ion-conductive properties between the electrode and the ion-selective membrane, thus improving the stability. Among many materials, the conductive polymer is commonly used as an intermediate layer of ISE because it perfectly conforms to these properties [49]. Studies have shown that the ISE using a conductive polymer as the intermediate layer has improved response stability, detection, and selectivity coefficient compared with traditional ion electrodes [50]. Common conductive polymers mainly include polyacetylene, polypyrrole, polythiophene, polyphenylene, polyphenylacetylene, polyaniline, etc. Their basic structure and conductivity are shown in Table 2.4 [51].

Table 2.4 Structure and conductivity of common conductive polymers [51]

Conductive polymers	Structure	Electrical conductivity

polyacetylene		$1.7*10^4$ S/cm
polypyrrole		$7.5*10^2$ S/cm
polythiophene		$1.0*10^2$ S/cm
polyphenylene		$1.0*10^2$ S/cm
polyphenylacetylene		$5.0*10^2$ S/cm
polyaniline		$2.0*10^1$ S/cm

Among many materials, poly (3, 4-ethylenedioxythiophene) -poly (sodium p-styrene sulfonate) copolymer (PEDOT: PSS) has a good performance in reducing the potential drift of ISE. In this thesis, PEDOT: PSS is used as the intermediate layer of sodium and potassium ion-selective electrodes.

2.4.2 Electrochemical Deposition of PEDOT: PSS

PEDOT: PSS is one of the polythiophene polymers and its structure is shown in Figure 2.10. Its common synthesis methods include electrochemical deposition, chemical oxidation synthesis, and so on. Chemical oxidation synthesis catalyzes the polymerization of EDOT by oxidant and then purified it by a series of methods to obtain PEDOT: PSS. Electrochemical Deposition catalyzes the polymerization of EDOT by applying an electric field, and the electroplating speed and thickness can be adjusted by changing the potential value and deposition time. This thesis adopts the electrochemical deposition method.

In the electrodeposition process, first of all, EDOT is oxidized and loses electrons to become PEDOT. PEDOT is neutral, non-conductive, and insoluble in water. Neutral PEDOT is further oxidized and loses electrons to form oxidized PEDOT with a positive charge, while PSS itself has a negative charge. Since the negative ion of PSS is fixed on the polymer chain, so does the positive ion of PEDOT, which forms a poly complex like a zipper.
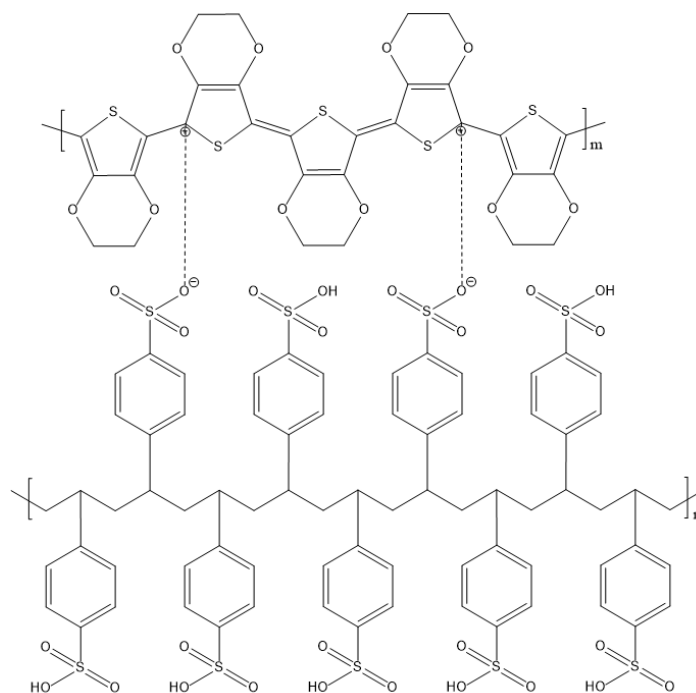
Figure 2.10 Structure of PEDOT: PSS

In addition, it should be noted that EDOT polymerization is caused by the reaction of cationic free radicals formed by the loss of an electron at No. 2 and 5 carbon atoms. In terms of reaction mechanism, electron loss belongs to oxidation reaction, so electrodeposition at the anode is required.

An electrochemical platform is used for the electrodeposition process. Before electrodeposition, the gold electrode is ultrasonically cleaned with deionized water, methanol, and deionized water for 30 seconds respectively, and the surface is blown dry with nitrogen after the cleaning. A certain amount of PSS and EDOT is weighed and configured into a mixed solution, in which the concentration of PSS is 0.1 mol/L and the concentration of EDOT is 0.01 mol/L. An external Ag/AgCl electrode and a platinum counter electrode are used for electrodeposition. A recommended method is to use chronopotentiometry (CP) and the current density is set to 0.2 mA/cm^2. According to the deposition time, the amount of charge on the electrode is different, so as to obtain different PEDOT: PSS film thickness. The PSS$^-$ anion is more conducive to the polymerization of EDOT molecules, which reduces the polymerization potential of EDOT to about 0.85 V [52].

During the deposition process, it can be seen that the electrode surface is gradually covered by PEDOT: PSS and the color of the surface become darker, as shown in Figure 2.11(a). The CP curve of the electrodeposition process is shown in Figure 2.11 (b). After electrodeposition, the

change of electrode surface can be observed obviously. PEDOT: PSS on gold electrode appears dark blue under strong white light, as shown in Figure 2.12.

(a)   (b)
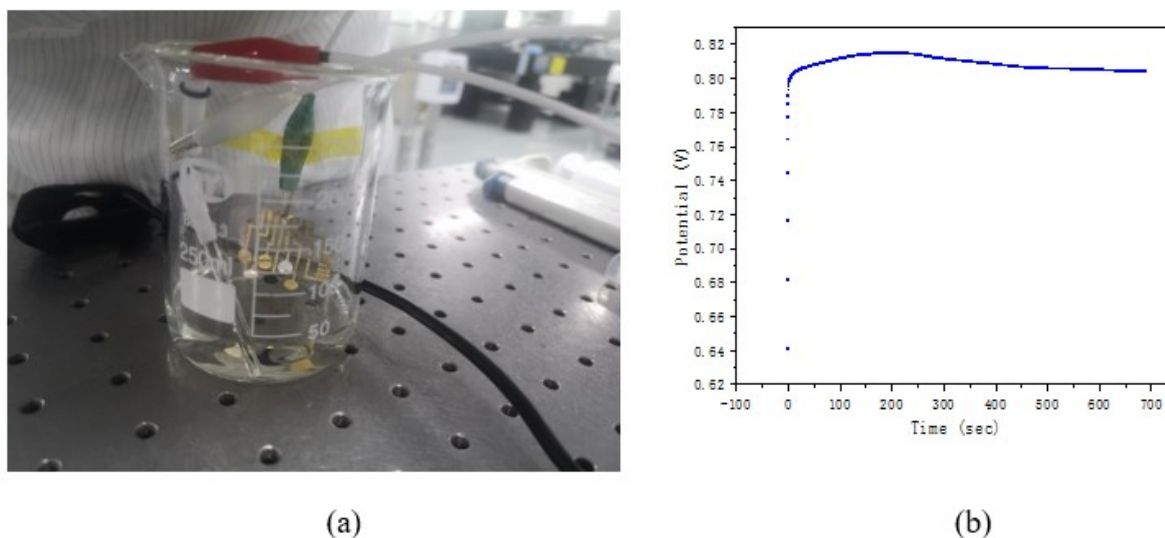
Figure 2.11 Electrodeposition of PEDOT: PSS (a) Deposition process (b) CP curve of deposition process
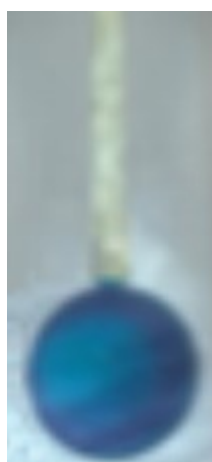
Figure 2.12 Dark blue color of PEDOT: PSS

2.4.3 Preparation of Potassium ISE

In general, ion selectivity of ISE is achieved through specific ion-selective membranes. The ISE used in this thesis is a kind of non-crystalline electrode structure, which covers the ion-selective membrane on the conductive polymer intermediate layer of ISE. Generally speaking, the main components of ion-selective membranes based on non-crystalline electrodes include ion-selective carriers (1%, w/w), lipophilic macromolecules (0.6%, w/w), non-conductive polymers (33%, w/w), and plasticizers (65.6%, w/w) while tetrahydrofuran is usually used as an organic solvent [53]. Among them, lipophilic macromolecules are used to improve the

detection limit of ISE electrodes, non-conductive polymers and plasticizers are used to support and improve the surface structure of electrodes [54].

Preparation of potassium ion ISE membrane solution is as follows:

3 mg valinomycin, 0.9 mg Na-TFPB, 49 mg PVC, and 97 mg DOS are dissolved in 780 µL tetrahydrofuran and ultrasound treatment is applied for 30 min. During this period, part of the solid powder may adhere to the wall of the tube without being dissolved due to its high viscosity. The ultrasonic can be continued after gently stirring with a stirring bar. The potassium ion-selective membrane solution is obtained after mixing uniformly and stored at 4 ℃ for future use.

Apply 4 µL K^+ ion-selective membrane solution with pipette gun to the PET gold electrode after depositing PEDOT: PSS, wait for a natural drying and preserve at 4 ℃.

2.4.4 Preparation of Sodium ISE

The composition and ratio of sodium ion-selective membrane solution are very similar compared with potassium. Preparation of sodium ion ISE membrane solution is as follows:

1.5 mg sodium ionophore X, 0.9 mg Na-TFPB, 49.5 mg PVC, and 98.1 mg DOS are dissolved in 660 µL tetrahydrofuran, and Na^+ selective membrane solution is prepared by ultrasound for 30 minutes. Due to the high viscosity, part of solid powder may stick to the wall of the tube without being dissolved, so ultrasound can be continued after gently stirring with a stirring bar. The sodium ion-selective membrane solution is obtained after mixing uniformly and stored at 4 ℃ for future use.

Apply 10 µL Na^+ ion-selective membrane solution with pipette gun to the PET gold electrode after depositing PEDOT: PSS, wait for natural drying and preservation at 4 ℃.

2.4.5 Preparation of Reference Electrode

Ag/AgCl is usually used as a reference electrode because it has good potential stability, is environmentally friendly, and is easy to make. By dropping a certain concentration of ferric chloride solution to the surface of the silver electrode, the electrode surface can be made to react as Equation (2.9):

$$FeCl_3 + Ag \rightarrow AgCl \downarrow + FeCl_2 \qquad (2.9)$$
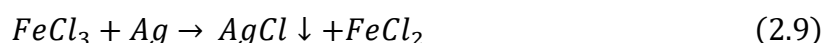
Among them, the standard electrode potential of Fe^{3+} reduced to Fe^{2+} is 0.77 V, and the standard electrode potential of Ag^+ reduced to elemental silver is 0.7996 V. Therefore, the elemental silver will be oxidized by Fe^{3+} into Ag^+, which in turn combines with Cl^- to generate AgCl.

The silver-deposited electrode is dripped with 10 µL $FeCl_3$ solution of 0.1 mol/L with a pipetting gun, and the reference electrode is washed with pure water after the full covering reaction for 1 minute. The Ag/AgCl reference electrode can be obtained after nitrogen drying.

Ulteriorly, because the concentration of Cl^- in the liquid to be tested affects the reaction balance on the reference electrode, the potential stability of the reference electrode will be affected. Therefore, the reference electrode needs to be modified. By using F127 and multi-walled carbon nanotubes, the potential stability of the reference electrode can be greatly improved [55]. In addition, PVB membrane containing electrolytes can form porous nanostructures which also play a role in potential stabilization [53]. Preparation of reference electrode modification solution is as follows:

0.2 mg MWCNT,50 mg NaCl,79.2 mg PVB, and 2 mg F127 are dissolved in 1000 µL methanol, and the solution is prepared by ultrasound for 30 minutes. Stored at 4 ℃ for future use.

Apply 10 µL of reference electrode modification solution with pipette gun to the PET Ag/AgCl electrode, wait for natural drying and preservation at 4 ℃.

2.5 Fabrication of Enzyme Electrodes

2.5.1 Introduction to Prussian Blue

The hydrogen peroxide molecule produced after the decomposition of organic matter catalyzed by oxidase is a kind of thermodynamically unstable but dynamically stable substance. For the semi-reaction of Equation (2.10):

$$O_2 + 2H^+ + 2e^- \rightarrow H_2O_2 \tag{2.10}$$

Its standard electrode potential is about 0.70 V; For the semi-reaction of Equation (2.11):

$$H_2O_2 + 2H^+ + 2e^- \rightarrow 2H_2O \tag{2.11}$$
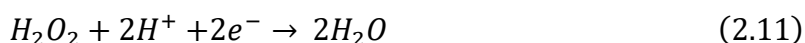
Its standard electrode potential is about 1.78 V. Therefore, from the perspective of thermodynamics, any "substance" with redox potential between 0.7 V and 1.78 V can catalyze the decomposition of hydrogen peroxide. Among these substances, Prussian Blue not only has

a significant electrocatalytic effect but also has good film formation properties. After film formation, hydrogen peroxide molecules can pass through, and then its decomposition is catalyzed by $Fe^{3+/2+}$ in the PB film. The crystal structure of PB is shown in Figure 2.13, there's one potassium ion in every two lattices.
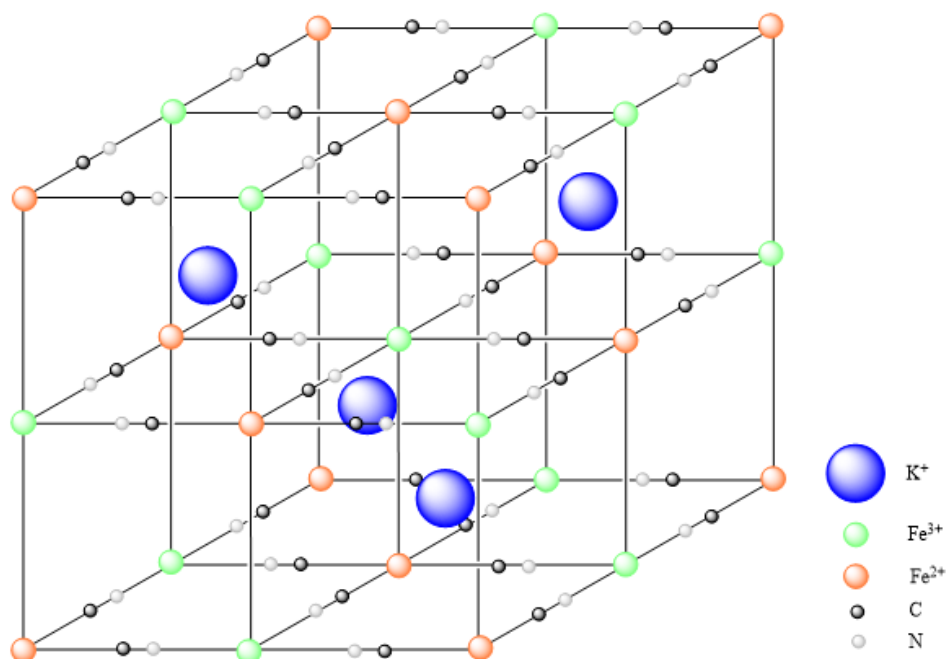
Figure 2.13 Crystal structure of PB

Prussian Blue has a better catalytic performance for hydrogen peroxide at low potential, which can reduce the interference of other easily oxidized substances. Moreover, after deposition and subsequent treatment, it also has relatively high operational stability, as well as high sensitivity and selectivity [56].

Prussian Blue is synthesized by precipitation synthesis, hydrothermal synthesis, and electrodeposition. Among them, the precipitation synthesis method is to generate Prussian Blue precipitation through the reaction of Fe^{3+} and $Fe(CN)_6^{4-}$ or Fe^{2+} and $Fe(CN)_6^{3-}$, and then separation and purification. The hydrothermal synthesis and electrodeposition of Prussian Blue are achieved through the redox reaction of Fe^{3+} and $Fe(CN)_6^{3-}$. Electrochemical synthesis is used in this thesis.

2.5.2 Electrochemical Deposition of PB

By applying a voltage or current to the electrode, the redox reaction of Fe^{3+} and $Fe(CN)_6^{4-}$ in the electrolyte takes place, and PB is complexed on the electrode surface. By optimizing

electrochemical synthesis parameters, such as the pH of electrolyte, the concentration of ions, electrodeposition potential, current, electrodeposition time, cycle times, etc., a relatively stable PB crystal structure can be obtained. The electrolyte used in the experiment is a mixed solution containing 2.5 mmol/L ferric chlorides, 2.5 mmol/L potassium ferricyanide, 0.1 mol/L potassium chloride, and 0.1 mol/L hydrochloric acids. Ferric chloride and potassium ferricyanide are the main reactants. Hydrochloric acid is present to maintain the pH value of the solution below 1, which prevents the Fe^{3+} from hydrolyzing to iron hydroxide and thus protects deposition of PB films. Potassium chloride is added to offer a sufficient amount of K^+ into the electrolyte. The activity of K^+ can affect the redox potential during deposition, and it can also penetrate the PB film to maintain the charge balance [56].

For the lactate electrode and glucose oxidase electrode, due to their different detection sensitivity and range, different PB film thickness is also required. The thinner Prussian Blue layer has a smaller detection range, but its sensitivity is high and is suitable for the detection of glucose concentration in sweat [57]. Conversely, the thicker Prussian Blue layer is suitable for detecting lactate concentration in sweat. The thickness of Prussian Blue is determined by the number of electrodeposition cycles. The electrodeposition process is shown in Figure 2.14.
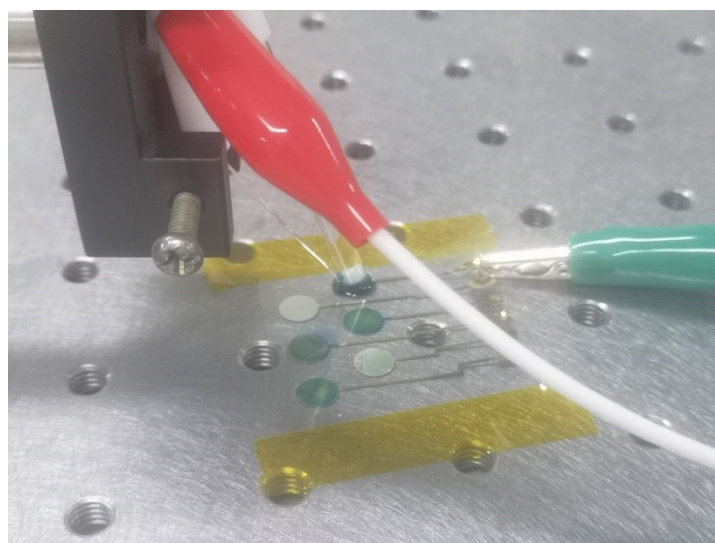
Figure 2.14 Electrodeposition process of Prussian Blue

● The Prussian Blue deposition of the glucose oxidase electrode:

30 μL of newly configured electrolyte is dropped onto the gold electrode, and the gold electrode, commercial counter electrode, and commercial Ag/AgCl reference electrode are connected to the corresponding clamps of the electrochemical platform. Cyclic voltammetry is used to form a pathway by scanning the solution. The voltage range of scanning is 0-0.5 V, and the scanning

rate is 20 mV/s. After one cycle of scanning, the thin Prussian Blue intermediate layer can be deposited on the gold electrode corresponding to the glucose. The scanning curve is shown in Figure 2.15.

As can be seen from Figure 2.15, a pair of redox peaks appear at 0.11 V and 0.156 V, which is the redox process of $Fe^{3+/2+}$.

● The Prussian Blue deposition of the lactate oxidase electrode:

Prussian Blue deposition of lactate electrode is roughly the same as that of glucose oxidase electrode. The difference lies in the specific parameters of cyclic voltammetry. The voltage range of scanning is 0-0.5 V, and the scanning rate is 50 mV/s. After two cycles of scanning, the electrolyte on the surface of the gold electrode is blown evenly with a pipette gun, and then the scanning is continued for another two cycles, a total of seven times, and 14 cycles are scanned. The thick Prussian Blue intermediate layer can be deposited on the gold electrode corresponding to the lactate. The scanning curve is shown in Figure 2.16.
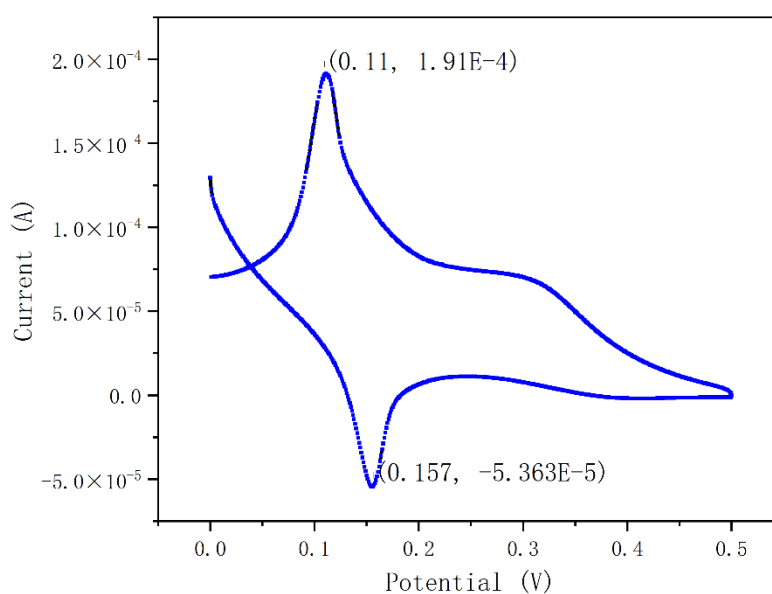
Figure 2.15 Electrodeposition CV curve of PB on glucose oxidase electrode
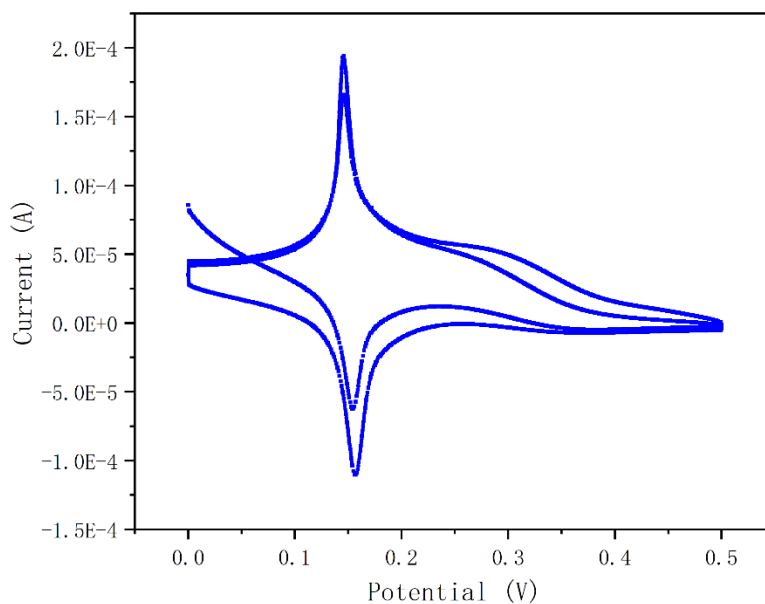
Figure 2.16 2 cycles of electrodeposition CV curve of PB on lactate oxidase electrode

2.5.3 Preparation of Glucose Oxidase Electrode

An enzyme electrode can be obtained by configuring an enzyme electrode membrane solution and dropping it onto a Prussian Blue medium layer. In order to ensure the stability of the electrode, Nafion is usually added after the oxidase membrane is formed to protect the electrode. In this thesis, chitosan and single-walled carbon nanotubes (SWCNT) are used to immobilize enzymes.

● Preparation of the viscous solution including chitosan and SWCNT:

Chitosan is dissolved in 2% acetic acid solution and magnetically stirred for 1 h to obtain 1% chitosan solution, followed by the addition of SWCNT at the ratio of 2 mg/mL. The viscous solution of chitosan and SWCNT can be obtained by ultrasonic stirring for 1h [58].

● Preparation of glucose oxidase membrane solution:

The glucose oxidase is dissolved in the PBS buffer (pH = 7, contains 0.2 mol/L NaH_2PO_4 and 0.2 mol/L Na_2HPO_4 with a volume ratio of 19: 31) at the concentration of 20 mg/mL. And then glucose oxidase membrane solution is completely mixed with the chitosan and SWCNT viscous solution mentioned above at the volume ratio of 2: 1 by ultrasonic stirring for 30 min.

Apply 1.6 µL enzyme electrode membrane solution with pipette gun to the PET gold electrode after depositing PB, drying at 4 °C. Then 2.5 µL 0.5%wt. Nafion is dropped on the electrode to make the glucose oxidase electrode.

2.5.4 Preparation of Lactate Oxidase Electrode

● Preparation of the viscous solution including chitosan and SWCNT:

See 2.5.3 for details.

● Preparation of lactate oxidase membrane solution:

The lactate oxidase is dissolved in the PBS buffer (pH = 7, contains 0.2 mol/L NaH_2PO_4 and 0.2 mol/L Na_2HPO_4 with a volume ratio of 19: 31) at the concentration of 50 mg/mL.

Apply 3 µL chitosan and SWCNT viscous solution, 2 µL lactate oxidase membrane solution, 3 µL chitosan, and SWCNT viscous solution in sequence with pipette gun to the PET gold electrode after depositing PB. Be sure that the electrode is completely dried at 4 °C before applying the next layer. Then 2.5 µL 0.5%wt. Nafion is dropped on the electrode to make the lactate oxidase electrode.

2.5.5 Preparation of Reference Electrode

The silver-deposited electrode is dripped with 10 µL $FeCl_3$ solution of 0.1 mol/L with a pipetting gun, and the reference electrode is washed with pure water after the full covering reaction for 1 minute. The Ag/AgCl reference electrode can be obtained after nitrogen drying.

2.6 Summary of the Chapter

This chapter mainly describes three aspects: the basic sensing principle of ion and enzyme electrodes, the fabrication of electrode array on PET substrate, and the preparation process of enzyme and ion electrodes. The preparation process of enzyme and ion electrodes includes a brief introduction of conductive polymer and Prussian Blue. In addition, this chapter describes the manufacturing process of the whole electrode system.

The main work of this chapter includes:

● The graphic design of evaporation mask by related software, the fabrication of electrode array on PET, and its subsequent processing such as insulation and activation.

- Modification of electrode surface based on different functions, including electrodeposition of PEDOT: PSS and PB interlayer, and preparation of Ag/AgCl electrode.

- Preparation of electrode membrane solution, as well as fabrication of ion electrode, enzyme electrode, and reference electrode. The complete electrode array is shown in Figure 2.17.
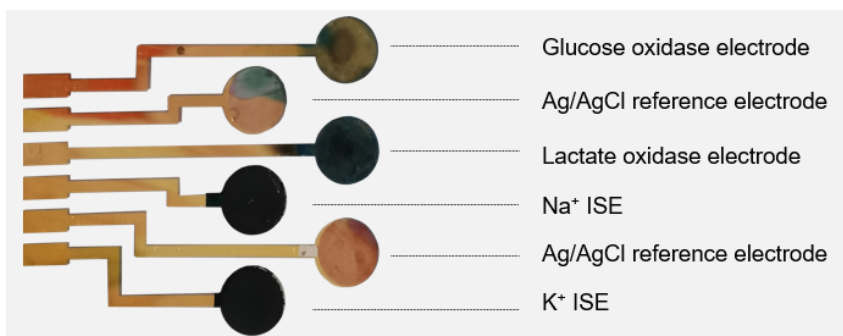
Figure 2.17 Complete electrode array

3 Response Testing and Data Analysis Based on Electrochemical Workstations

The previous chapter describes the principle of electrode array sensing and the fabrication process. In this chapter, the response of four typical sweat compositions is measured by an electrode array fabricated in chapter 2 and analyzed based on the response curves obtained from electrochemical workstations.

The main content of this chapter is mainly divided into the following aspects: ISE response and analysis of sodium and potassium, the effect of temperature on ISE, the selective test of ISE, response, and analysis of lactate and glucose oxidase electrodes.

3.1 ISE Response and Analysis

3.1.1 Test Method and Preparation

In order to achieve continuous measurement of the response without changing the surface state of the electrode, a small amount of the standard solution with a high concentration of the substance is added to a certain amount of solution to achieve the change of the overall concentration of the substance. According to the Nernst equation, the diffusion potential of ions between the two systems at room temperature is theoretically logarithmic to the concentration. In order to obtain a linear relationship that is easy to analyze, a linear change in voltage response is obtained by artificially controlling the concentration of the substance to be measured to increase exponentially during measurement. When the standard solution is added, the overall concentration will change and the response will fluctuate due to the diffusion effect. Therefore, data collecting shall be suspended during this period and shall be carried on after the molecular diffusion is uniform for some time.

The response test of the ISE electrode is realized by measuring the response of substrate solution with known concentration to obtain the linear relationship between concentration and electrical signal response. Since the ISE electrode presents voltage response, the chronopotentiometry method is used. During all subsequent experiments, no additional voltage or current will be applied to the system unless otherwise specified. The electrochemical workstation uses a three-electrode system mode, thus the reference electrode interface on the workstation is directly connected to the counter electrode interface, and then connected to the

Ag/AgCl reference electrode corresponding to ISE on the electrode array. The tests are performed at a constant room temperature (25 °C).

3.1.2 Potassium ISE Response

The concentration of potassium ions in human sweat fluctuates between 1-19 mmol/L according to individual differences [59]. Therefore, the total K^+ concentration of the solution to be tested is selected as 1 mmol/L, 2 mmol/L, 4 mmol/L, 8 mmol/L, 16 mmol/L, 32 mmol/L, and then the voltage response of potassium ISE at these concentrations is measured. The volume of the total solution is 30 mL. When the amount of standard solution added is far less than 30 mL, the volume change of the total solution can be ignored. According to the solubility of potassium chloride, a standard solution of potassium chloride with a concentration of 2 mol/L is prepared. For a total solution concentration change of Δc mmol/L, the ΔV amount of standard solution to be added is:

$$c_{total} + \Delta c = \frac{\Delta V * c_{standard} + V_{total}c_{total}}{V_{total}} \xrightarrow{simplified} \Delta c = \frac{\Delta V * c_{standard}}{V_{total}} \tag{3.1}$$

Where $c_{standard}$ is the standard solution concentration, and V_{total} is the total solution volume. Through the Equation (3.1), standard solution volumes need to be added each time can be calculated as 15 µL, 15 µL, 30 µL, 60 µL, 120 µL, 240 µL.

The response of potassium ISE at various concentrations is shown in Figure 3.1.
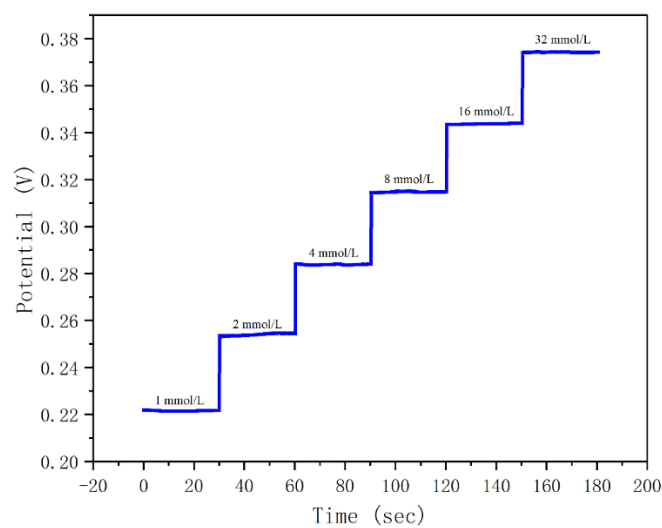
Figure 3.1 Potential-time response of potassium ISE

As can be seen from Figure 3.1, potassium ISE not only has good stability in the range of potassium ion concentration in sweat but also shows a linear increase trend in voltage.

3.1.3 Fitting of Potassium Ion Standard Curve

According to Equation (2.5), the diffusion potential formed by ions between the two systems at room temperature is:

$$\varphi = \varphi_0 + \frac{RT}{nF} lnA = \varphi_0 + \frac{0.0592}{n} lgA = \varphi_0 + \frac{0.0592}{3.322 * n} logA \tag{3.2}$$

Where A is the ratio of concentration and log stands for logarithm base 2. For the convenience of calculation and observation, φ_0 is taken as the potential value when the potassium ion concentration is 1 mmol/L, and A is the ratio between the present concentration and 1 mmol/L. With lgA as the abscissa and voltage data at different concentrations (1 mmol/L, 2 mmol/L, 4 mmol/L, 8 mmol/L, 16 mmol/L, 32 mmol/L) as the ordinate for fitting, the standard curve of potassium ion can be obtained, as shown in Figure. 3.2.
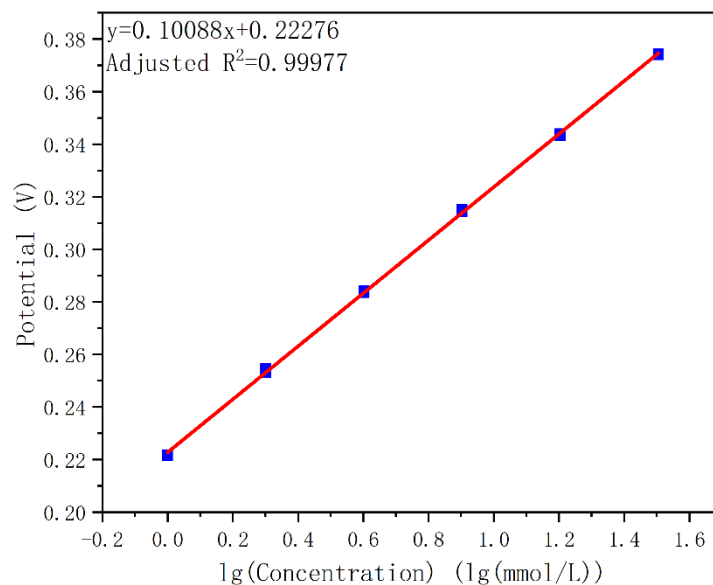
Figure 3.2 Standard curve of potassium ISE

It can be seen from the figure that the potassium ion-selective electrode shows a good linear state. By substituting the linear fitting equation $y = a + b * x$, detailed fitting parameters can be obtained as shown in Table 3.1.

Table 3.1 Fitting parameters of potassium ion concentration standard curve

Intercept		Slope	
Value	Standard error	Value	Standard error
0.22276	3.31274E-5	0.10088	3.63507E-05
Residual sum of squares		Adjusted R^2	
0.00114		0.99977	

According to the table, it can be seen that the sensitivity value of potassium ISE is 100.9 mV/lg[c(K$^+$)]. This value is far from the theoretical value of Nernst equation 59.2 mV, which is due to the introduction of chloride ions that influence the potential balance of the reference electrode. After testing and calculating, the response of the reference electrode to chloride ions is 40.1 mV/lg[c(Cl$^-$)]. After removing the influence of chloride ion, the sensitivity of potassium ion is 60.8 mV/lg[c(K$^+$)]. Discarding the influence of non-human factors, objective conditions, and systematic errors, the sensitivity is very close to the theoretical value, indicating that the design requirements are met.

3.1.4 Potassium ISE Response

Similar to potassium, the concentration of sodium in sweat is usually between 10 and 100 mmol/L, depending on the individual [59]. Therefore, the total Na$^+$ concentration of the solution to be tested is selected as 5 mmol/L, 10 mmol/L, 20 mmol/L, 40 mmol/L, 80 mmol/L, and 160 mmol/L, and then the response of sodium ISE potential at these concentrations is measured. Based on the solubility of sodium chloride in water, the concentration of sodium chloride standard solution is 5 mol/L. Other conditions are the same as when measuring potassium ISE. Standard solution volumes need to be added each time can be calculated as 30 μL,30 μL, 60 μL, 120 μL, 240 μL, 480 μL.

The response of sodium ISE at various concentrations is shown in Figure 3.3.

As can be seen from Figure 3.3, sodium ISE also has good stability in the range of sodium ion concentration in sweat, with a linear increase trend in voltage.
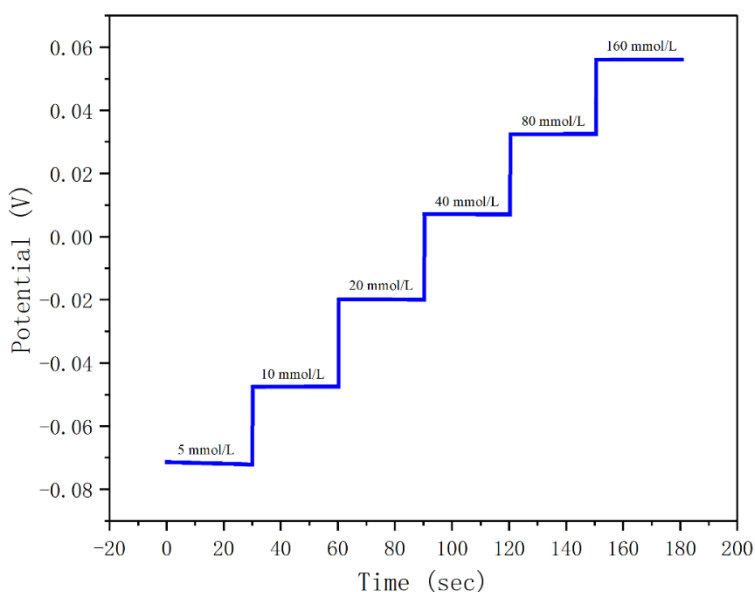
Figure 3.3 Potential-time response of sodium ISE

3.1.5 Fitting of Sodium Ion Standard Curve

For the convenience of calculation and observation, according to Equation (3.2), φ_0 is the potential value corresponding to the sodium ion concentration of 5 mmol/L, and A is the ratio of the present concentration to 5 mmol/L. Taking lgA as abscissa and potential data of different sodium ion concentrations (5 mmol/L, 10 mmol/L, 20 mmol/L, 40 mmol/L, 80 mmol/L, and 160 mmol/L) as coordinates, the standard curve of potassium ion is obtained, as shown in Figure 3.4.

As can be seen from the figure, sodium ISE also presents a good linear dependence. Substituting linear fitting equation $y = a + b * x$, the detailed fitting parameters are shown in Table 3.2.

Table 3.2 Fitting parameters of sodium ion concentration standard curve

Intercept		Slope	
Value	Standard error	Value	Standard error
-0.07198	4.4942E-5	0.08599	4.93152E-05
Residual sum of squares		Adjusted R^2	
0.00209		0.99941	
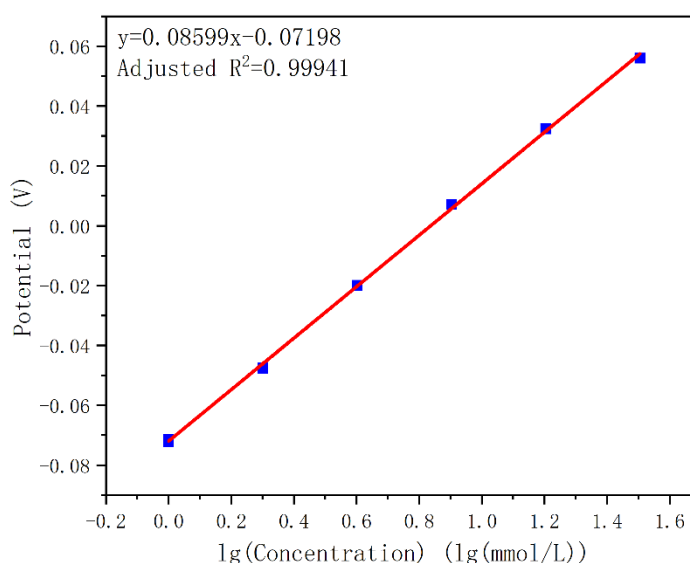
Figure 3.4 Standard curve of sodium ISE

As can be seen from the table, the ISE sensitivity of sodium is 86.0 mV/lg[c(Na$^+$)]. Because sodium and potassium ISE share a reference electrode, the sensitivity of sodium ion is 45.9 mV/lg[c(Na$^+$)] after removing the influence of chloride ion. The sensitivity is close to the theoretical value and meets the design requirements after eliminating the influence of non-human factors, objective conditions, and systematic errors.

3.2 Influence of temperature on ISE

The temperature has a certain influence on the response of the ion-selective electrode. According to the Nernst equation, the electric potential increases gradually as the temperature increases. As the characteristics of the temperature of ISE do not distinguish ions in theory, potassium ISE is taken as an example for measurement. The specific measurement method is to drop the standard potassium chloride solution into the water to make the solution become a certain concentration (4 mmol/L is used in this thesis) and then observe the concentration change through the method of water bath heating. In order to avoid the influence of other factors, a commercial Ag/AgCl reference electrode is used.

The potential response is measured for 100 seconds at room temperature of 25 °C (0-100 s) and water bath heated to 30 °C (100-200 s), 35 °C (200-300 s) and 37 °C (300-400 s). The response is shown in Figure 3.5.
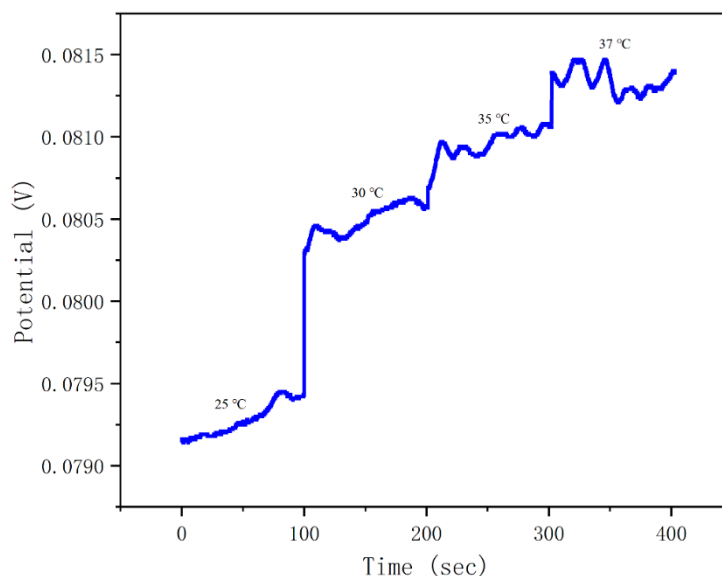
Figure 3.5 ISE response under different temperature

The response of ISE fluctuates due to a series of objective factors such as intermittent heating of water bath equipment. But on the whole, it can be seen that the potential response of ISE increases with the temperature, which is consistent with the theoretical expectation.

3.3 Selective Test of ISE

The selective test is one of the most important indexes to evaluate ion-selective electrodes. Unlike enzymes, which have high specificity and high catalytic efficiency for their substrates, ISE reflects the change of ion concentration through potential. Therefore, it is necessary to explore its anti-interference ability under different ion conditions.

In addition to sodium and potassium ions, there are a small amount of calcium and magnesium ions in human sweat. Calcium ion's concentration in human sweat is usually 0.3-4 mmol/L, while magnesium ions are usually 0.03-0.5 mmol/L [59]. The selective test is measured in the same way as the sodium and potassium ion response. Referring to the ion concentration in human sweat, the standard solution concentration of calcium chloride and magnesium chloride is 1 mol/L and 0.1 mol/L, respectively. If 30 μL standard solution is dropped into 30 mL total solution system, the concentration changes of Ca^{2+} and Mg^{2+} are 1mmol/L and 0.1mmol/L, respectively.

3.3.1 Potassium ISE Selective Test

A certain amount of magnesium, calcium, and sodium ion standard solutions are added to a certain concentration of potassium chloride solution in turn, and the response changes are observed. In order to control the variables, the dripping amount of interference solution, electrode test method, electrode system, and CP curve parameters are the same as those of the sodium ion test.

The potassium ISE is scanned in 2 mmol/L KCl solution until the response is stable, and then a certain amount of ion standard solution is dropped at regular intervals. The CP curve obtained is shown in Figure 3.6.
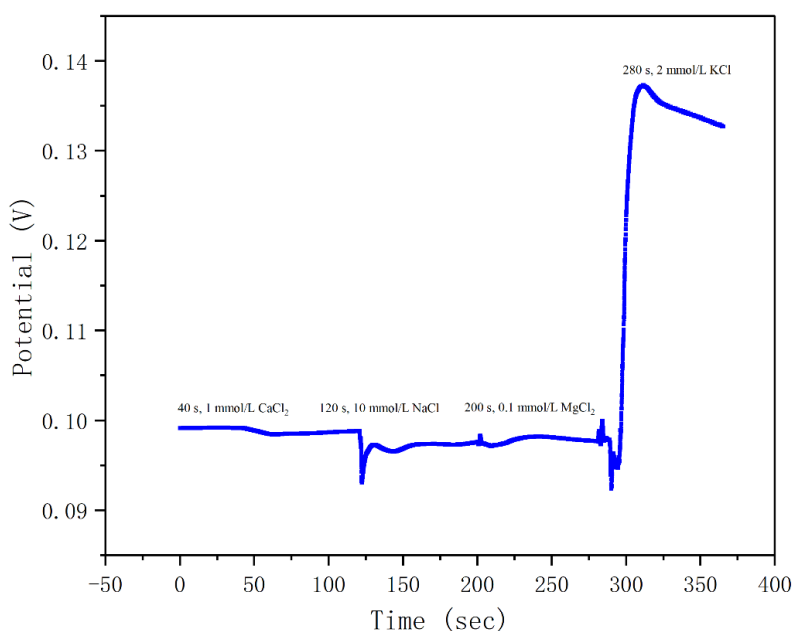
Figure 3.6 CP curve of K$^+$ ISE selective test

In Figure 3.6, standard solutions of different ions are dropped at 40 s, 120 s, 200 s, and 280 s respectively. With the introduction of various ions, the influence of the components of other ions on the potential response is much less than that of potassium ions, indicating that the curve can better reflect the selectivity of potassium ions.

3.3.2 Sodium ISE Selective Test

Same as the Potassium ISE selective test, a certain amount of standard solution of magnesium, calcium, and sodium ions are successively added to a certain concentration of sodium chloride

solution to observe its response changes. The sodium ISE is scanned in 10 mmol/L NaCl solution until the response is stable, and then a certain amount of ion standard solution is dropped at regular intervals. The CP curve obtained is shown in Figure 3.7.
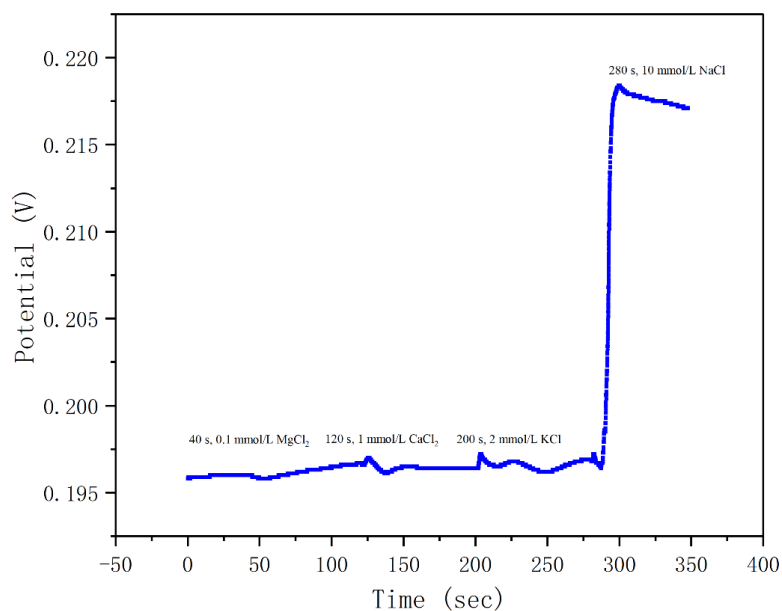
Figure 3.7 CP curve of Na$^+$ ISE selective test

In Figure 3.7, standard solutions of different ions are dropped at 40 s, 120 s, 200 s, and 280 s respectively. The influence of other ions on the potential response is much less than that of sodium ions, which means that the curve can better reflect the selectivity of sodium ions.

3.4 Response and Analysis of Enzyme Electrodes

3.4.1 Test Method and Preparation

According to the analysis in 2.1.3, the substrate of the enzyme electrode has a linear relationship with its response. Similar to the ISE response measurement, in order to achieve continuous measurement of the response without changing the surface state of the electrode, a small amount of high concentration of the substance standard solution is added to a certain solution to achieve the change of the total concentration of the substance. Due to the diffusion effect, the response will fluctuate in a certain period in the beginning, and data collection shall be carried out after the molecular diffusion is uniform.

Because of the current response characteristic of the enzyme electrode, chronoamperometry is adopted. Similarly, no additional voltage or current is applied to the system unless otherwise stated. The mode, connection method, and test environment of the electrochemical workstation are the same as those of ISE. Note that the counter electrode clamp should be connected to the corresponding Ag/AgCl electrode.

Unlike ions, the response of the enzyme electrode is measured in phosphate-buffered saline (PBS) instead of pure water in both the total and standard solution. Generally, active biological agents are diluted with it because of its salt-balanced and pH-adjustable properties. Pure water may destroy the structure and biological properties of biological proteins. To simplify the configuration process of PBS, sodium dihydrogen phosphate and disodium hydrogen phosphate are used to configure sodium phosphate buffer with pH = 7.0. The solution protects the enzyme structure while providing appropriate pH and ion concentration.

3.4.2 Glucose Oxidase Electrode Response

The glucose concentration in human sweat is generally about 0.3 mmol/L, and the concentration will decrease accordingly when exercising [60]. Therefore, the total glucose concentration of the solution to be tested is selected as 0.1-0.6 mmol/L with a 0.1 mmol/L interval. Then measure the current response of the glucose enzyme at these concentrations. The volume of the total solution is 30 mL, and the concentration of 0.1 mol/L glucose standard solution is prepared.

The electrode is placed in a PBS buffer solution for scanning until the current is relatively stable. Then 30 µL standard glucose solution is successively added to PBS solution and waited for diffusion. Measure the relatively stable response curve for 10 seconds, shown in Figure 3.8.

As can be seen from Figure 3.8, due to the decrease of the substrate, uneven diffusion, decreased activity of the enzyme, and other objective problems, the current response has drifted to some extent, but the glucose oxidase electrode still has good stability in the range of glucose concentration in sweat, while there is a relatively linear increase trend in current.
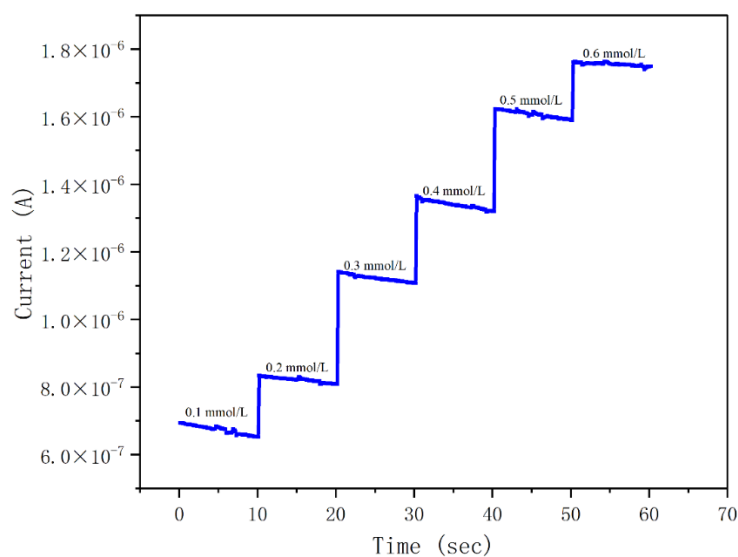
Figure 3.8 Current-time response of glucose oxidase electrode

3.4.3 Fitting of Glucose Standard Curve

Taking concentration of glucose as abscissa and current response of different glucose concentrations (0.1-0.6 mmol/L, with a 0.1 mmol/L interval) as coordinates, the standard curve of glucose is obtained, as shown in Figure 3.9.
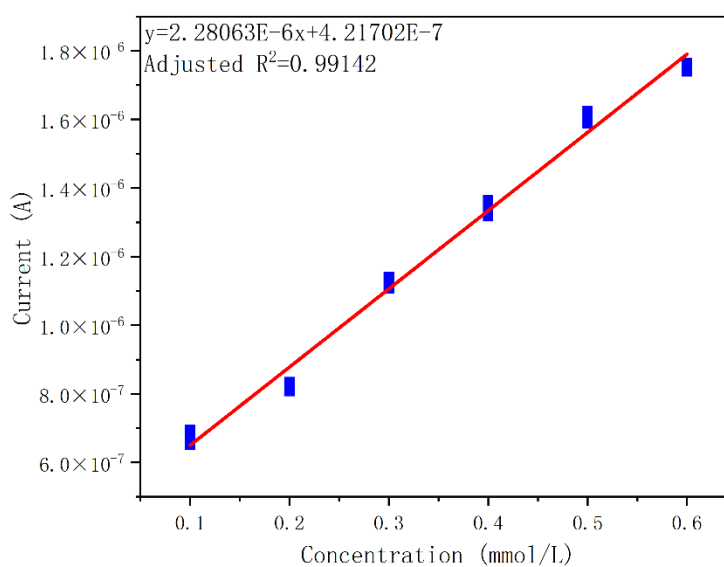
Figure 3.9 Standard curve of glucose oxidase electrode

As can be seen from the figure, the glucose oxidase electrode response presents a linear dependence. Substituting linear fitting equation $y = a + b * x$, the detailed fitting parameters are shown in Table 3.3.

Table 3.3 Fitting parameters of glucose concentration standard curve

Intercept		Slope	
Value	Standard error	Value	Standard error
4.21702E-7	3.36567E-9	2.28063E-6	8.65245E-09
Residual sum of squares		Adjusted R^2	
7.90215E-13		0.99142	

From the table, the sensitivity of the glucose oxidase electrode is 2.28 µA·L/mmol. The parameter meets the design requirements after eliminating the influence of non-human factors, objective conditions, and systematic errors.

3.4.4 Lactate Oxidase Electrode Response

The concentration of lactate in human sweat is generally about 7 mmol/L, and it will change according to the state of exercise [60]. Lactate is the product of anaerobic respiration in the body's cells. Therefore, when people do anaerobic exercise, the lactate content in sweat will increase, and very few people sweat lactate concentration can reach 15-20 mmol/L. Therefore, the total lactate concentration of the solution to be tested is selected as 6-14 mmol/L with a 2 mmol/L interval. The current response of the lactate oxidase electrode at these concentrations is then measured. The total volume of solution is 30 mL, and the concentration of lactate standard solution is 2 mol/L.

The electrode is scanned in PBS buffer solution until the current is relatively stable. Then 30 µL standard lactate solution is successively added to PBS solution and waited for diffusion. The relatively stable response curve within 10 seconds is measured, as shown in Figure 3.10.

As can be seen from Figure 3.10, compared with glucose electrode, the drift of current response of lactate electrode is increased, which is caused by different substrate concentration and reaction rates on the electrode surface. In addition to the objective reasons, the lactate oxidase electrode still has good stability in the range of lactate concentration in sweat, and the current has a relatively linear trend of increase.
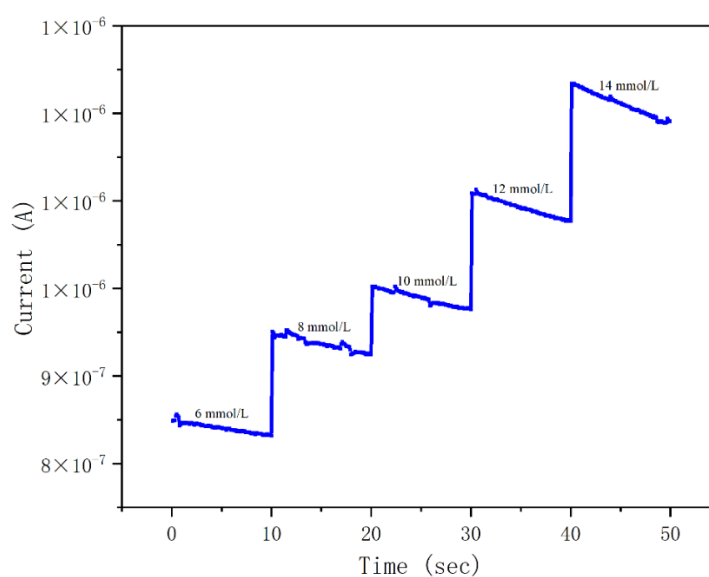
Figure 3.10 Current-time response of lactate oxidase electrode

3.4.5 Fitting of Lactate Standard Curve

Taking lactate concentration as abscissa and current response of different lactate concentrations (6-14 mmol/L, with a 2 mmol/L interval) as coordinates, the standard curve of lactate is obtained, as shown in Figure 3.11.
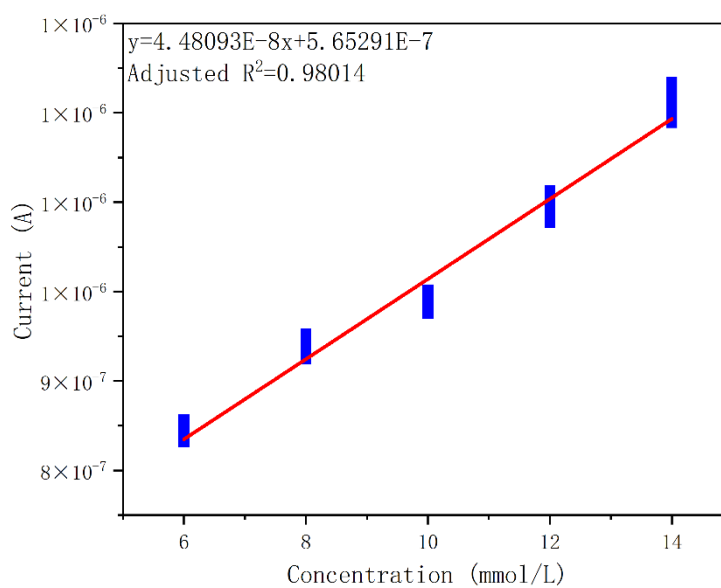
Figure 3.11 Standard curve of lactate oxidase electrode

As can be seen from the figure, the response of the lactate oxidase electrode shows a linear relationship. The linear fitting equation $y = a + b * x$ is substituted, and the detailed fitting parameters are shown in Table 3.4.

Table 3.4 Fitting parameters of lactate concentration standard curve

Intercept		Slope	
Value	Standard error	Value	Standard error
5.65291E-7	3.04295E-9	4.48093E-8	2.93047E-10
Residual sum of squares		Adjusted R^2	
1.70039E-13		0.98014	

It can be seen from the table that the sensitivity of the lactate oxidase electrode is 45 nA·L/mmol. After eliminating the influence of non-human factors, objective conditions, and systematic errors, the design requirements are satisfied.

3.5 Summary of the Chapter

This chapter mainly introduces the electrochemical response and standard curve of the electrode array. In addition to the temperature response and selectivity test of ISE.

The main work of this chapter includes:

- The relationship between the concentration of Na^+, K^+, and potential is tested, and the linear relationship between the logarithm of ion concentration and the potential signal is confirmed.

- Anti-interference of ISE is tested, including temperature response and ion selectivity.

- The relationship between glucose, lactate concentrations, and current is tested, and the linear relation between its concentration and the current signal is confirmed.

4 Response Testing and Data Analysis Based on Electrochemical Workstations

The previous chapter describes the response of electrode arrays and their standard curves. In this chapter, the standard curve is measured based on a self-designed circuit rather than an electrochemical workstation, and the sweat is measured online in vitro under the real motion state according to the standard curve.

The main content of this chapter is mainly divided into the following aspects: circuit design of signal acquisition module, standard curve verification based on the circuit, simulated sweat response, and real sweat measurement online under real motion state in vitro. The control and communication module, process design, and manufacture are not the work content of this thesis, so it will not be elaborated on and explained in detail.

4.1 Overall Architecture of Flexible Electronic System

In theory, flexible electronic systems have the same functionality as electrochemical workstations: they take signals from electrodes and display them on mobile devices after a series of transformations done by the circuit. Therefore, the flexible electronic system mainly includes two parts: signal acquisition module and control and communication module. The entire electronic system is assembled on a flexible printed circuit board (FPC).

As shown in Figure 4.1, the signal acquisition module mainly includes a signal amplification circuit, filter circuit, multiplexer, and ADC part. The control and communication module includes NFC modules and related software for mobile devices.

The electrode array converts the substrate concentration into current and voltage signals, but due to its small amplitude, it cannot meet the input requirements of ADC and needs to be amplified. The circuit is more convenient for voltage acquisition and processing than current, so the enzyme electrode and ISE amplification circuit are not the same. For ISE, an instrument amplifier (IA) is used to collect voltage signal directly and amplify it. For the enzyme electrode, a trans-impedance amplifier (TIA) is used to convert the current into voltage and realize acquisition and amplification.

The signal will remove the interference of other signals through the filter, and then the filtered signals of the four components are selected and output to the ADC according to the feedback signal of the control and communication module.
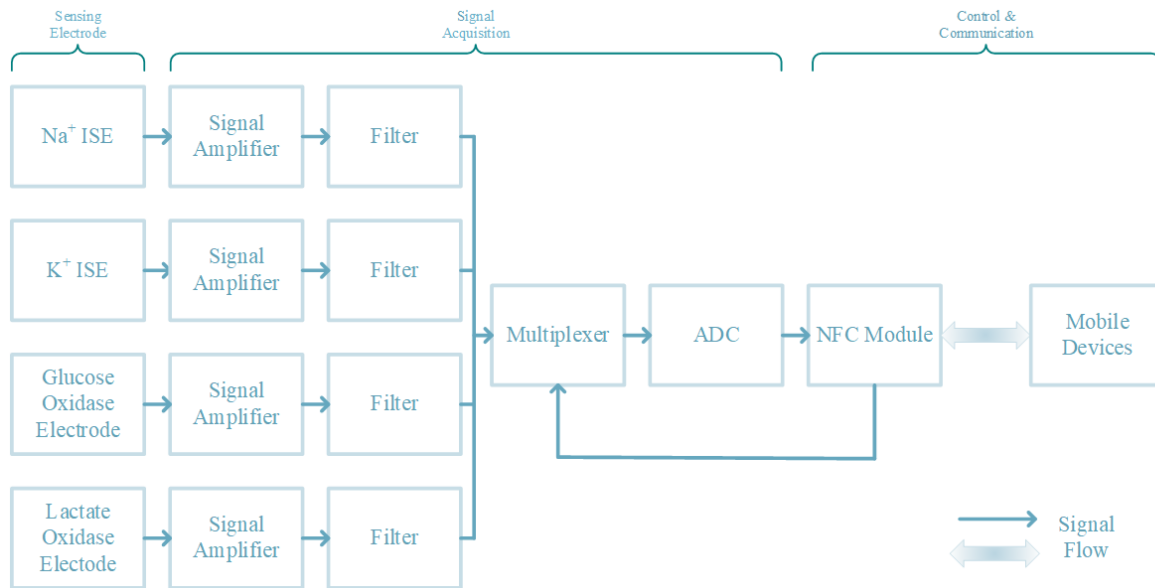
Figure 4.1 Structure diagram of flexible electronic system

ADC quantifies the received analog signal and converts it to a digital signal for the convenience of NFC module transmission and further processing on a mobile device.

4.2 Design of Signal Acquisition Circuit

4.2.1 Design of ISE Signal Amplifier Circuit

According to Equation (3.2), at room temperature (298 K), the relation between the potential of ISE and ion concentration to be measured is as follows:

$$\varphi = \varphi_0 + \frac{0.0592}{n} lgA \tag{4.1}$$

In Formula (4.1), n is the number of electron transfers during ion reactions. For ISE, it is related to the technological level of the membrane. In the ideal case, the membrane can transfer ions and electrons completely without hindrance, so the value of n under this circumstance is 1.

In general, if the concentration to be measured has a linear relationship with the electrochemical response, the slope is the sensitivity of the electrode response. In contrast, if the concentration is to be measured and the electrochemical response is nonlinear, the sensitivity is usually characterized by the first derivative of the electrochemical response with respect to the concentration. Take the derivative of both ends of Equation (4.1) with respect to concentration ratio A, we can get:

$$\frac{d\varphi}{dA} = \frac{0.0592}{A} \tag{4.2}$$

With the increase of concentration ratio A, the sensitivity of ISE will decrease gradually. The design of the ISE amplifier circuit should be able to collect accurate ISE potential signals even when the sensitivity is at the lowest level, that is, when the concentration to be measured is at the highest level.

In addition to the above conditions, the design of the ISE amplifier circuit and the selection of devices should also meet the following requirements:

I. The input resistance of the preamplifier should be much larger than the equivalent DC input resistance to avoid the voltage dividing of the electrode and solution system on the response. Similarly, because of resistance, the preamplifier must have a very low bias current and thermal drift to prevent interference with the ISE signal [61].

II. Depending on the process, the ISE input voltage is generally in the range of -0.5-0.5 V, which will result in a negative output voltage. But the analog-to-digital conversion only allows positive voltage input values, so voltage conversion is required.

III. Since the Ag/AgCl reference potential varies in the presence of different chloride ion concentrations, the reference electrode cannot connect to the ground, and the potential difference between the working electrode and the reference electrode should be measured. To do this, two voltage buffers are connected to the working electrode and reference electrode respectively, followed by a differential amplifier. The common-mode interference can be greatly reduced by this structure.

Based on the above requirements, the INA333 instrument amplifier from Texas Instruments (TI) is selected in this thesis. Some of its basic parameters are shown in Table 4.1.

Table 4.1 Basic parameters of INA333 instrument amplifier

Input voltage	-0.3-0.3 V	Max input bias current	200 pA
Input impedance	100 GΩ/3 pF	Operating temperature range	-40-125 ℃
Voltage Noise Density	50 nV/$\sqrt{\text{Hz}}$	Voltage temperature drift	0.1 μV/℃
CMRR	100 dB	DC operating voltage range	1.8-5.5 V

Calculated with the linear sensitivity of 45.9 mV of sodium ion, the minimum voltage is required to achieve the resolution of 3 mmol/L at the maximum concentration of 160 mmol/L is:

$$V_{min} = c * \frac{d\varphi}{dA} = 3\,mmol/L * \frac{45.9\,mV}{160\,mmol/L} = 0.861\,mV \tag{4.3}$$

Similarly, the minimum voltage is required to achieve the resolution of 1 mmol/L potassium ion is 1.9 mV. It is clear that the noise condition of INA333 can meet the application requirements.

A 3.3 V DC power is used to supply INA333. Since the maximum voltage swing allowed by the amplifier input is 300 mV, the gain can be designed (And can be adjusted according to the input voltage range) after considering the two-fold margin:

$$G = \frac{3.3\,V/2}{300\,mV * 2} = 2.75 \tag{4.4}$$

Therefore, according to the electrical schematic diagram of INA333 and the design requirements and parameters in this section, the circuit diagram can be designed as shown in Figure 4.2. The gain can be adjusted by different values of R_G:

$$G = 1 + \frac{100\,k\Omega}{R_G} \tag{4.5}$$
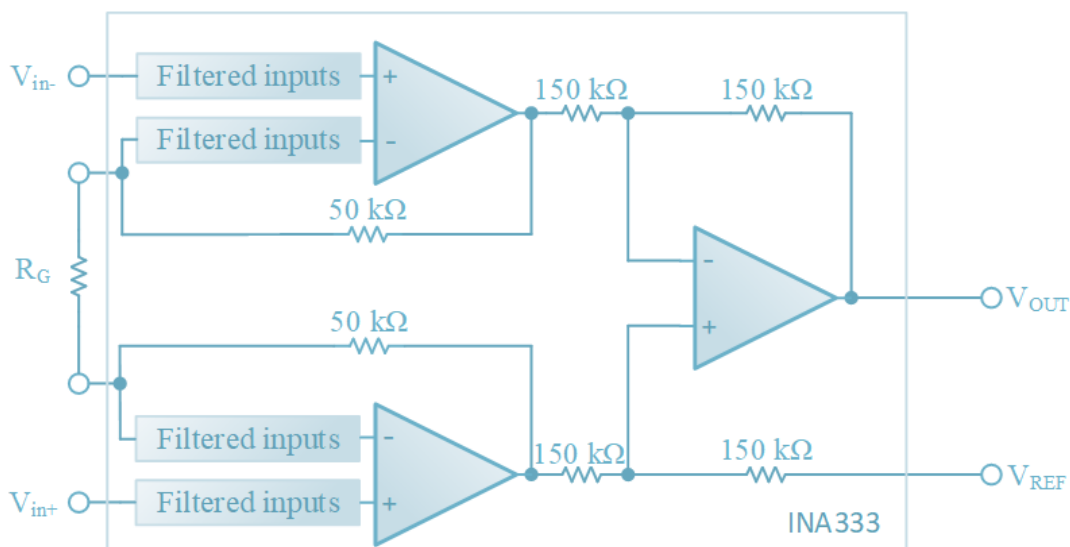
Figure 4.2 Signal Amplifier Circuit of ISE

The output voltage of the INA333 is referenced to V_{REF}. According to the virtual short of the operation amplifier and the characteristics of the zero-input current, the relation between V_{in-}, V_{in+}, $V_{REF,}$ and V_{OUT} can be deduced as:

$$V_{OUT} = V_{in-} - V_{in+} + V_{REF} \qquad (4.6)$$

In general, V_{REF} is grounded, and the V_{OUT} is the amplified waveform of the input voltage. However, since the output potential of ISE may be negative, V_{REF} should be set properly so that the output V_{OUT} is always positive within 3.3 V. In this thesis, ADA4841-1 of Analog Devices, Inc. (ADI) is used to implement V_{REF} of 1.65 V (bisect of 3.3 V power supply). The generating circuit of V_{REF} is shown in Figure 4.3.
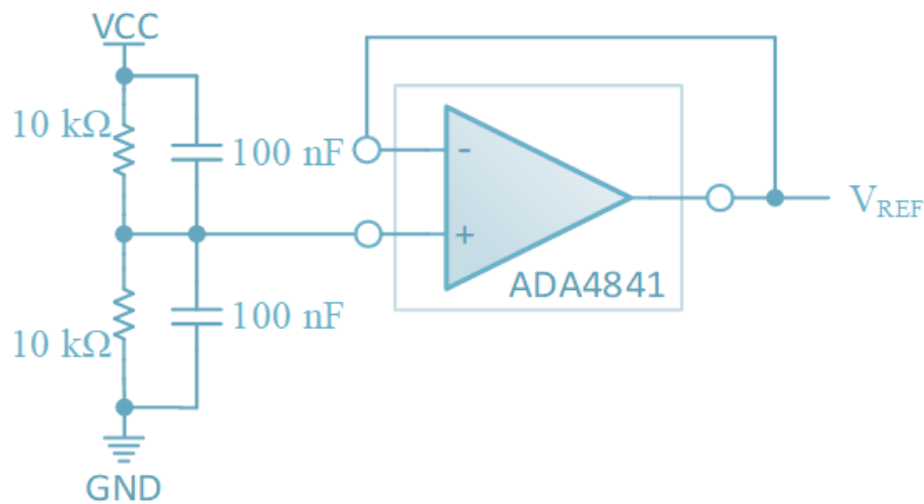
Figure 4.3 Generating circuit of V_{REF}

4.2.2 Design of Enzyme Electrode Signal Amplifier Circuit

Similar to ISE, enzyme electrode amplifier circuit design should be able to meet the sensitivity, maximum current range, and accurate current signal acquisition. The design of the enzyme electrode amplifier circuit and the selection of the device need to meet the following conditions:

I. The signal acquisition circuit of the enzyme electrode should be completely isolated from the ISE signal acquisition circuit to avoid mutual interference between paths.

II. The voltage after trans-impedance amplification should be in the input voltage range of ADC.

III. Due to the small amplitude of the current signal, the circuit design needs to be able to reflect current changes as low as nanoampere, and the corresponding Ag/AgCl reference electrode needs to be connected to a constant reference potential due to the trans-impedance amplifier.

Based on the above requirements, the AD8657 operational amplifier from Analog Devices, Inc. (ADI) is selected. Some of its basic parameters are shown in Table 4.2.

Table 4.2 Basic parameters of AD8657 operational amplifier under 3.3 V power supply

Input voltage	0-2.7 V	Input bias current	10 pA
Gain Bandwidth Product (Av = 100)	200 kHz	Operating temperature range	-40-125 ℃
Voltage Noise Density (f = 1kHz)	60 nV/$\sqrt{\text{Hz}}$	CM input capacitance	3.5 pF
Current noise density (f = 1kHz)	0.1 pA/$\sqrt{\text{Hz}}$	DM input capacitance	11 pF

The design of the trans-impedance amplifier circuit based on AD8657 is shown in Figure 4.4.
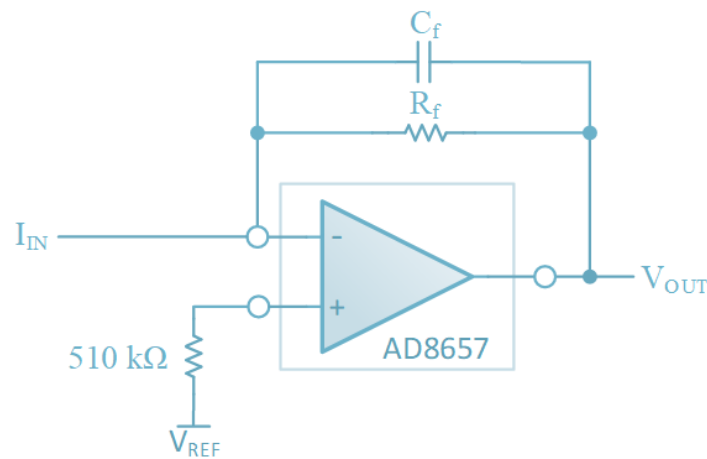
Figure 4.4 Trans-impedance amplifier circuit of the enzyme electrode

For the trans-impedance amplifier, the feedback circuit is a feedback resistance R_f and a feedback capacitor C_f in parallel, which can be assumed 1 MΩ and 10 pF for noise calculating. The parasitic capacitance of the enzyme electrode is C_p, which can be assumed 100 pF. The parasitic resistance of the enzyme electrode is large and negligible.

Since the feedback circuit is a first-order RC circuit, its thermal noise is only related to C_f:

$$N_R = \sqrt{\frac{kT}{C_f}} = 20.3 \ \mu V_{RMS} \tag{4.7}$$

And the noise voltage generated by the current noise density i_n flowing through the feedback circuit is:

$$N_I = \frac{i_n}{2}\sqrt{\frac{R_f}{C_f}} = 15.8\ \mu V_{RMS} \tag{4.8}$$

For trans-impedance amplifier circuits, the voltage noise of the operational amplifier can be calculated accurately by the zero and pole values of the system transfer function. To simplify the calculation, N_{OA} can be estimated by the GBP. When the gain is 0 dB (voltage gain is 1), the value of GBP is the maximum frequency that the circuit can respond to:

$$N_{OA} < \sqrt{e_n{}^2 * \frac{C_f + C_{DM} + C_{CM} + C_p}{C_f} * GBP} = 94.7\ \mu V_{RMS} \tag{4.9}$$

In Formula (4.9), the second term of the product is the maximum gain of voltage noise density. Thus the total equivalent output noise is the sum of the voltage noise N_{OA} of the operational amplifier, the thermal voltage noise N_R of the resistance, and the voltage noise N_I generated by the current noise flowing through the resistance:

$$N_{RMS} = \sqrt{N_{OA}{}^2 + N_R{}^2 + N_I{}^2} < 98.13\ \mu V_{RMS} \tag{4.10}$$

To achieve accurate quantization of the voltage, the current converted by the trans-impedance amplifier should be at least 10 times greater than the effective value of the output noise N_{RMS}. The typical current range of lactate and glucose oxidase electrodes is -1.5 µA to 3 µA, while the sensitivity of lactate and glucose oxidase electrodes is 2.28 µA·L/mmol and 45 nA·L/mmol. Therefore, in order to achieve the detection accuracy of 1 µmol/L glucose and 50 µmol/L lactate, the current detection capability of 2.28 nA and 2.25 nA is needed. According to Figure 4.4, the relationship between the output voltage and input current can be obtained as follows:

$$V_{OUT} = V_{REF} - I_{in} * R_f \tag{4.11}$$

If 510 kΩ feedback resistance is used, it can be calculated that when the current change is 2.28 nA and 2.25 nA, the output voltage change is 1.16 mV, which is more than 10 times larger than the total output noise.

In addition, to provide sufficient phase margin, the value of the feedback capacitance can be confirmed by the Formula (4.12):

$$C_f = \sqrt{\frac{C_{DM} + C_{CM} + C_p}{2\pi * R_f * GBP}} \qquad (4.12)$$

Therefore, for the selected 510 kΩ feedback resistance, the feedback capacitance can be calculated as 13.4 pF through Equation (4.12).

4.2.3 Design of Low-pass Filter

Since all signals are similar to DC signals, low-pass filtering is needed to filter out high-frequency noise and interference. The cut-off frequency of the low-pass filter is designed to be 1 Hz. Normally the filter has a unit gain to ensure a small degree of signal distortion.

Compared with common types of filters, Sallen-Key active filter can control the quality factor, and the transition band drop of this type of filter is steeper, so it is selected in this thesis. Through the cascade of two Sallen-Key second-order filters, a 4-order Butterworth filter can be formed. At this time, the filtering effect is enhanced and can meet the measurement requirements.

OPA2333 of Texas Instruments (TI) is selected to constitute the low-pass filter because it has a voltage shift of nearly 0 (0.05 μV/°C) and satisfies low-frequency noise (1.1 μV$_{PP}$) from 0.01-10 Hz. The design of a fourth-order low-pass filter circuit based on OPA2333 is shown in Figure 4.5.
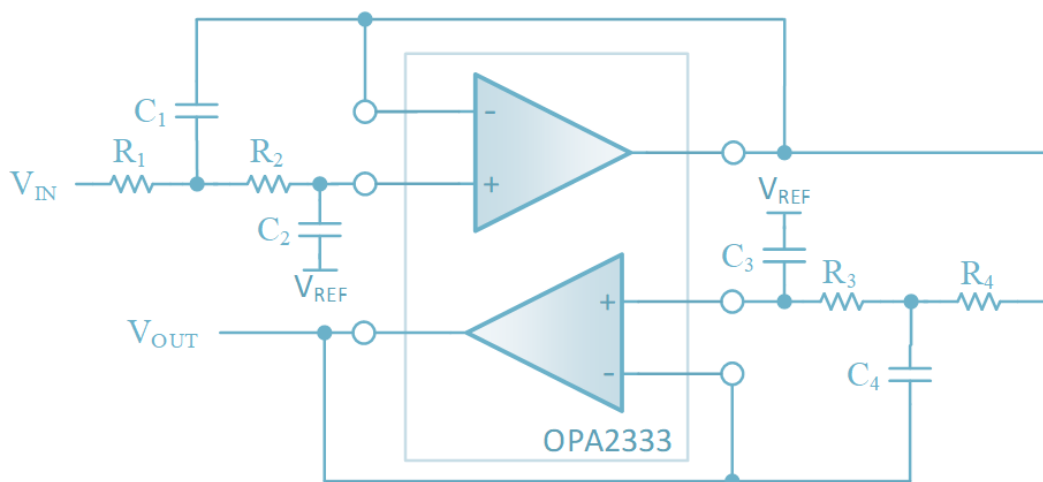
Figure 4.5 Low-pass filter circuit

According to Figure 4.5, the cut-off frequency of the low-pass filter can be calculated as:

$$f_{-3\,dB} = \frac{1}{2\pi \sqrt[4]{R_1 R_2 R_3 R_4 C_1 C_2 C_3 C_4}} \qquad (4.13)$$

According to the system function formula of even order Butterworth low-pass filter:

$$H(s) = \prod_{k=1}^{\frac{N}{2}} \frac{\omega_C^2}{s^2 + 2\left[\sin\left(\frac{2k-1}{2N}\pi\right)\right]\omega_C s + \omega_C^2} \qquad (4.14)$$

Where N is the total order of the filter. Therefore, we can obtain the damping factor ξ_1, ξ_2 of the two Sallen-Key filters by Formula (4.14):

$$\xi_1 = \sin\left(\frac{1}{8}\pi\right), \xi_2 = \sin\left(\frac{3}{8}\pi\right) \qquad (4.15)$$

Taking the first Sallen-Key filter as an example, its capacitance ratio should meet the following relationship:

$$\frac{C_2}{C_1} < \xi_1^2 + A - 1 = \ \xi_1^2 \approx 0.146 \qquad (4.16)$$

Let the capacitance ratio be 0.14. Meanwhile, capacitance C_1 and C_2 also satisfy the following relationship:

$$\frac{1}{2\pi\sqrt{R_1 R_2 C_1 C_2}} = 1\,Hz \qquad (4.17)$$

For the convenience of design, we take the resistance values $R_1 = R_2 = 180$ kΩ. Based on Formula (4.16) and (4.17), $C_1 = 2.36$ μF and $C_2 = 330$ nF can be solved by simultaneous equations. Similarly, we can calculate $C_3 = 816$ nF and $C_4 = 960$ nF. The capacitance value selected in the experiment is $C_1 = 2.2$ μF, $C_2 = 330$ nF, $C_3 = 820$ nF and $C_4 = 1$ μF. Put the resistance and capacitance values into Formula (4.13) for verification:

$$f_{-3\,dB} = \frac{1}{2\pi R \sqrt[4]{C_1 C_2 C_3 C_4}} \approx 1.007 Hz \qquad (4.18)$$

Thus, the design of the filter meets the requirements.

4.2.4 Selection of Multiplexer and ADC

Since an ADC cannot perform A/D conversion on multiple signals at the same time, A multiplexer is required before the ADC. ADG704 multiplexer from Analog Devices, Inc. (ADI) is selected to implement the circuit. The ADG704 has low on-resistance (2.5 Ω), low power consumption (< 0.01 μW) and fast switching time (t_{ON} = 20 ns, t_{OFF} = 13 ns), which can meet the requirements of the circuit.

In consideration of the design accuracy of each sensor channel, the low power consumption, and the constraints sampling rate, AD7091R from Analog Devices, Inc. (ADI) is selected.

AD7091R is a 1 MSPS, 12-bit ADC. It provides a high precision 2.5 V reference voltage internally, and when using this voltage, the REF_{IN} and REF_{OUT} pins are decoupled by a 2.2 μF capacitance. Under the condition, a least significant bit (LSB) input voltage change is:

$$V_{LSB} = \frac{V_{REF}}{2^{12}} \approx 610 \ \mu V \tag{4.19}$$

The relationship between the minimum voltage amplitude of each channel and the voltage of LSB is shown in Table 4.3, which means the ADC selection meets the requirements.

Table 4.3 Relation between LSB and input voltage of ADC

Channel	Channel Voltage	Ratio with LSB voltage
Sodium ion	0.861 mV	1.41
Potassium ion	1.9 mV	3.11
Glucose	1.16 mV	1.90
Lactate	1.15 mV	1.89

The output signal of the ADC is transmitted to the mobile device through the NFC module. Since the ADC has a 12-bit output, the reading data from software is usually three hexadecimal numbers.

According to the previous acquisition circuit design and ADC parameters, we can get the conversion relation between hexadecimal numbers N_{HEX} obtained from the software on the device, ISE input voltage V_{in} and enzyme electrode input current I_{in}:

$$V_{in} = \frac{\frac{Dec(N_{HEX}) * 2.5 \ V}{2^{12}} - V_{REF}}{G} \tag{4.20}$$

$$I_{in} = \frac{V_{REF} - \frac{Dec(N_{HEX}) * 2.5\,V}{2^{12}}}{R_f} \tag{4.21}$$

In the formula above, $Dec(N_{HEX})$ represents the decimal value corresponding to N_{HEX}; V_{REF} and G are the reference voltage and gain respectively mentioned in chapter 4.2.1; R_f is the feedback resistance mentioned in chapter 4.2.2.

4.3 Electronic System Verification

4.3.1 Overview of Self-designed Flexible Electronic System

After layout design and wiring, PCB design, process manufacturing, and integration of electrode and electronic system, the complete system structure (excluding mobile devices) are shown in Figure 4.6. The circuit parts and coils are FPC circuit boards with a total thickness of 125μm, allowing for greater flexibility from thinner substrates.
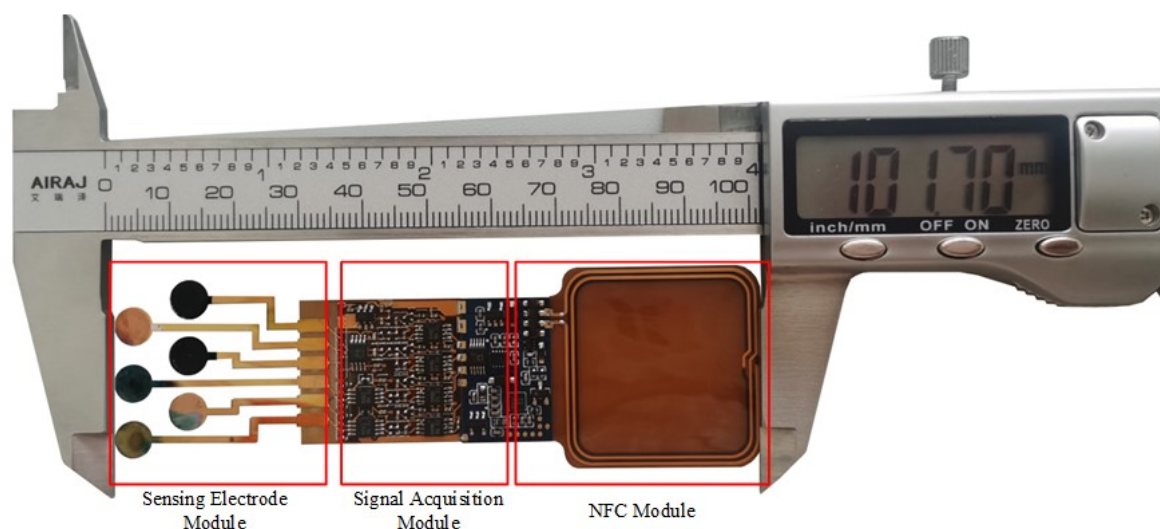
Figure 4.6 A diagram of the complete system (excluding mobile devices)

To verify the functional feasibility of the electronic system, the sodium and potassium ions, glucose, and lactate in sweat are tested systematically. The specific measurement method is to calculate and fit the curve by taking the average value of the data collected within 10 seconds when it is stable.

4.3.2 System Verification of ISE

The potassium ISE system is verified in potassium chloride solution of 1 mmol/L, 2 mmol/L, 4 mmol/L, 8 mmol/L, 16 mmol/L, and 32 mmol/L, respectively. The average value of collected data is shown in Table 4.4, and the fitting curve is shown in Figure 4.7.

Table 4.4 Average value of potassium ion data collected from mobile device

Concentration	Data (in hexadecimal)	Corresponding Voltage
1 mmol/L	82E	-0.1240 V
2 mmol/L	8DE	-0.0882 V
4 mmol/L	98E	-0.0524 V
8 mmol/L	A46	-0.0149 V
16 mmol/L	AF4	0.0205 V
32 mmol/L	BB1	0.0589 V
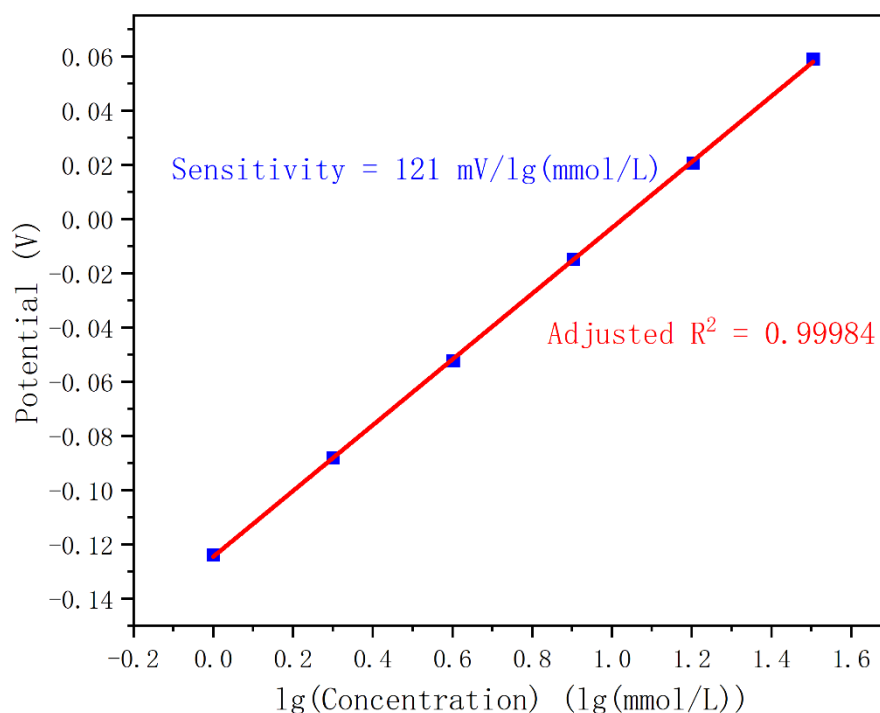
Figure 4.7 Standard curve of potassium ion data collected from the mobile device

The sodium ISE system is verified in sodium chloride solution of 5 mmol/L, 10 mmol/L, 20 mmol/L, 40 mmol/L, 80 mmol/L, and 160 mmol/L, respectively. The average value of collected data is shown in Table 4.5, and the fitting curve is shown in Figure 4.8.

Table 4.5 Average value of sodium ion data collected from mobile device

Concentration	Data (in hexadecimal)	Corresponding Voltage
5 mmol/L	942	-0.0672 V
10 mmol/L	9C1	-0.0420 V
20 mmol/L	A55	-0.0119 V
40 mmol/L	AEE	0.0193 V
80 mmol/L	B72	0.0461 V
160 mmol/L	C00	0.0750 V
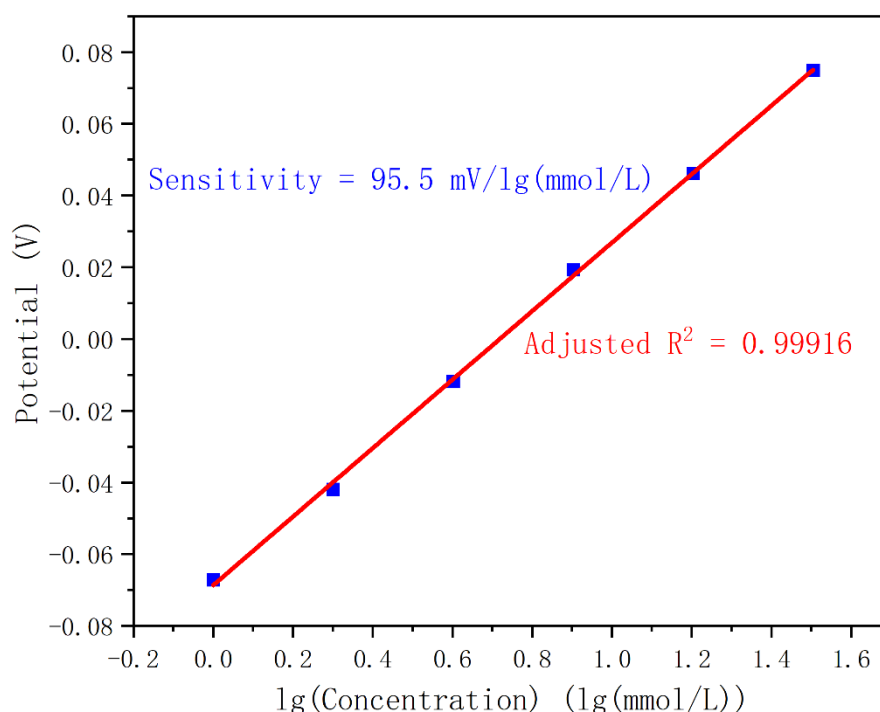
Figure 4.8 Standard curve of sodium ion data collected from the mobile device

It can be seen that the self-designed flexible electronic systems have good linearity to measure the response of ISE, and also has good sensitivity after excluding the influence of chloride ions, which meets the design requirements.

4.3.3 System Verification of Enzyme Electrode

The glucose oxidase electrode is verified in glucose solution of 0.1 mmol/L, 0.2 mmol/L, 0.3 mmol/L, 0.4 mmol/L, 0.5 mmol/L and 0.6 mmol/L, respectively. The average value of collected data is shown in Table 4.6, and the fitting curve is shown in Figure 4.9.

Table 4.6 Average value of glucose data collected from the mobile device

Concentration	Data (in hexadecimal)	Corresponding Current
0.1 mmol/L	8F8	0.488 µA
0.2 mmol/L	89A	0.600 µA
0.3 mmol/L	831	0.726 µA
0.4 mmol/L	78D	0.922 µA
0.5 mmol/L	6EF	1.110 µA
0.6 mmol/L	65B	1.288 µA
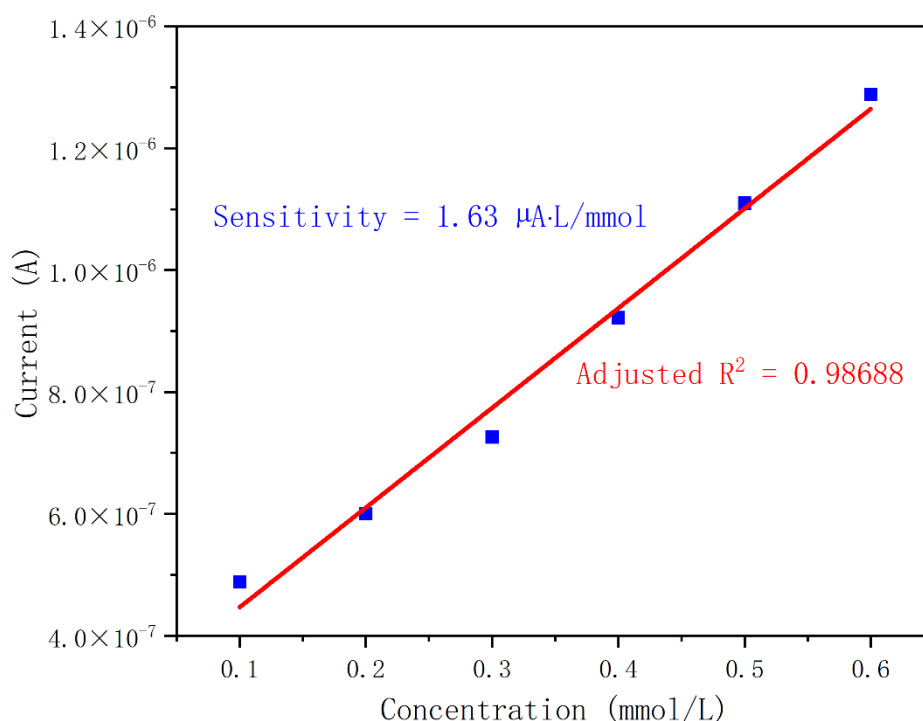
Figure 4.9 Standard curve of glucose data collected from the mobile device

The lactate oxidase electrode is verified in lactate solution of 2 mmol/L, 4 mmol/L, 6 mmol/L, 8 mmol/L, 10 mmol/L, 12 mmol/L, and 14 mmol/L respectively. The average value of collected data is shown in Table 4.7, and the fitting curve is shown in Figure 4.10.

Table 4.7 Average value of lactate data collected from mobile device

Concentration	Data (in hexadecimal)	Corresponding Current
2 mmol/L	CDB	-0.703 µA
4 mmol/L	CD3	-0.694 µA

Concentration	Data (in hexadecimal)	Corresponding Current
6 mmol/L	CC2	-0.673 µA
8 mmol/L	CB8	-0.661 µA
10 mmol/L	CB0	-0.652 µA
12 mmol/L	CA7	-0.641 µA
14 mmol/L	C9F	-0.631 µA
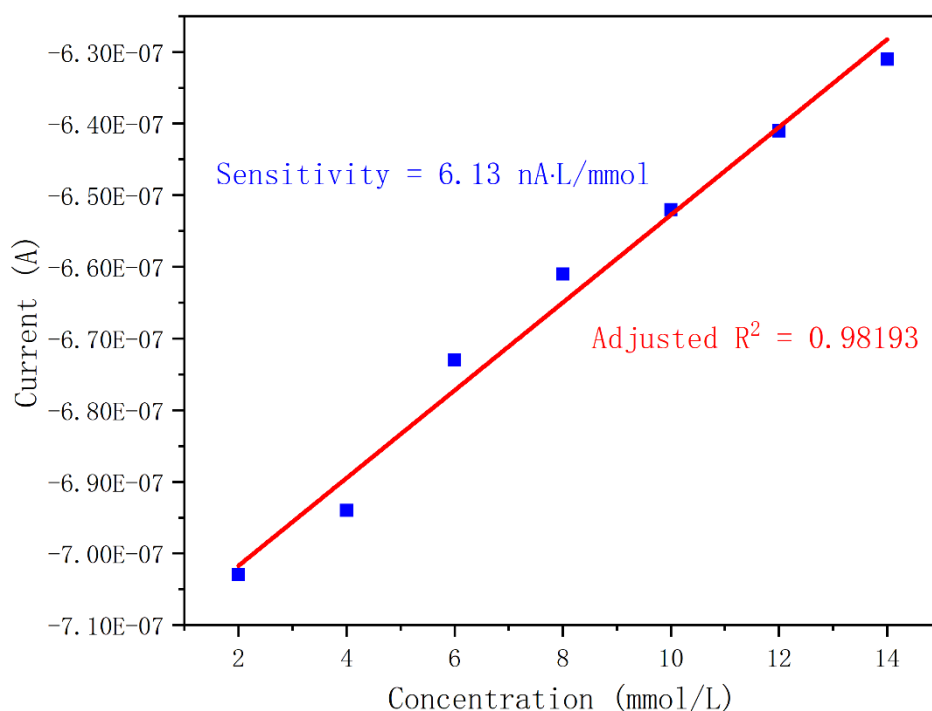
Figure 4.10 Standard curve of lactate data collected from the mobile device

It can be seen that the self-designed flexible electronic systems have relatively good linearity to measure the response of enzyme electrodes. It also has good sensitivity in measuring glucose, which meets the design requirements. The sensitivity of lactate measured by the system is low due to the unstable response of the electrode itself and enzyme activity, but the parameter of the electronic system can still meet the measurement requirement.

4.4 Sweat Response Measurement and Analysis

4.4.1 Clip Plate Measuring Method

Nowadays, most of the sensors have been based on the premise of wearability, because of the difficulty of collecting and measuring sweat. In order to collect data from sweat, the sensor has to be in close contact with the skin for the best results, while taking into account factors like ease of wearing, impact on a person's health, and abrasion on the sensor [62].

Different from the previous measurement methods, this thesis adopts an in vitro measurement method of sweat based on non-wearing conditions, which can ensure the primitiveness of sweat samples while realizing the continuous and real-time measurement as much as possible. This method can reduce the wear of the electrode surface while minimizing external interference, thus providing the possibility of repeated use.

The implementation of this method is based on the hydrophobicity of PET and parylene. PET and parylene are hydrophobic, so water molecules do not wet the surface of the substrate [63-64]. A small amount of sweat is dripped onto the electrode array so that the sweat is evenly distributed over the surface of the electrode by compression with the clip plate. The clip plate itself is made of highly electric-insulating material. In this case, the clip plate can insulate the electrode from external environmental interference and prevent the measurement error caused by the evaporation of sweat.

After the measurement, open the clip plate to remove the sample. Due to the hydrophilicity of the clip plate, it will be moistened by sweat, and acting forces are created between them, thus removing most of the sweat. The remaining sweat on the electrode array will condense into droplets due to hydrophobicity and can be cleaned by a capillary tube to minimize the impact on the next measurement. A schematic diagram of the Clip Plate method is shown in Figure 4.11.

The advantages of this method are as follows: 1. It can be completely measured in vitro, which reduces the wear on the electrode surface. 2. Can greatly reduce the amount of sweat sample (the actual test amount can be as low as 30 μL) 3. Can prevent external factors to the response caused by interference.

The following measurements of simulated and real sweat are based on the method mentioned above.
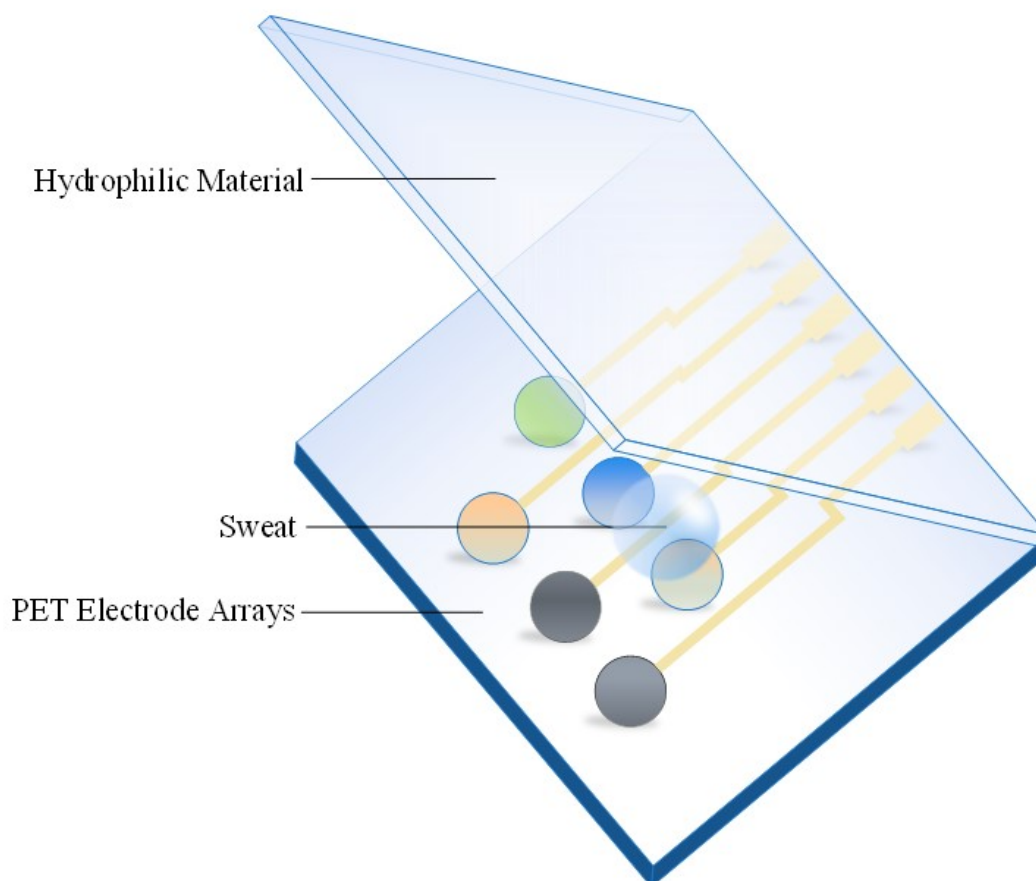
Figure 4.11 Schematic diagram of Clip Plate method

4.4.2 Simulated Sweat Response Measurements and Verification

To verify the feasibility of the method in 4.4.1 and to verify the sensor's response changes to each component of sweat, artificially simulated sweat response is first measured.

First, the initially simulated sweat (0.1 mmol/L glucose, 2 mmol/L KCl, and 20 mmol/L NaCl) is prepared and dropped on the electrode array for scanning until the response is relatively stable. Then the change of component concentration in sweat is simulated by dropping lactate, glucose, potassium chloride, and sodium chloride standard solutions into the initial solution respectively. The amount of added standard solution is controlled so that the total concentration varies linearly. The response of the electrode array to simulated sweat is shown in Figure. 4.12.

In the figure, the response-concentration coordinates of lactate and glucose are in the lower left, and the response-concentration coordinates of ions are in the upper right. It can be seen that the linearity and sensitivity of this method are relatively good, and it can reflect the changing trend of component concentration in sweat.
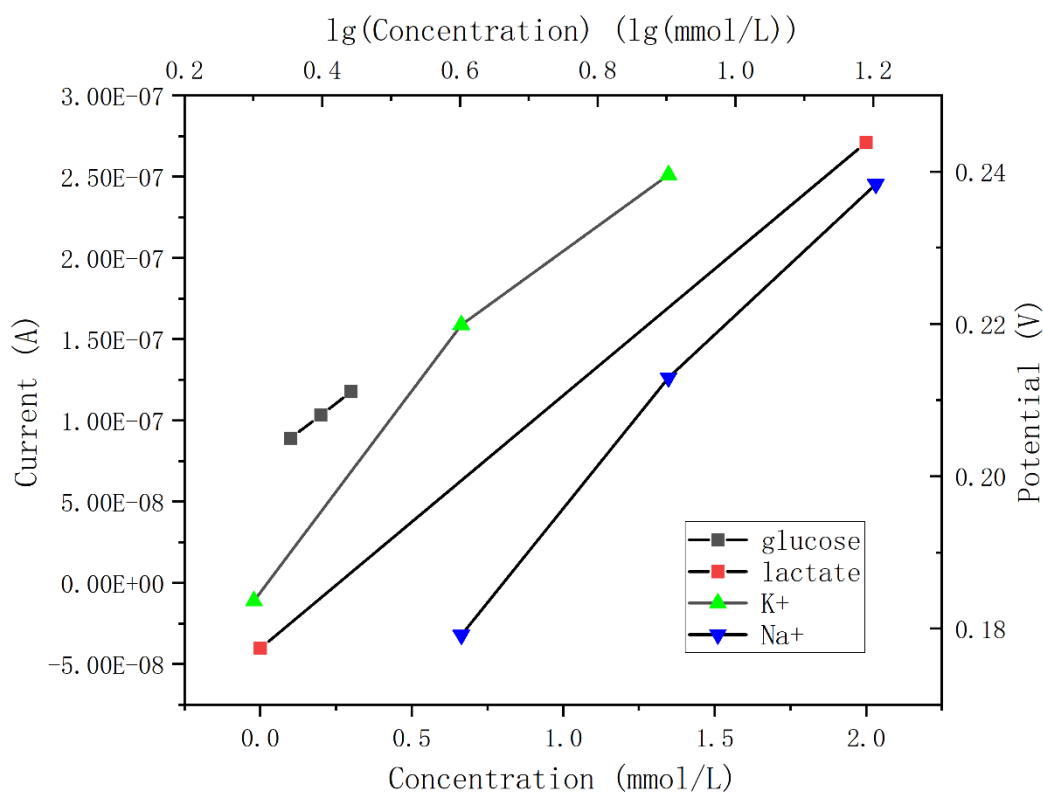
Figure 4.12 Simulated sweat response curve based on the electrode array

4.4.3 Real Sweat Response Measurements and Analysis

A flexible electrode array is used to measure the change of compounds in sweat during exercise. To observe the changes of exercise status more obviously, sodium ion, glucose, and lactate which changed significantly during exercise are selected for measurement.

The sweating of the human body is achieved by exercising on a cycling machine, as shown in Figure 4.13(a). Through preliminary preparation and observation, the load of gear 3 and gear 5 are selected as the gear of the formal experiment. Every ten minutes, sweat is collected from the testee's foreheads with a pipette gun or disposable pipette. The collected sweat is immediately loaded into a centrifugal tube, labeled and measured in real-time, as shown in Figure 4.13(b). After each collection, wipe the sweat on the forehead of the subject with a non-woven cloth to prevent the mixed contamination of sweat. During the whole exercise, the testee does not drink water to ensure control variables.

The flexible electrode needs to be recalibrated with a standard solution of known concentrations to obtain a standard curve with the lowest possible error before each use. The relationship between time and concentration can be obtained after calibration, as shown in Figure 4.14. The

testee begins to sweat at 20 min and adjusts the cycling machine to gear 5 loads at 40 min until the end of the experiment. During the test, the testee will have an appropriate rest depending on the situation.

(a)   (b)
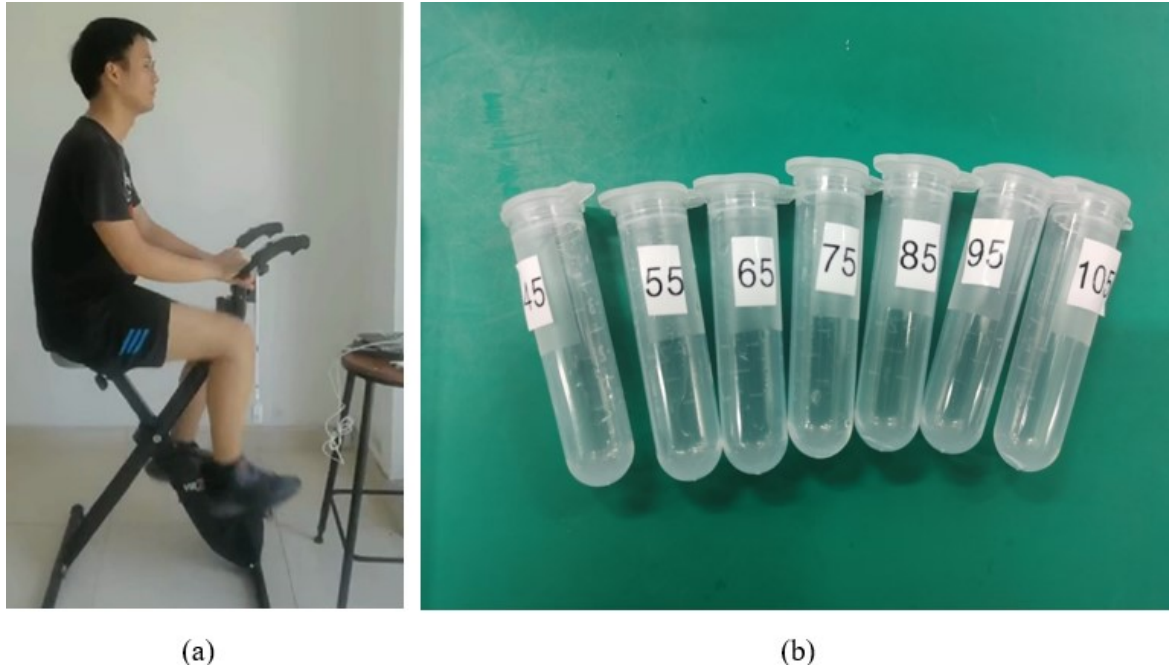
Figure 4.13 During the sweat collection progress. (a) Testee exercises on a cycling machine; (b) Sweat collected from testee
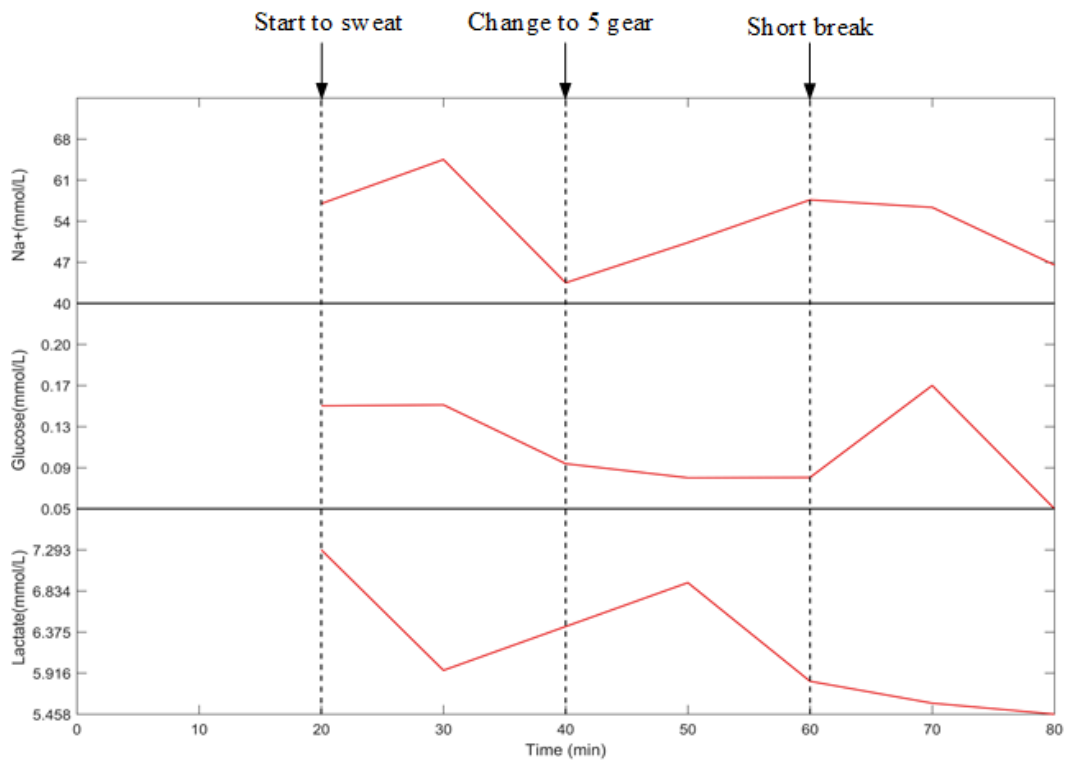
Figure 4.14 Changes in sweat concentration during cycling

It can be seen that the concentration of sodium ions, glucose, and lactate in sweat is high at the beginning of the exercise. As the movement continued, they all have a dedine trend. Sodium ions and lactate concentrations rise and glucose concentrations fall further when the load is changed to gear 5. After a short rest, sweat glucose levels rise, while lactate and sodium ions tend to decline. The average sweat concentration during the overall exercise is shown in Table 4.8.

Table 4.8 Average sweat component concentration during the exercise

	Sodium Ion	Glucose	Lactate
Concentration	53.9 mmol/L	0.112 mmol/L	5.948 mmol/L

It can be seen that although the sweat composition concentration varies greatly with the environment, the amount of exercise and the physical condition of the tested person, the concentration changes of sodium ion, lactate, and glucose are relatively consistent with the theoretical expectations, and their content values are also within the normal range, meeting the requirements.

In addition, we explore the relationship between heart rate, body temperature, oxygen saturation (SpO2), and the concentration of sodium ions and glucose in sweat. To reduce the error of experiments, we find another testee to participate in the experiment due to individual differences. The physical information of the two testees is shown in Table 4.9.

Table 4.9 Physical information of two testees

	Testee 1	Testee 2
Height	186cm	170cm
Weight	74kg	87.5kg

For testee 2, the exercise state should be kept the same as testee 1 so as to control the variables. The sodium ion and glucose concentration in the sweat of the two testees and their heart rate, body temperature and oxygen saturation changes during the exercise are shown in Figure 4.15.

Compared with testee 1, which has a lower body mass index, the sweat of testee 2 is higher in both sodium ion concentration and glucose concentration according to the figure. The oxygen saturation changes of the two testees tend to be the same: the oxygen saturation has an opposite trend with exercise intensity, and it will slightly increase after a short rest. The body temperature of both testees has raised with the increase of exercise intensity, and eventually stabilized at around 36.6-36.8 °C. The exact relationship between the concentration of sodium ions, glucose

in sweat and the physiological indices has not been found due to the large individual differences and the limitations of physiological indices measurement methods.
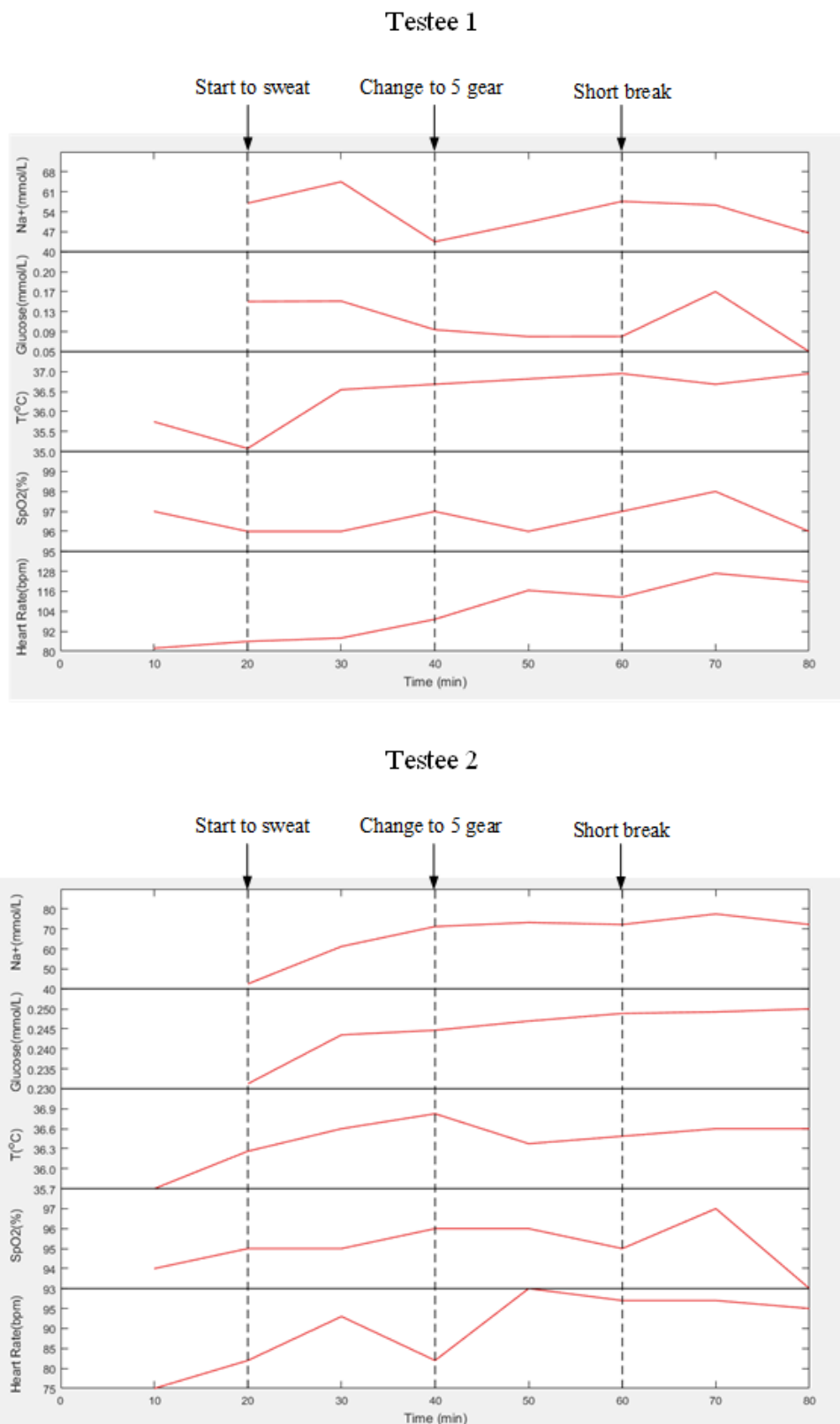
Figure 4.15 Changes in glucose, Na$^+$, HR, SpO$_2$ and temperature of two testees during cycling

4.5 Summary of the Chapter

This chapter mainly introduces the design of the signal acquisition circuit, verification of the system, and sweat measurement and analysis. In addition, a new method of in vitro online measurement is proposed.

The main work of this chapter includes:

- Circuit of ISE, enzyme electrode signal amplification, and low pass filter are designed, while appropriate hardware is selected to implement the self-designed flexible electronic systems.

- The response of the system to different concentrations of sweat components is verified.

- The response verification of simulated sweat is completed, and then the sweat of the testee in the exercise state is collected, which has been further measured and analyzed.

5 Preliminary Study of Flexible Enzyme Electrode Based on Viologen Compounds

The previous chapter describes circuit design, system verification, and sweat sample measurement. In order to improve the stability and linearity of the enzyme electrode compared with the conventional one, this chapter improved the enzyme electrode by using viologen compounds. In this chapter, the response of the flexible enzyme electrode based on viologen compounds, including glucose and lactate, is preliminarily studied.

The main content of this chapter is mainly divided into the following aspects: brief introduction of viologen compounds, preparation of sulfhydryl viologen-based enzyme electrode, response measurement, and standard curve analysis.

5.1 Introduction of Viologen Compounds

Viologen compounds are a kind of chemical substance containing the structure of 1, 1' - disubstituted 4, 4' - bipyridine salts. The core structure of viologen is shown in Figure 5.1.
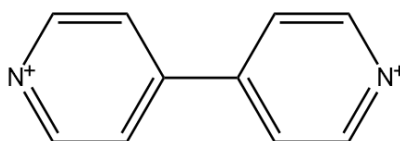
Figure 5.1 Structure of viologen

Its structure was first discovered in the widely used herbicide paraquat [65], with two methyl groups added to two nitrogen atoms based on the structure shown in Figure 5.1. The substance got its current name in 1932 when chemist Michaelis discovered that a reduction state of the substance appears purple [66]. Under normal conditions, the viologen compound exists stably in the form of a double cation (V^{2+}). When it receives an electron, it will turn into the form of a single cation radical (V^+). At this time if the electron is continually provided, the material will be further reduced into neutral (V) (due to its strong reducibility, the molecules is not stable compared with V^{2+} and V^+, but they are all thermodynamic stable), the reaction mechanism is shown in Figure 5.2 [67]. Because the potential of the two redox reactions is very similar, the reaction is reversible, which is also the reason why viologen is often used in electrochemical and photochemical applications. For example, viologen can be used in electrochromic devices [68-69], transistors [70] and storage device materials [71-72].
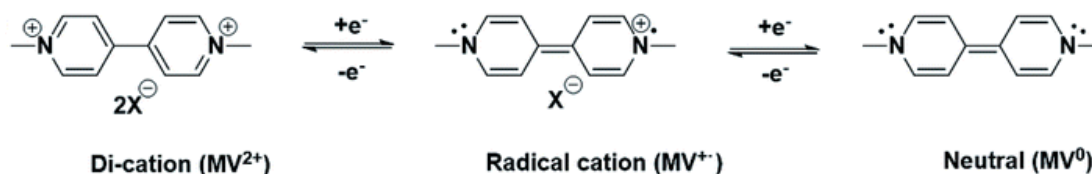
Figure 5.2 Reversible redox reaction mechanism of viologen [67]

Viologen can be used as an intermediate layer for enzyme electrodes based on its unique redox properties. Since the oxidase electrode catalyzes the decomposition of substrates to generate electrons, viologen can play a good role in electron transfer as an intermediate layer. In addition, when different initial voltages are used, the degree of the redox reaction of viologen is different, and its response sensitivity can change accordingly. Sulfhydryl viologen (HSC_6VC_6SH) is the derivative of viologen used in this thesis, and its basic structure is shown in Figure 5.3.
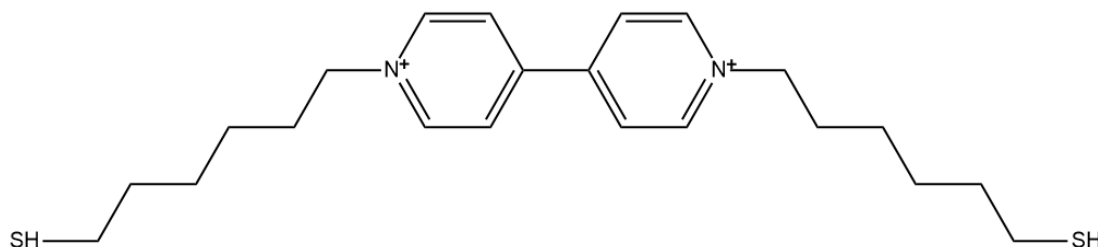
Figure 5.3 Chemical construction of sulfhydryl viologen (HSC6VC6SH)

5.2   Preparation of Enzyme Electrode Based on Viologen

5.2.1 Base Materials and Reagents

Acetonitrile is procured from China National Pharmaceutical Group CO., LTD. (Sinopharm). Horseradish peroxidase is purchased from Shanghai Aladdin Biochemical Technology CO., LTD. Sulfhydryl viologen is synthesized by professor Dongjin Qian's research group at Fudan University.

Other reagents and material sources are introduced in chapter 2.2.1.

5.2.2 Immobilization of Viologen on Enzyme Electrode

Sulfhydryl viologen fixation is preceded by pretreatment and the activation of the gold electrode. The pretreatment and activation process are described in Chapter 2. For sulfhydryl viologen immobilization in this thesis, two methods are adopted in this study and will be introduced separately in the following part.

●   Sulfhydryl viologen self-assembles on the surface of the gold electrode:

Sulfhydryl groups can be chemically bonded to some transition metals: with the breaking of the sulfur-hydrogen bond, the sulfur atom and the metal interact in the form of coordination bonds, thus realizing the self-assembly of sulfhydryl compounds. Among many transition metals, the interaction between sulfur and gold is strong and has a good fixation effect [73]. Therefore, for gold electrodes, molecular self-assembly can be adopted. The self-assembly procedure is as follows:

Sulfhydryl viologen is dissolved in acetonitrile with a concentration of 2 mg/ mL, and the electrode is placed in it for 24 hours. Then the electrode is removed from the solution and cleaned with water and ethanol to remove the weak fixed viologen. Nitrogen is applied for 20 minutes to remove the dissolved oxygen in the PBS solution and prevent the interference of oxygen redox peak. Set the parameter to -0.9-0 V and the rate to 100 mV/s, and scan for 7 cycles to obtain the complete and stable CV characteristic curve as shown in Figure 5.4. The assembly is successful the redox peak can be observed.
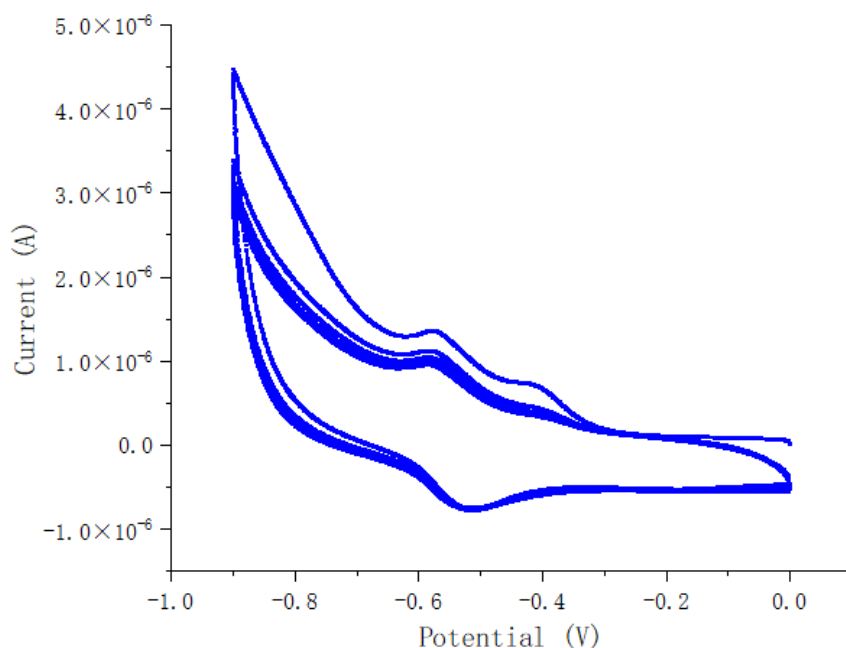
Figure 5.4 CV characteristic curve of sulfhydryl viologen self-assembled on the gold electrode

Two oxidation peaks can be clearly observed from Figure 5.4, corresponding to the process in which neutral V is oxidized to V^+ and V^+ is oxidized to V^{2+} respectively. However, there is only one reduction peak, and the area is larger than the respective area of the two oxidation peaks, indicating that after V^{2+} is reduced to V^+, a part of V^+ is further reduced to neutral V.

● Sulfhydryl viologen solution drops on the surface of the gold electrode:

Due to the molecular properties of sulfhydryl viologen, it is extremely insoluble in water and ethanol. Therefore, an acetonitrile solution (4 mg/mL) of sulfhydryl viologen can be prepared and dropped on the surface of the gold electrode. When completely dried, the viologen can be adsorbed to the negatively charged gold (111) surface due to its positive charge, and thus fixed to the electrode surface. Then the electrode is cleaned with water and ethanol. Nitrogen is applied for 20 minutes to remove the dissolved oxygen in the PBS solution and prevent the interference of oxygen redox peak. Set the parameter to -0.7-0 V and the rate to 100 mV/s, and scan for 7 cycles to obtain the complete and stable CV characteristic curve as shown in Figure 5.5. The viologen is fixed on the electrode if the redox peak can be observed.
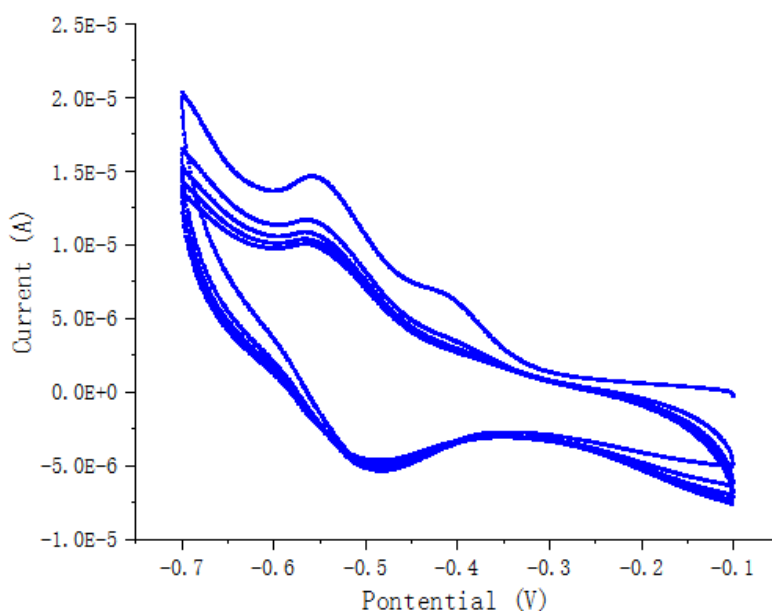
Figure 5.5 CV characteristic curve of sulfhydryl viologen dropped on the gold electrode

It can be seen that the CV curve is roughly the same as the self-assembly method, but the response value is larger. This is due to a large amount of viologen dropped on the electrode surface, so both the overall response and the peak value are increased. In addition, it is also related to the pretreatment of the gold electrode surface.

5.2.3 Preparation of Viologen on Enzyme Electrode

The enzyme electrode can be further prepared after immobilizing the viologen on the gold electrode. The specific procedures are as follows:

● Preparation of Glucose Oxidase Electrode:

See 2.5.3 for details.

● Preparation of Lactate Oxidase Electrode:

Unlike Prussian Blue, viologen does not have the catalytic properties of hydrogen peroxide. Since the measurement range of lactate concentration is wide, in order to improve the response sensitivity of lactate oxidase electrode, horseradish peroxidase (HRP) is used to catalyze the decomposition of hydrogen peroxide on the basis of 2.5.4.

HRP is further added to lactate oxidase membrane solution. When oxidase and HRP have the same activity, the optimum enzyme ratio is 1: 1 [74]. Therefore, lactate oxidase and HRP is dissolved in the PBS buffer (pH = 7, contains 0.2 mol/L NaH_2PO_4 and 0.2 mol/L Na_2HPO_4 with a volume ratio of 19: 31) at the concentration of 50 mg/mL and 31 mg/mL.

Apply 3 µL chitosan and SWCNT viscous solution, 2 µL lactate oxidase and HRP membrane solution, 3 µL chitosan and SWCNT viscous solution in sequence with pipette gun to the PET gold electrode after viologen immobilizing. Be sure that the electrode is completely dried at 4 ℃ before applying the next layer. Then 2.5 µL 0.5%wt. Nafion is dropped on the electrode to make the lactate oxidase electrode.

5.3 Electrode Response and Analysis of Viologen Enzyme Electrode

5.3.1 Test Method and Preparation

See 3.4.1 for details.

5.3.2 Glucose Oxidase Electrode Current Response

The total glucose concentration of the solution to be tested is selected as 0.1-0.8 mmol/L with a 0.1 mmol/L interval. Then the current response at these concentrations is measured. The total volume of solution is 30 mL, and the concentration of glucose standard solution is 0.1 mol/L.

The electrode is scanned in PBS buffer solution under -100 mV initial potential until the current is relatively stable. Then 30 µL standard glucose solution is added to PBS solution in turn and wait for diffusion. The relatively stable response curve within 10 seconds is measured, as shown in Figure 5.6.
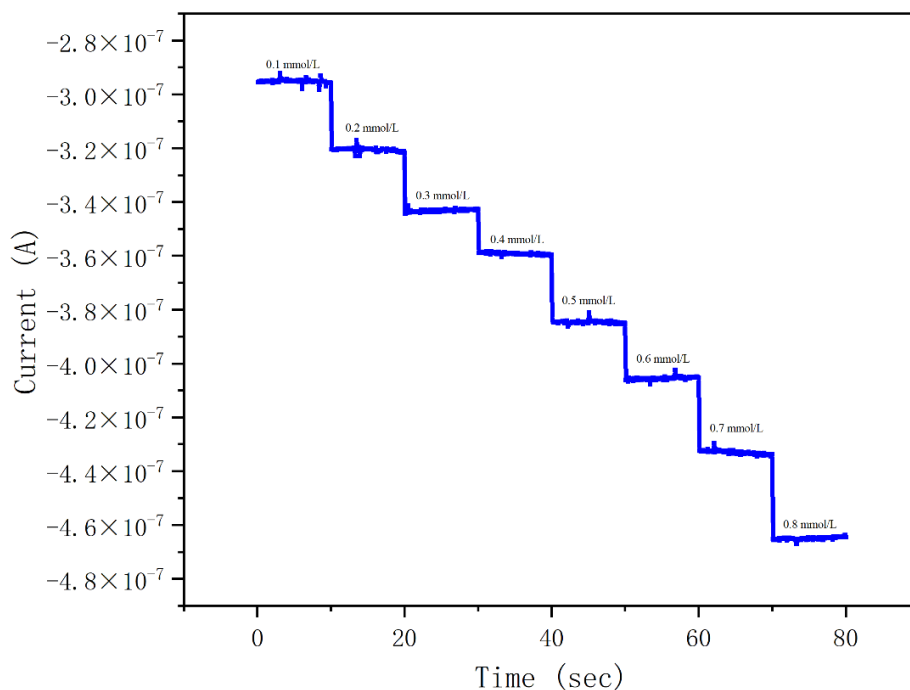
Figure 5.6 Current-time response of glucose oxidase electrode based on viologen

As can be seen from Figure 5.6, compared with the electrode in Chapter 3, the drift of current response is greatly improved, and the glucose oxidase electrode based on viologen still has good stability in the range of glucose concentration in sweat.

5.3.3 Fitting of Glucose Standard Curve

Taking concentration of glucose as abscissa and current response of different glucose concentrations (0.1-0.8 mmol/L, with a 0.1 mmol/L interval) as coordinates, the standard curve of glucose is obtained, as shown in Figure 5.7.

Substituting linear fitting equation $y = a + b * x$, the detailed fitting parameters are shown in Table 5.1.
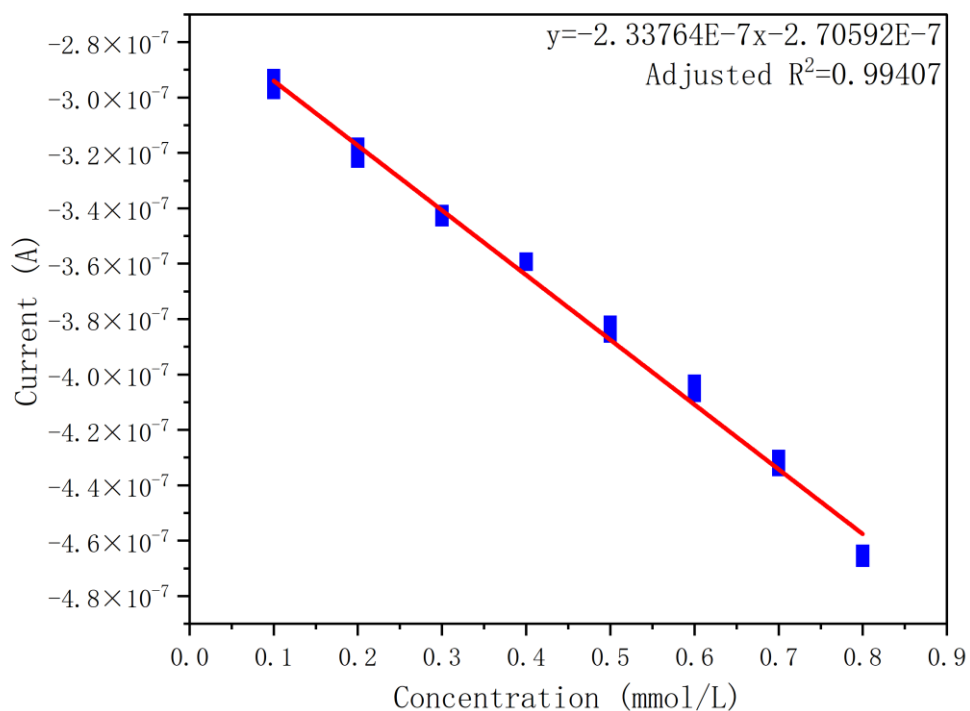
Figure 5.7 Standard curve of glucose oxidase electrode based on viologen

Table 5.1 Fitting parameters of glucose concentration standard curve

Intercept		Slope	
Value	Standard error	Value	Standard error
-2.70592E-7	3.22524E-10	-2.33764E-7	6.38693E-10
Residual sum of squares		Adjusted R^2	
1.36722E-14		0.99407	

From the table, the sensitivity of the glucose oxidase electrode is -0.234 µA·L/mmol. Compared with the electrode in Chapter 3, the viologen glucose oxidase electrode is less sensitive but has better response stability and linearity, and the measurement range of concentration is relatively large.

5.3.4 Lactate Oxidase Electrode Current Response

The total lactate concentration of the solution to be tested is selected as 4-20 mmol/L with a 1 mmol/L interval. Then the current response at these concentrations is measured. The total volume of solution is 30 mL, and the concentration of lactate standard solution is 2 mol/L.

The electrode is scanned in PBS buffer solution under -200 mV initial potential until the current is relatively stable. Then 15 μL standard lactate solution is added to PBS solution in turn and wait for diffusion. The relatively stable response curve within 10 seconds is measured, as shown in Figure 5.8.
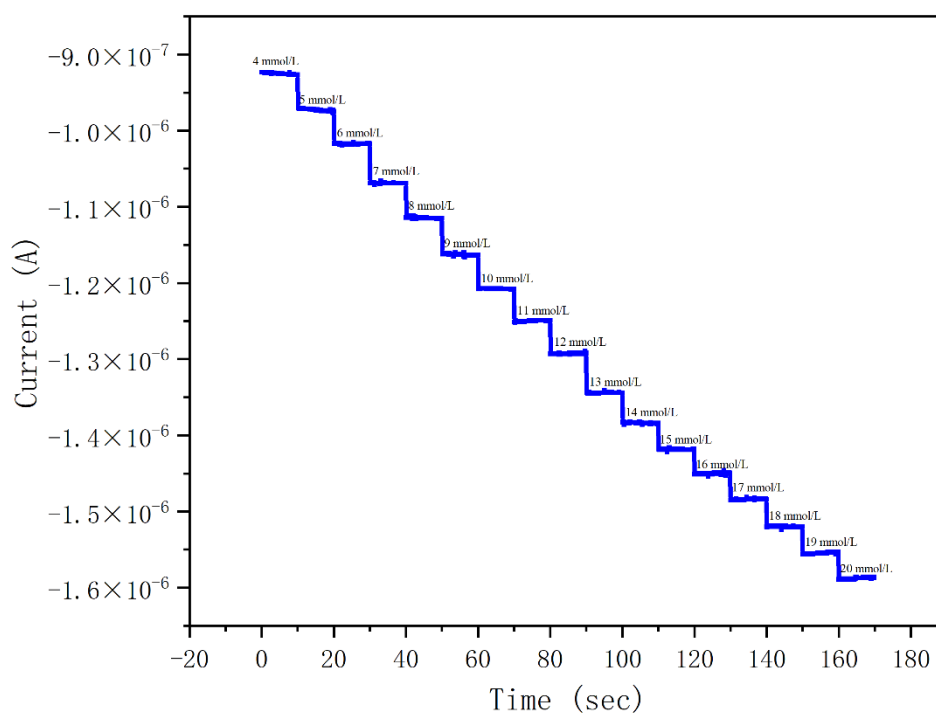
Figure 5.8 Current-time response of lactate oxidase electrode based on viologen

As can be seen from Figure 5.8, compared with the electrode in Chapter 3, the drift of current response of lactate electrode decreases significantly. Lactate oxidase electrode based on viologen shows good stability in the range of lactates concentration in sweat, and the current increased linearly.

5.3.5 Fitting of Lactate Standard Curve

Taking concentration of lactate as abscissa and current response of different lactate concentrations (4-20 mmol/L, with a 1 mmol/L interval) as coordinates, the standard curve of lactate is obtained, as shown in Figure 5.9.
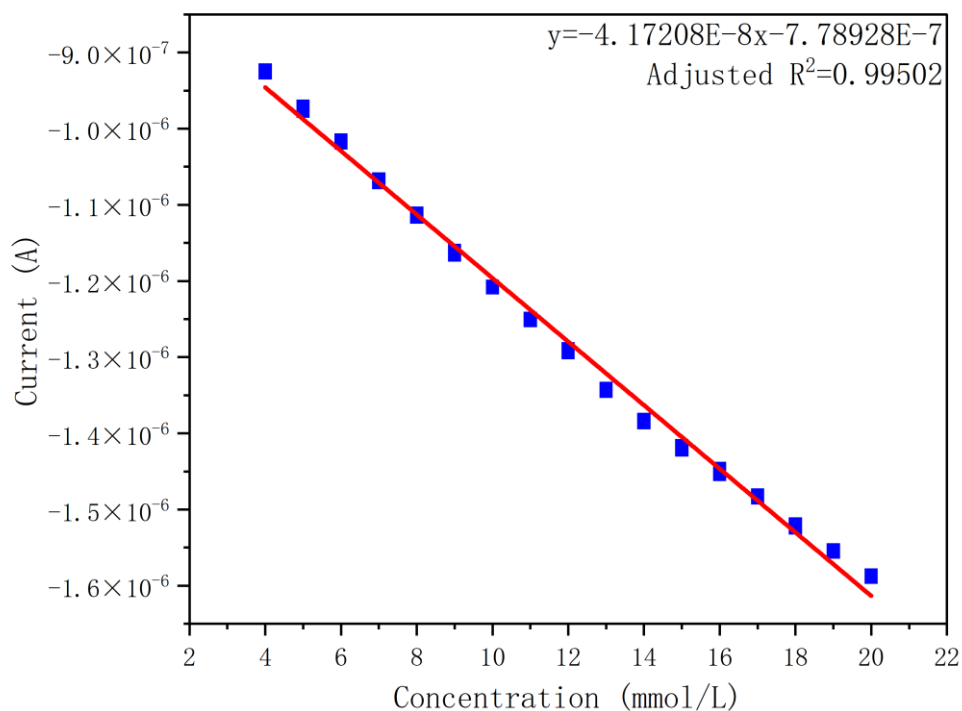
Figure 5.9 Standard curve of lactate oxidase electrode based on viologen and HRP

Substituting linear fitting equation y = a + b * x, the detailed fitting parameters are shown in Table 5.2.

From the table, the sensitivity of the lactate oxidase electrode is -41.7 nA·L/mmol. The viologen lactate oxidase electrode has nearly the same sensitivity compared with the electrode in Chapter 3, but it has better response stability and linearity, and the measurement range of concentration is relatively large.

Table 5.2 Fitting parameters of lactate concentration standard curve

Intercept		Slope	
Value	Standard error	Value	Standard error
-7.78928E-7	9.27915E-10	-4.17208E-8	7.15973E-11
Residual sum of squares		Adjusted R^2	
3.54846E-13		0.99502	

5.4 Summary of the Chapter

This chapter mainly introduces the property of viologen and the fabrication of enzyme electrodes based on viologen as an intermediate layer, in addition to the electrochemical response and standard curve of the electrode.

The main work of this chapter includes:

● Immobilization of sulfhydryl viologen on the surface of the gold electrode.

● Preparation of lactate and glucose oxidase electrodes based on sulfhydryl viologen.

● The relationship between glucose, lactate concentrations, and current is tested, and the linear relation between its concentration and the current signal is confirmed.

6 Summary and Prospect

In this thesis, a sweat composition analysis system based on a flexible electrode array is developed to complete the detection of four representative components of sodium ion, potassium ion, glucose, and lactic acid in sweat. The main work includes:

Firstly, a sweat analysis electrode array integrating ion sensing module, enzyme sensor module, and reference module is prepared based on PET flexible substrate, and the sensor performance is tested. The corresponding linear relationship is obtained by fitting. For ion sensing module: The sensitivity of potassium ISE is 60.8 mV/lg[c(K$^+$)], and the sensitivity of sodium ISE is 45.9 mV/lg[c(Na$^+$)]. In comparison, the potassium ISE has better sensitivity than the sodium ISE. In general, the ion sensing system has good anti-interference and linearity, but the change of temperature will interfere with the response. For enzyme sensing module: The sensitivity of glucose oxidase electrode is 2.28 µA·L/mmol, and the sensitivity of lactate oxidase electrode is 45 nA·L/mmol. Compared with lactate, the glucose oxidase electrode has better sensitivity and linearity.

Secondly, complete the design of the signal acquisition module of the electronic system, and integrate it into the electrode array. According to the response of the electrode test, the circuit design is carried out, and then the system level verification of the four components has proceeded. Verification results show that the design of the electronic system can meet the requirements of sensitivity and linearity. Finally, the whole system is used to measure and analyze human sweat in real motion.

Thirdly, the electrochemical responses of glucose and lactate oxidase electrodes are fabricated and verified based on viologen compounds. The sensitivity of the glucose oxidase electrode is -0.234 µA·L/mmol, and the sensitivity of the lactate oxidase electrode is -41.7 nA·L/mmol. Compared with the common enzyme electrode, the sensitivity of the glucose oxidase electrode is decreased, while the sensitivity of the lactate oxidase electrode is basically unchanged. But the linearity and stability of enzyme electrodes are significantly increased.

Due to the time limit and the complexity of the sweat analysis system, this thesis only realizes the analysis and measurement of four typical components in sweat and the preliminary exploration of the response of viologen-based enzyme electrodes. Based on the work in this thesis, there are also the following possibilities for improvement and development:

I. Further optimization of electrode material and response, and improvement of electrode array manufacturing process. For example, focus on the wear of the electrode surface.

II. Further improvements to the electronic circuit and the addition of current and voltage excitation, which may allow additional electrochemical methods to be used for verification and measurement of other substances.

III. Add other function modules as well as algorithms, so as to realize automatic sweat monitoring and online reminder, alarm functions.

IV. The response of the enzyme electrode based on viologen can be further explored and optimized to develop a new electrode superior to the existing enzyme electrode.

References

[1] BANDODKAR A J, JEANG W J, GHAFFARI R, ROGERS J A. Wearable Sensors for Biochemical Sweat Analysis[J]. Annual review of analytical chemistry (Palo Alto, Calif.), 2019, 12(1): 1-22.

[2] SMITH R E, TOTTI S, VELLIOU E, CAMPAGNOLO P, HINGLEY-WILSON S M, WARD N I, VARCOE J R, CREAN C. Development of a novel highly conductive and flexible cotton yarn for wearable pH sensor technology[J]. Sensors & Actuators: B. Chemical, 2019, 287 : 338-345.

[3] ONOR M, GUFONI S, LOMONACO T, GHIMENTI S, SALVO P, SORRENTINO F, BRAMANTI E. Potentiometric sensor for non invasive lactate determination in human sweat[J]. Analytica Chimica Acta, 2017, (989): 80-87.

[4] BARIYA M, NYEIN H Y Y, JAVEY A. Wearable sweat sensors[J]. Nature Electronics, 2018, 1(3): 160-171.

[5] PATTERSON M J, HALLOWAY S D R, NIMMO M A. Variations in regional sweat composition in normal human males[J]. Experimental physiology, 2000, 85(6): 869-875.

[6] JASON HEIKENFELD. Non-invasive Analyte access and sensing through Eccrine sweat: challenges and outlook circa 2016[J]. Electroanalysis, 2016,28(6): 1242-1249.

[7] REEDER J T, CHOI J, XUE Y G, GUTRUF P, HANSON J, LIU M, RAY T, BANDODKAR A J, AVILA R, XIA W, KRISHNAN S, XU S, BARNES K, PAHNKE M, GHAFFARI R, HUANG Y, ROGERS J A. Waterproof, electronics-enabled, epidermal microfluidic devices for sweat collection, biomarker analysis, and thermography in aquatic settings[J]. Science Advances, 2019, 5(1): eaau6356.

[8] KIM J, SEMPIONATTO J R, IMANI S, HARTEL M C, BARFIDOKHT A, TANG G D, CAMPBELL A S, MERCIER P P, WANG J. Simultaneous monitoring of sweat and interstitial fluid using a single wearable biosensor platform[J]. Advanced Science,2018,5(10): 1800880.

[9] BAKER L B, WOLFE A S. Physiological mechanisms determining eccrine sweat composition[J]. European journal of applied physiology,2020,120(4):719-752.

[10] HE X C, YANG S J, PEI Q B, SONG Y C, LIU C H, XU T L, ZHANG X J. Integrated smart Janus textile Bands for self-pumping sweat sampling and analysis[J]. ACS sensors, 2020, 5(6): 1548-1554.

[11] LIU G, HOB C, SLAPPEY N, ZHOU Z, SNELGROVE S E, BROWN M, GRABINSKI A, GUO X, CHEN D Y, MILLER K, EDWARDS J, KAYA T. A wearable conductivity sensor for wireless real-time sweat monitoring[J]. Sensors and Actuators: B. Chemical,

2016, 227: 35-42.

[12] KOH A, KANG D, XUE Y, LEE S, PIELAK R M, KIM J, HWANG T, MIN S, BANKS A, BASTIEN P, MANCO M C, WANG L, AMMANN K R, JANG K I, WON P, HAN S, GHAFFARI R, PAIK U, SLEPIAN M J, BALOOCH G, HUANG Y G, ROGERS J A. A soft, wearable microfluidic device for the capture, storage, and colorimetric sensing of sweat[J]. Science Translational Medicine, 2016, 8(366): 366ra165.

[13] NIGEL A T, CHRISTIANO A M. Regional variations in transepidermal water loss, eccrine sweat gland density, sweat secretion rates and electrolyte composition in resting and exercising humans[J]. 2013, 2(1): 4.

[14] CHOI J, KANG D, HAN S. Thin, soft, skin-mounted microfluidic networks with capillary bursting valves for chrono-sampling of sweat[J]. Advanced healthcare materials, 2017, 6(5): 1601355.

[15] SONNER Z, WILDER E, HEIKENFELD J. The microfluidics of the eccrine sweat gland, including biomarker partitioning, transport, and biosensing implications[J]. Biomicrofluidics, 2015, 9(3): 031301.

[16] GHAFFARI R, YANG D, KIM J, MANSOUR A, WRIGHT J A, MODEL J B, WRIGHT D E, ROGERS J A, RAY T R. State of sweat: emerging wearable systems for real-time, noninvasive sweat sensing and analytics[J]. ACS sensors, 2021, 6(8): 2787–2801.

[17] ZAFAR S, LU M, JAGTIANI A. Comparison between Field Effect Transistors and Bipolar Junction Transistors as Transducers in Electrochemical Sensors[J]. Scientific reports, 2017, 7: 41430.

[18] ZHANG Y, CLAUSMEYER J, BABAKINEJAD B, CORDOBA A L, ALI T, SHEVCHUK A, TAKAHASHI Y, NOVAK P, EDWARDS C, LAB M, GOPAL S, CHIAPPINI C, ANAND U, MAGNANI L, COOMBES R C, GORELIK J, MATSUE T, SCHUHMANN W, KLENERMAN D, SVIDERSKAYA E V, KORCHEV Y. Spearhead nanometric field-effect transistor sensors for single-cell analysis[J]. ACS nano, 2016, 10(3): 3214-3221.

[19] MATZEU G, FLOREA L, DIAMOND D. Advances in wearable chemical sensor design for monitoring biological fluids[J]. Sensors & Actuators: B. Chemical, 2015, 211: 403-418.

[20] HAMMOND K B, TURCIOS N L, GIBSON L E. Clinical evaluation of the macroduct sweat collection system and conductivity analyzer in the diagnosis of cystic fibrosis[J]. 1994, 124(2): 255-260.

[21] RODBARD D. Continuous glucose monitoring: a review of successes, challenges, and opportunities[J]. Diabetes technology & therapeutics, 2016, 18(S2): S2-3-S2-13.

[22] LIN L, SHIH J. Immobilized fullerence C60-enzyme-based electrochemical glucose

sensor[J]. Journal of the Chinese Chemicla Society,2011,58: 228-235.

[23]ABDEL-LATIF M S, SULEIMAN A A, GUILBAULT G G. Enzyme-based fiber optic sensor for glucose determination[J]. Analytical letters, 1988, 21(6) : 943-951.

[24]CHEN W,CHEN Y Q. Fabrication of flexible continuous glucose monitoring sensor by non-patterning method[J]. Chinese Journal of Analytical Chemistry, 2016,44(4): 654-659.

[25]EMAMINEJAD S, GAO W, WU E, DAVIES Z A, NYEIN H Y Y, CHALLA S, RYAN S P, FAHAD H M, CHEN K, SHAHPAR Z, TALEBI S, MILLA C, JAVEY A, DAVIS R W. Autonomous sweat extraction and analysis applied to cystic fibrosis and glucose monitoring using a fully integrated wearable platform[J]. Proceedings of the National Academy of Sciences of the United States of America.,2017,114(18):4625-4630.

[26]GAO W, NYEIN H Y Y, SHAHPAR Z, FAHAD H M, CHEN K, EMAMINEJAD S, GAO YJ , TAI L C, OTA H, WU E, BULLOCK J, ZENG Y P, LIEN D H, JAVEY A. Wearable microsensor array for multiplexed heavy metal monitoring of body fluids[J]. ACS sensors, 2016, 1(7): 866-874.

[27]GAO W, EMAMINEJAD S, NYEIN H Y Y, CHALLA S, CHEN K V, PECK A, FAHAD H M, OTA H, SHIRAKI H, KIRIYA D, LIEN D H, BROOKS G A, DAVIS R W, JAVEY A. Fully integrated wearable sensor arrays for multiplexed in situ perspiration analysis[J]. Nature, 2016, 529(7587): 509-514.

[28]REEDER J T, XUE Y G, FRANKLIN D, DENG Y J, CHOI J, PRADO O, KIM R, LIU C, HANSON J, CIRALDO J, BANDODKAR A J, KRISHNAN S, JOHNSON A, PATNAUDE E, AVILA R, HUANG Y G, ROGERS J A. Resettable skin interfaced microfluidic sweat collection devices with chemesthetic hydration feedback[J]. Nature communications, 2019, 10(1): 5513-5513.

[29]SEMPIONATTO J R, NAKAGAWA T, PAVINATTO A, MENSAH S T, IMANI S, MERCIER P, WANG J. Eyeglasses based wireless electrolyte and metabolite sensor platform.[J]. Lab on a chip, 2017, 17(10): 1834-1842.

[30]BOYSEN T C, YANAGAWA S, SATO F, SATO K. A modified anaerobic method of sweat collection[J]. Journal of applied physiology: respiratory, environmental and exercise physiology, 1984, 56(5): 1302-7.

[31]SONNER Z, WILDER E, HEIKENFELD J, KASTING G, BEYETTE F, SWAILE D, SHERMAN F, JOYCE J, HAGEN J, KELLEY-LOUGHNANE N, NAIK R. The microfluidics of the eccrine sweat gland, including biomarker partitioning, transport, and biosensing implications[J]. Biomicrofluidics, 2015, 9(3): 031301.

[32]Yu C, SUN X L, WANG D X, DU C, LIU N, KONG L. The latest research progress of enzyme immobilization carrier and immobilization method[J]. Guangdong Chemical

Industry,2021,48(02): 60-62+78

[33] BRADY D, JORDAAN J, SIMPSON C, CHETTY A, ARUMUGAM C, MOOLMAN F S. Spherezymes: A novel structured self-immobilisation enzyme technology[J]. BMC Biotechnology, 2008, 8(1): 8.

[34] LIU Q Q, HUA Y F, KONG X Z, ZHANG C M, CHEN Y M. Covalent immobilization of hydroperoxide lyase on chitosan hybrid hydrogels and production of C6 aldehydes by immobilized enzyme[J]. Journal of molecular catalysis b-enzymatic 2013, 95: 89-98.

[35] TEMBE S, KUBAL B S, KARVE M, D'SOUZA S F. Glutaraldehyde activated eggshell membrane for immobilization of tyrosinase from Amorphophallus companulatus: Application in construction of electrochemical biosensor for dopamine[J]. Analytica Chimica Acta, 2008, 612(2): 212-217.

[36] ZDARTA J, MEYER A S, JESIONOWSKI T, PINELO M. A general overview of support materials for enzyme immobilization: characteristics, properties, practical utility[J]. Catalysts, 2018, 8(2): 92.

[37] LIU Y, WANG M K, ZHAO F, XU Z A, DONG S J. The direct electron transfer of glucose oxidase and glucose biosensor based on carbon nanotubes/chitosan matrix[J]. Biosensors and Bioelectronics, 2005, 21(6): 984-988.

[38] CHEN Y, LU S, ZHANG S. Skin-like biosensor system via electrochemical channels for noninvasive blood glucose monitoring[J]. Science advances, 2017, 3(12): e1701629

[39] GERLACHE M, KAUFFMANN J M, QUARIN G, VIRE J C, BRYANT G A, TALBOT J M. Electrochemical analysis of surfactants: An overview[J]. Talanta, 1996, 43(4): 507-519.

[40] LABIB M, SARGENT E H, KELLEY S O. Electrochemical methods for the analysis of clinically relevant biomolecules[J]. Chemical reviews, 2016, 116(16): 9001-90.

[41] NYEIN H Y Y, BARIYA M, KIVIMAKI L, UUSITALO S, LIAW T S, JANSSON E, AHN C H, HANGASKY J A, ZHAO J Q, LIN Y J, HAPPONEN T, CHAO M H, LIEDERT C, ZHAO Y B, TAI L C, HILTUNEN J, JAVEY A. Regional and correlative sweat analysis using high-throughput microfluidic sensing patches toward decoding sweat[J]. Science Advances, 2019, 5(8): eaaw9906.

[42] ROSE D P, RATTERMAN M E, GRIFFIN D K, HOU L L, KELLEY-LOUGHNANE N, NAIK R R, HAGEN J A, PAPAUTSKY I, HEIKENFELD J C. Adhesive RFID sensor patch for monitoring of sweat electrolytes[J]. IEEE transactions on bio-medical engineering, 2015, 62(6): 1457-65.

[43] NYEIN H Y Y, GAO W, SHAHPAR Z, EMAMINEJAD S, CHALLA S, CHEN K, FAHAD H M, TAI L C, OTA H, DAVIS R W, JAVEY A. A wearable electrochemical

platform for noninvasive simultaneous monitoring of Ca(2+) and pH[J]. ACS nano, 2016, 10(7): 7216-24.

[44] SATISH K T, CONNOR O, SURESH N. Noninvasive label-free detection of cortisol and lactate using graphene embedded screen-printed electrode[J]. Nano-Micro Letters, 2018, 10(3): 1-10.

[45] GAMELLA M, CAMPUZANO S, MANSO J, DE RIVERA G G, LOPEZ-COLINO F, REVIEJO A J, PINGARRON J M. A novel non-invasive electrochemical biosensing device for in situ determination of the alcohol content in blood by monitoring ethanol in sweat[J]. Analytica Chimica Acta, 2014, 806: 1-7.

[46] BUCK R P, LINDNER E. Recommendations for nomenclature of ionselective electrodes (IUPAC Recommendations 1994)[J]. Pure and Applied Chemistry, 2013, 66(12): 2527-2536.

[47] FIKRET K. Generalized rate equation for single-substrate enzyme catalyzed reactions[J]. Biochemical and Biophysical Research Communications, 2009, 382(1): 157-159.

[48] TAYLOR D M. Vacuum-thermal-evaporation: the route for roll-to-roll production of large-area organic electronic circuits[J]. Semiconductor Science and Technology, 2015, 30(5): 054002.

[49] MICHALSKA A. All-solid-state ion selective and all-solid-state reference electrodes[J]. Electroanalysis, 2012, 24(6): 1253-1265.

[50] AGATA M. Optimizing the analytical performance and construction of ion-selective electrodes with conducting polymer-based ion-to-electron transducers[J]. Analytical and Bioanalytical Chemistry, 2006, 384(2): 391-406.

[51] LU C. Research progress of conductive polymer materials[J]. Modern Chemical Research, 2018(12): 162-163.

[52] JOHAN B, ANDRZEJ L, ARI I. Electrochemical impedance spectroscopy of oxidized poly(3,4-ethylenedioxythiophene) film electrodes in aqueous solutions[J]. Journal of Electroanalytical Chemistry, 2000, 489(1-2): 17-27.

[53] BANDODKAR A J, MOLINNUS D, MIRZA O, GUINOVART T, WINDMILLER J R, VALDES-RAMIREZ G, ANDRADE F J, SCHONING M J, WANG J. Epidermal tattoo potentiometric sodium sensors with wireless signal transduction for continuous non-invasive sweat monitoring[J]. Biosensors and Bioelectronics, 2014, 54: 603-609.

[54] MALON A, RADU A, QIN W, QIN Y, CERESA A, MAJ-ZURAWSKA M, BAKKER E, PRESTCH E. Improving the detection limit of anion-selective electrodes: an iodide-selective membrane with a nanomolar detection limit[J]. Analytical chemistry, 2003, 75(15): 3865-71.

[55] ZHU J W, QIN Y, ZHANG Y H. Preparation of all solid-state potentiometric ion sensors with polymer-CNT composites[J]. Electrochemistry Communications, 2009, 11(8): 1684-1687.

[56] KARYAKIN A A, KARYAKINA E E. Electroanalytical applications of Prussian Blue and its analogs[J]. Russian Chemical Bulletin, 2001, 50(10): 1811-1817.

[57] WANG Y S. Flexible electrode electrochemical sensor for determination of glucose and lactate in sweat[D]. Zhejiang University, 2019.

[58] GUAN D R. Sweat monitoring system based on flexible sensor array[D]. Fudan University, 2021.

[59] VERDE T, SHEPHARD R J, COREY P, MOORE R. Sweat composition in exercise and in heat[J]. Journal of applied physiology: respiratory, environmental and exercise physiology, 1982, 53(6): 1540-5.

[60] SUZHOU PSB. Analysis and study on the composition of human sweat (in Chinese)[J]. Forensic Science and Technology, 1978(05): 24-30.

[61] FILIPKOWSKI A, OGRODZKI J, OPALSKI L J, RYBANIEC R, WIECZOREK P Z. Data acquisition system for ion-selective potentiometric sensors[C]. Photonics Applications in Astronomy, Communications, Industry and High Energy Physics, 2009, 7502.

[62] CHUNG M, FORTUNATO G, RADACSI N. Wearable flexible sweat sensors for healthcare monitoring: a review[J]. Journal of the Royal Society Interface, 2019, 16(159): 20190217.

[63] BRANCATO L, DECROP D, LAMMERTYN J, PUERS R. Surface nanostructuring of parylene-C coatings for blood contacting implants[J]. Materials, 2018, 11(7): 1109.

[64] JASMEE S, OMAR G, MASRIPAN N A B, KAMAROLZAMAN A A, ASHIKIN A S, ANI F C. Hydrophobicity performance of polyethylene terephthalate (PET) and thermoplastic polyurethane (TPU) with thermal effect[J]. Materials research express, 2018, 5(9): 096304.

[65] HAN X, BAI Y. Research progress on synthesis and applications of the viologens [J]. Chinese Journal of Synthetic Chemistry, 2019,27(07): 576-583.

[66] MICHAELIS L, HILL E S. The viologen indicators[J]. The Journal of general physiology, 1933, 16(6): 859-73.

[67] DING J J, ZHENG C N, WANG L X, LU C B, ZHANG B, CHEN Y, LI M Q, ZHAI G Q, ZHUANG X D. Viologen-inspired functional materials: synthetic strategies and applications[J]. Journal of Materials Chemistry, A. Materials for energy and sustainability,2019,7(41): 23337-23360.

[68] HWANG E, SEO S, BAK S, LEE HA, MIN M, LEE HY. An electrolyte-free flexible electrochromic device using electrostatically strong graphene quantum dot-viologen nanocomposites[J]. Advanced Materials,2014,26(30): 5129-5136.

[69] WADHWA K, NURYYEVA S, FAHRENBACH A C, ELHABIRI M, PLATAS-IGLESIAS C, TRABOLSI A. Intramolecular redox-induced dimerization in a viologen dendrimer[J]. Journal of Materials Chemistry, C. materials for optical and electronic devices, 2013,1(12): 2302-2307.

[70] NGUYEN Q V, MARTIN P, FRATH D, DELLA ROCCA M L, LAFOLET F, BELLINCK S, LAFARGE P, LACROIX J C. Highly efficient long-range electron transport in a viologen-based molecular junction[J]. Journal of the American Chemical Society, 2018, 140(32): 10131-10134.

[71] WANG L X, SUN S, HE Y F, HE N, ZHANG F, YAO Y F, ZHANG B, ZHAUNG X D, CHEN Y. Viologen-bridged polyaniline based multifunctional heterofilms for all-solid-state supercapacitors and memory devices[J]. European Polymer Journal, 2018, 98: 125-136.

[72] ZHANG P P, ZHU F, WANG F X, WANG J H, DONG R H, ZHAUNG X D, SCHMIDT O G, FENG X L. Stimulus-responsive micro-supercapacitors with ultrahigh energy density and reversible electrochromic window.[J]. Advanced materials (Deerfield Beach, Fla.), 2017, 29(7): 1604491.

[73] LI X, XUE Y R, SONG Y, ZHANG W K. Coordinate interaction between monosulfide and Au surfaces [J]. Chemical Journal of Chinese Universities, 2018,39(12): 2774-2780.

[74] MACKEY D, KILLARD A J, AMBROSI A, SMYTH M R. Optimizing the ratio of horseradish peroxidase and glucose oxidase on a bienzyme electrode: Comparison of a theoretical and experimental approach[J]. Sensors & Actuators: B. Chemical, 2006, 122(2): 395-402.